

Copyright  
by  
Landon Paul Lockhart  
2018

**The Thesis Committee for Landon Paul Lockhart  
Certifies that this is the approved version of the following thesis:**

**Pore Pressure Prediction: From Vertical Stress to Mean Stress to the  
Full Stress Tensor**

**APPROVED BY  
SUPERVISING COMMITTEE:**

**Supervisor:**

---

Peter B. Flemings

---

Maria A. Nikolinakou, Co-Supervisor

---

Luc Lavier

**Pore Pressure Prediction: From Vertical Stress to Mean Stress to the  
Full Stress Tensor**

**by**

**Landon Paul Lockhart**

**Thesis**

Presented to the Faculty of the Graduate School of

The University of Texas at Austin

in Partial Fulfillment

of the Requirements

for the Degree of

**Master of Science in Geological Sciences**

**The University of Texas at Austin**

**May 2018**

## **Acknowledgements**

First, I would like to thank my family for their unconditional love and support (and for taking my endless phone calls). I thank my parents, for they have sacrificed a lot and done an incredible job raising my two siblings and me. Undoubtedly, my parents are responsible for all of my success and none of my shortcomings. I thank my sister for telling me what to do and where to go in Austin (without you, I'd probably have never explored anything beyond my office, apartment, or HEB). I especially want to thank my brother for helping me to navigate through the unfamiliar waters of higher education during my time as an undergraduate and graduate student, and for editing nearly everything I ever wrote. You inspired me to be a geologist, and for that I am forever grateful.

Second, I would like to thank my friends, classmates, and professors here at UT. I am grateful to have worked with and learned from some truly exceptional people. Will and Kevin, we had many fun times together in the office. I guess if some guys from Texas, Massachusetts, and Georgia can get along, anybody can. Kris and Baiyuan, thanks for your willingness to always help me with anything technical, from math to MATLAB to how to format this thesis.

Third, I would like to thank everyone in our GeoFluids group. Thanks Dr. Germaine always being lighthearted when times got stressful, and for teaching me how to give a professional talk. Thanks Tessa, Colleen, and Jac for your administrative support and fitting me into Dr. Flemings' busy schedule.

Lastly, I would like to thank my advisor, Dr. Flemings, and my co-advisor, Maria Nikolinakou. Dr. Flemings, I am truly fortunate to have been advised by such an exceptional leader and scientist. Thank you for never ceasing to push me to be my very

best and for always demanding the highest standard of excellence and professionalism. Maria, you served as an incredible source of insight and advice. Thank you for your willingness to always stop whatever you were working on (something that I did not deserve) to indulge my endless questions. I learned more from you than any textbook I read during my time as a master's student. Dr. Flemings and Maria, I could not have asked for two better advisors. Anything good in this thesis is a direct result of your expertise and oversight; any errors and shortcomings are solely mine.

*Esse quam videri.*

## **Abstract**

### **Pore Pressure Prediction: From Vertical Stress to Mean Stress to the Full Stress Tensor**

Landon Paul Lockhart, M.S. Geo. Sci.

The University of Texas at Austin, 2018

Supervisor: Peter B. Flemings

Co-Supervisor: Maria A. Nikolinakou

My thesis focuses on evaluating the relative contribution of both mean stress and deviatoric (shear) stress and understanding how to incorporate their role in order to better predict pore pressure. In Chapter 1, I introduce my thesis by providing a brief background of pore pressure prediction, discussing the importance of using the full stress tensor (mean and shear stress) to predict stress and pressure, and summarizing the agenda of the following two Chapters. In Chapter 2, I predict pore pressure in the deepwater Gulf of Mexico Mad Dog Field, using three different methods that are based on (i) the vertical effective stress (VES), (ii) the mean effective stress (MES), and (iii) the full stress tensor (FES). The VES and MES methods are traditional workflows, whereas the FES method is a new technique. I use ultra-high resolution sonic velocity data, geomechanical modeling, and the Modified Cam Clay soil model. I compare the predicted pore pressures against those that were measured while drilling. I also evaluate the fraction of pore pressure induced by the mean stress and deviatoric (shear) stress. I show that the MES method can

account for the mean stress-induced pressure, but neither VES nor MES can account for the deviatoric (shear) stress-induced pressure. In Chapter 3, I present the new University of Texas Full Application of Stress Tensor to Predict Pore Pressure (UT-FAST-P<sup>3</sup>) online software that I developed to predict pore pressure. I created the software to be a learning tool to illustrate how pore pressure and stress interact in non-uniaxial settings. I wrote the program to predict pore pressure based on the VES, MES, and FES methods. I communicate the results in a velocity vs. mean effective stress plot, and a mean effective stress vs. deviatoric (shear) stress plot. This allows for a side-by-side comparison of each method, thus providing physical insight into the relative contribution of mean stress and deviatoric (shear) stress to compression and pore pressure development. Overall, my thesis contributes to our understanding of the interaction of pressure and stress in the subsurface, demonstrates the importance of using the full stress tensor to predict pore pressure, and explores a new technique (FES approach) that is applicable to a wide range of complex geological environments where the traditional VES and MES methods underperform.

## Table of Contents

List of Tables .....	x
List of Figures .....	xi
Chapter 1: Introduction .....	1
Chapter 2: Influence of Mean and Deviatoric (shear) Stress on Pore Pressure Prediction at the Mad Dog Field, Gulf of Mexico .....	4
Abstract .....	4
2.1 Introduction .....	5
2.2 Soil Compaction and Stress States .....	10
2.3 Pore Pressure Methods: VES, MES, and FES .....	15
2.3.1 Vertical Effective Stress (VES) Method .....	16
2.3.2 Mean Effective Stress (MES) Method .....	18
2.3.3 Full Stress Tensor (FES) Method .....	19
2.4 Application of VES, MES, and FES Methods .....	20
2.4.1 Data and Methods .....	20
2.4.2 Mad Dog Field .....	21
2.4.3 Geomechanical Model .....	22
2.4.4 Assumptions .....	23
2.4.5 Calibration .....	23
2.4.6 Prediction .....	27
2.5 Results .....	31
Pressure Prediction along Calibration Well 826-1 .....	33
Pressure Prediction along Well 825-1 .....	37
Pressure Prediction along Well 826-5 .....	40
Pressure Prediction along Well 782-1 .....	43
2.6 Discussion .....	45
2.7 Conclusions .....	52

Chapter 3: UT-FAST-P <sup>3</sup> GeoFluids Software .....	53
Abstract .....	53
3.1 Introduction.....	53
3.2 Material Model Set-up and Assumptions .....	54
3.3 Display of Results in Mean Effective Stress – Deviatoric (shear) Stress Space .....	62
3.4 List of Inputs .....	64
3.5 Material Model Calibration.....	65
3.6 Pore Pressure from VES Method.....	66
3.7 Pore Pressure from MES Method .....	70
3.8 Pore Pressure from FES Method.....	75
3.9 Simulations .....	81
3.9.1 Simulation 1: Uniaxial Compression.....	82
3.9.2 Simulation 2: Isotropic Compaction (shear lower than uniaxial).....	86
3.9.3 Simulation 3: Shear Higher than Uniaxial .....	93
3.10 Conclusions and Discussion .....	99
Appendix A: Derivation of Mean Total Stress for VES Method.....	102
Appendix B: Derivation of Mean Total Stress for MES Method .....	104
Appendix C: Derivation of Mean Total Stress for FES Method .....	106
Bibliography .....	108

## List of Tables

Table 2.1: Nomenclature. *M = mass, L = Length, and T = time. ....	8
Table 2.1: (continued) .....	9
Table 2.1: (continued) .....	10
Table 2.2: List of input parameters for the geomechanical models. ....	23

## List of Figures

Figure 2.1: Stress paths and volumetric responses of a material compacted with various stress ratios: isotropic (Iso.;  $K=1$ ; dash-dot black path), critical state (C.s.; solid black path), uniaxial ( $K_0$ ; red path), and anything in between ( $K$ ; green paths). A) In  $\sigma'_m:q$  space, iso-porosity curve (iso-n; solid turquoise) captures relationship between mean effective stress and deviatoric (shear) stress for given porosity (horizontal turquoise line in (B)). Yield surface (Y.s.; bright blue) is shown for comparison. B) In  $\sigma'_m:e$  space, compression curves capture relationship between void ratio (or porosity) and mean effective stress for different stress states. Same void ratio corresponds to different mean effective stresses, depending on stress ratio ( $K$ ).....13

Figure 2.2: Schematic showing how pore pressure is calculated for the VES, MES, and FES methods. The VES and MES methods obtain mean effective stress from a uniaxial porosity (velocity) vs. mean effective stress relationship. Both methods assume a unique relationship between porosity and mean effective stress (vertical end-cap (dashed red line)). The FES method obtains mean effective stress from porosity and deviatoric (shear) stress acquired from a geomechanical model. The VES method derives the mean total stress from the overburden, whereas the MES and FES methods acquire the mean total stress from a geomechanical model.....18

Figure 2.3: Location, salt thickness, and cross-sectional profiles of the Mad Dog Field, Gulf of Mexico. (A) The Mad Dog Field is located approximately 190 mi southwest of New Orleans and extends over the Green Canyon. (B) A large-scale 3D wide-azimuth towed-streamer (WATS) survey is used to define the seafloor bathymetry and salt body (seismic data provided by BP and Partners). Pore pressure is predicted in four wells: 825-1, 826-1, 826-5, and 782-1. The smaller red dots mark the surface well locations, and the large black dots mark the bottom hole locations. (C) Interpreted cross-sections A-A', B-B', and C-C' of the salt body (shown in red on B) are used to build the geomechanical models....21

Figure 2.4: Effective stress ratio ( $K$ ) in sediments around Mad Dog salt along section B-B' (Figure 3C). The stress ratio is higher than the uniaxial value,  $K_0=0.8$ :  $K=1$  in the minibasin (isotropic stress state) and  $K>1$  in front of the salt, indicating elevated horizontal stresses (Heidari et al., in press). .....22

Figure 2.5: Calibration well 826-1. Gamma ray, resistivity and sonic logs acquired while drilling. Shear stress obtained from the geomechanical model. MDT measurements (black dots) and total mean stress,  $\sigma_m$  (less hydrostatic pressure) obtained from the geomechanical model (red line). The mean effective stress ( $\sigma'_m$ ) is calculated as the difference between the mean total stress and the MDT pressure measurements. ....25

Figure 2.6: Diagram depicting relationship between velocity ( $v$ ), original stress state (open circles), and equivalent effective stress (filled circles) used to develop a predictive relationship. Pressure measurements are acquired at calibration well 826-1. A) The mean effective stress-deviatoric (shear) stress combination (or original stress state, open circle) is transformed into an equivalent effective stress (filled circle) using equation 22 (graphically, the intersection of the iso-porosity curve with x-axis, where  $q = 0$ ). B) The process described in (A) is repeated for the remainder of MDT locations where pressure measurements allowed for the calculation of mean effective stress (Figure 2.5). C) The equivalent effective stress and corresponding velocities are cross-correlated using linear regression analysis. D) Velocity values corresponding to iso-porosity curves in  $\sigma'_m:q$  space; velocity values calculated from the equivalent effective stress using equation 32.....26

Figure 2.7: Example VES, MES, and FES pore pressures prediction from a single velocity measurement. A) The equivalent effective stress ( $\sigma'_e$ ) is determined from the measured velocity using equation 32. B) An iso-porosity curve is generated from  $\sigma'_e$  (equation 22). C) VES and MES methods: mean effective stress ( $\sigma_m, K_0'$ ) is obtained from intersection of iso-porosity curve and uniaxial compression line ( $\eta K_0$ ; equation 17); FES method: mean effective stress ( $\sigma'_{m,K}$ ) is obtained from intersection of iso-porosity curve with deviatoric (shear) stress ( $q_{GM}$ ) obtained from geomechanical model. D) Mean total stress under uniaxial strain ( $\sigma_m, K_0$ ) for VES derived from vertical total stress and  $K_0$  (equation 28); Mean total stress ( $\sigma_{m,K}$ ) for MES and FES obtained from geomechanical model. Pore pressure is calculated as difference between mean total stress and mean effective stress (VES: equation 29; MES: equation 30; FES: equation 31).....30

Figure 2.8: Schematic showing how to quantify the increment of pore pressure due to non- $K_0$  mean total stress and deviatoric (shear) stress. In this example, increment of pore pressure due to non- $K_0$  mean total stress is negative, and deviatoric (shear) stress is positive. ....32

Figure 2.9: Calibration well 826-1. A1) True vertical depth subsea (TVDSS). A2) Deviatoric (shear) stress from geomechanical model (Shear (K)) and proportional to  $K_0$  (Shear ( $K_0$ )). A3) Increment of pore pressure due to geomechanical deviatoric (shear) stress greater than  $K_0$  deviatoric stress (positive  $\Delta u_q$ ; dark yellow) or lower than  $K_0$  (negative  $\Delta u_q$ ; light yellow) A4) Increment of pore pressure due to geomechanical mean total stress greater than  $K_0$  (positive  $\Delta u_{\sigma m}$ ; dark purple) or lower than  $K_0$  (negative  $\Delta u_{\sigma m}$ ; light purple); A5) Stress and pressure less hydrostatic value,  $u_h$ : vertical total stress ( $\sigma_v$ ; solid black line), mean total stress from geomechanical model ( $\sigma_m, K$ ; solid red line), mean total stress proportional to  $K_0$  ( $\sigma_m, K_0$ ; dashed red line), MDT pressure measurements (black dots); pore pressures predicted by the FES (orange dots), MES (green dots) and VES approach (gray dots). B) Contours of deviatoric (shear) stresses from geomechanical model along section B-B' (Figure 2.3). C) Contours of mean total stresses from geomechanical model along section B-B' (Figure 2.3). .....34

Figure 2.10: Well 825-1 results. A1) True vertical depth subsea (TVDSS). A2) Deviatoric (shear) stress from geomechanical model (Shear (K)) and proportional to  $K_0$  (Shear ( $K_0$ )). A3) Increment of pore pressure due to geomechanical deviatoric (shear) stress greater than  $K_0$  deviatoric stress (positive  $\Delta u_q$ ; dark yellow) or lower than  $K_0$  (negative  $\Delta u_q$ ; light yellow) A4) Increment of pore pressure due to geomechanical mean total stress greater than  $K_0$  (positive  $\Delta u_{\sigma m}$ ; dark purple) or lower than  $K_0$  (negative  $\Delta u_{\sigma m}$ ; light purple); A5) Stress and pressure less hydrostatic value,  $u_h$ : vertical total stress ( $\sigma_v$ ; solid black line), mean total stress from geomechanical model ( $\sigma_m, K$ ; solid red line), mean total stress proportional to  $K_0$  ( $\sigma_m, K_0$ ; dashed red line), MDT pressure measurements (black dots); pore pressures predicted by the FES (orange dots), MES (green dots) and VES approach (gray dots). B) Contours of deviatoric (shear) stresses from geomechanical model along section A-A' (Figure 2.3). C) Contours of mean total stresses from geomechanical model along section A-A' (Figure 2.3).....38

Figure 2.11: Well 826-5 results. A1) True vertical depth subsea (TVDSS). A2) Deviatoric (shear) stress from geomechanical model (Shear (K)) and proportional to  $K_0$  (Shear ( $K_0$ )). A3) Increment of pore pressure due to geomechanical deviatoric (shear) stress greater than  $K_0$  deviatoric stress (positive  $\Delta u_q$ ; dark yellow) or lower than  $K_0$  (negative  $\Delta u_q$ ; light yellow) A4) Increment of pore pressure due to geomechanical mean total stress greater than  $K_0$  (positive  $\Delta u_{\sigma m}$ ; dark purple) or lower than  $K_0$  (negative  $\Delta u_{\sigma m}$ ; light purple); A5) Stress and pressure less hydrostatic value,  $u_h$ : vertical total stress ( $\sigma_v$ ; solid black line), mean total stress from geomechanical model ( $\sigma_m, K$ ; solid red line), mean total stress proportional to  $K_0$  ( $\sigma_m, K_0$ ; dashed red line), MDT pressure measurements (black dots); pore pressures predicted by the FES (orange dots), MES (green dots) and VES approach (gray dots). B) Contours of deviatoric (shear) stresses from geomechanical model along section A-A' (Figure 2.3). C) Contours of mean total stresses from geomechanical model along section A-A' (Figure 2.3).....41

Figure 2.12: Well 782-1 results. A1) True vertical depth subsea (TVDSS). A2) Deviatoric (shear) stress from geomechanical model (Shear (K)) and proportional to  $K_0$  (Shear ( $K_0$ )). A3) Increment of pore pressure due to geomechanical deviatoric (shear) stress greater than  $K_0$  deviatoric stress (positive  $\Delta u_q$ ; dark yellow) or lower than  $K_0$  (negative  $\Delta u_q$ ; light yellow) A4) Increment of pore pressure due to geomechanical mean total stress greater than  $K_0$  (positive  $\Delta u_{\sigma m}$ ; dark purple) or lower than  $K_0$  (negative  $\Delta u_{\sigma m}$ ; light purple); A5) Stress and pressure less hydrostatic value,  $u_h$ : vertical total stress ( $\sigma_v$ ; solid black line), mean total stress from geomechanical model ( $\sigma_m, K$ ; solid red line), mean total stress proportional to  $K_0$  ( $\sigma_m, K_0$ ; dashed red line), MDT pressure measurements (black dots); pore pressures predicted by the FES (orange dots), MES (green dots) and VES approach (gray dots). B) Contours of deviatoric (shear) stresses from geomechanical model along section C-C' (Figure 2.3). C) Contours of mean total stresses from geomechanical model along section C-C' (Figure 2.3). .....44

Figure 2.13: Hypothetical well in front of salt body, in area of elevated deviatoric (shear) stress (Figure 2.4). A1) True vertical depth subsea (TVDSS). A2) Deviatoric (shear) stress from geomechanical model (Shear (K)) and proportional to  $K_0$  (Shear ( $K_0$ )). A3) Increment of pore pressure due to geomechanical deviatoric (shear) stress greater than  $K_0$  deviatoric stress (positive  $\Delta u_q$ ; dark yellow) or lower than  $K_0$  (negative  $\Delta u_q$ ; light yellow) A4) Increment of pore pressure due to geomechanical mean total stress greater than  $K_0$  (positive  $\Delta u_\sigma$ ; dark purple) or lower than  $K_0$  (negative  $\Delta u_\sigma$ ; light purple); A5) Stress and pressure less hydrostatic value,  $u_h$ : vertical total stress ( $\sigma_v$ ; solid black line), mean total stress from geomechanical model ( $\sigma_m, K$ ; solid red line), mean total stress proportional to  $K_0$  ( $\sigma_m, K_0$ ; dashed red line), MDT pressure measurements (black dots); pore pressures predicted by the FES (orange dots), MES (green dots) and VES approach (gray dots). B) Contours of deviatoric (shear) stresses from geomechanical model along section B-B' (Figure 2.3). C) Contours of mean total stresses from geomechanical model along section B-B' (Figure 2.3). .....49

Figure 2.14: Geologic cross section of Mad Dog Field. Figure modified from Merrell et al. (2014). .....51

Figure 3.1: Volumetric responses of a material for various stress state: isotropic (Iso.), critical state (C.s.), uniaxial ( $K_0$ ), and arbitrary (K). A) In mean effective stress vs. deviatoric (shear) stress ( $\sigma'_m:q$ ) space, yield surface (Y.s.; dashed blue) describes elasto-plastic behavior of material. Iso-porosity surface (iso-n; solid blue) captures relationship between mean effective stress and deviatoric (shear) stress for given porosity. B) In mean effective stress vs. void ratio ( $\sigma'_m:e$ ) space, compression curves capture relationship between porosity and mean effective stress for different stress states. ....57

Figure 3.2: Generation of iso-porosity curve. A) The velocity – vertical effective stress relationship (equation 17) is mapped to velocity – mean effective stress assuming uniaxial strain (equation 19). B) Velocity is related to any mean effective stress along the uniaxial compression line C) Shape of iso-porosity surface (equation 13) is anchored to the mean effective stress along the uniaxial ( $K_0$ ) compression line calculated from velocity. D) The iso-porosity (iso-velocity) line is used to relate velocity to mean effective stress for the isotropic stress state, critical stress state and any stress state in between (K). ....61

Figure 3.3: Radial compression curves corresponding to effective stress ratio ( $K$ ) varying from extensional to compressional failure. The region above the x-axis represents extensional loading in terms of geological conditions; the region below the y-axis represents compressional loading in terms of geological conditions. In this example,  $\phi=30$  deg. The slope of  $M$  in the extensional region is defined by equation 8; the slope of  $M$  in the compressional region is defined by equation 9. The loading cartoons illustrate the effective stress ratio from extensional failure (top), to uniaxial compression ( $K_0$ ), to isostatic compression (iso.), to compressional failure (bottom). For each of the stress states, the vertical stress is held constant while the horizontal stress is changed. ....63

Figure 3.4: Default inputs for UT-FAST-P<sup>3</sup> software found on home page ([Link](#)). .....65

Figure 3.5: Pore pressure and stress prediction based on VES method (diamond). Results shown use default input parameters (Figure 3.4). A) Compression curves for isotropic stress state (black dash-dot curve), uniaxial stress state (gray dashed curve), and critical state state (black dashed curve). B) Compression lines for the isotropic stress state (x-axis), uniaxial stress state (dashed gray line), and critical stress state (black line); pore pressure is the difference between mean total and effective stress ( $u_{VES}$ ; gray arrow). C) Mean total stress. ....69

Figure 3.6: Pore pressure and stress prediction based on MES method (square). Results shown use default input parameters (Figure 3.4). A) Compression curves for isotropic stress state (black dash-dot curve), uniaxial stress state (gray dashed curve), user-defined stress state (green dashed curve), and critical stress state (black dashed curve). B) Compression lines for the isotropic stress state (x-axis), uniaxial stress state (dashed gray line), user-defined stress state (green dashed line), and critical stress state (black line). MES method assumes a 1:1 relationship between velocity and mean effective stress that is independent of deviatoric (shear) stress; therefore, the iso-porosity line is vertical in  $\sigma'_m:q$  space (red dashed line). Pore pressure is the difference between mean total and effective stress ( $u_{MES}$ ; green arrow). C) Mean total stress. ....73

Figure 3.7: A) Radial compression curves corresponding to effective stress ratio (K) varying from extensional to compressional failure. MES method assumes a 1:1 relationship between velocity and mean effective stress that is independent of deviatoric (shear) stress; therefore, the iso-porosity line is vertical in  $\sigma'_m:q$  space (black dashed line). B) Change in mean total stress (green line) and therefore pore pressure (black arrows between A and B figures) as a function of K (from extensional failure to compressional failure).....74

Figure 3.8: A) Radial compression curves corresponding to effective stress ratio (K) varying from extensional to compressional failure. MES method assumes a 1:1 relationship between velocity and mean effective stress that is independent of deviatoric (shear) stress; therefore, the iso-porosity line is vertical in  $\sigma'_m:q$  space (black dashed line). B) Change in pore pressure predicted by the MES method (green curve) as a function of stress ratio K (from extensional to compressional failure). .....75

Figure 3.9: Pore pressure and stress prediction based on FES method (circle). Results shown use default input parameters (Figure 3.4). A) Compression curves for isotropic stress (black dash-dot curve), uniaxial stress (gray dashed curve), user-defined stress state (green dashed curve), and critical state (black dashed curve). B) Compression lines for the isotropic stress state (x-axis), uniaxial stress state (dashed gray line), user-defined stress state (green dashed line), and critical stress state (black line). For a given velocity, changes in mean effective stress and deviatoric (shear) stress follow curved iso-porosity path. Pore pressure is the difference between mean total and effective stress ( $u_{FES}$ ; dash-dot green arrow). C) Mean total stress. ....79

Figure 3.10: A) Radial compression curves corresponding to effective stress ratio (K) varying from extensional to compressional failure. For a given velocity, changes in mean effective stress and deviatoric (shear) stress follow curved iso-porosity path. B) Change in mean total stress (green line) and therefore pore pressure (black arrows between A and B figures) as a function of K (from extensional failure to compressional failure). ..80

Figure 3.11: A) Radial compression curves corresponding to effective stress ratio ( $K$ ) varying from extensional to compressional failure. For a given velocity, changes in mean effective stress and deviatoric (shear) stress follow curved iso-porosity path. B) Change in pore pressure predicted by the FES method (green dash-dot curve) as a function of stress ratio  $K$  (from extensional to compressional failure). .....81

Figure 3.12: Input table for uniaxial compaction ( $K=K_0$ ). .....82

Figure 3.13: Pore pressure and stress prediction based on VES (diamond), MES (square), and FES (circle) methods. A) Compression curves for isotropic stress state (black dash-dot curve), uniaxial stress state (gray dashed curve), user-defined stress state (dashed green curve) and critical stress state (black dashed curve). B) Compression lines for the isotropic stress state ( $x$ -axis), uniaxial stress state (dashed gray line), user-defined stress state (green dashed line), and critical stress state (black line). C) Mean total stress. B, C)  $u_{VES}$  pore pressure (gray arrows);  $u_{MES}$  pore pressure (green arrows);  $u_{FES}$  pore pressure (green dash-dot arrows). .....85

Figure 3.14: Predicted pore pressures in pressure & stress – depth plot.  $u_{VES}$  pore pressure (diamond);  $u_{MES}$  pore pressure (square);  $u_{FES}$  pore pressure (circle); hydrostatic gradient (blue dashed line); lithostatic gradient (red dashed line). The lithostatic gradient is derived from vertical total stress and user-defined input depth. ....86

Figure 3.15: Input table for isotropic compaction ( $K=1$ ). .....87

Figure 3.16: Pore pressure and stress prediction based on VES (diamond), MES (square), and FES (circle) methods. A) Compression curves for isotropic stress state (black dash-dot curve), uniaxial stress state (gray dashed curve), user-defined stress state (dashed green curve) and critical stress state (black dashed curve). B) Compression lines for the isotropic stress state (x-axis), uniaxial stress state (dashed gray line), user-defined stress state (green dashed line), and critical stress state (black line). C) Mean total stress. B, C)  $u_{VES}$  pore pressure (gray arrows);  $u_{MES}$  pore pressure (green arrows);  $u_{FES}$  pore pressure (green dash-dot arrows).....91

Figure 3.17: Predicted pore pressures:  $u_{ES}$  (diamond);  $u_{MES}$  (square);  $u_{FES}$  (circle) A) Predicted pore pressures in pressure & stress – depth plot: hydrostatic gradient (blue dashed line); lithostatic gradient (red dashed line). The lithostatic gradient is derived from vertical total stress and user-defined depth. B) Change in pore pressure predicted by MES (green solid curve) and FES (green dash-dot curve) as a function of stress ratio  $K$  (from extensional to compressional failure). .....92

Figure 3.18: Predicted pore pressure error range:  $u_{VES}$  (diamond);  $u_{MES}$  (square);  $u_{FES}$  (circle); capped lines represent predicted pore pressure based on minimum and maximum  $K$  values ( $K_{min.}$  &  $K_{max.}$ ). A) Pressure & stress – depth plot. Depth is the same but shown graphically as different to improve clarity. B) Error range for VES, MES, and FES methods. .93

Figure 3.19: Input table for shear higher than uniaxial ( $K < K_0$ ). .....94

Figure 3.20: Pore pressure and stress prediction based on VES (diamond), MES (square), and FES (circle) methods. A) Compression curves for isotropic stress state (black dash-dot curve), uniaxial stress state (gray dashed curve), user-defined stress state (dashed green curve) and critical stress state (black dashed curve). B) Compression lines for the isotropic stress state (x-axis), uniaxial stress state (dashed gray line), user-defined stress state (green dashed line), and critical stress state (black line). C) Mean total stress. B, C)  $u_{VES}$  pore pressure (gray arrows);  $u_{MES}$  pore pressure (green arrows);  $u_{FES}$  pore pressure (green dash-dot arrows). .....97

Figure 3.21: Predicted pore pressures:  $u_{ES}$  (diamond);  $u_{MES}$  (square);  $u_{FES}$  (circle) A) Predicted pore pressures in pressure & stress – depth plot: hydrostatic gradient (blue dashed line); lithostatic gradient (red dashed line). The lithostatic gradient is derived from vertical total stress and user-defined depth. B) Change in pore pressure predicted by MES (green solid curve) and FES (green dash-dot curve) as a function of stress ratio K (from extensional to compressional failure). .....98

Figure 3.22: Predicted pore pressure error range:  $u_{VES}$  (diamond);  $u_{MES}$  (square);  $u_{FES}$  (circle); capped lines represent predicted pore pressure based on minimum and maximum K values ( $K_{min.}$  &  $K_{max.}$ ). A) Pressure & stress – depth plot. Depth is the same but shown graphically as different to improve clarity. B) Error range for VES, MES, and FES methods. .99

## Chapter 1: Introduction

Pore pressure prediction is a complex, evolving science. As geology, law, and an increase in global demand for energy continue to push exploration farther offshore into more complex geologic settings, progress in our ability to predict pore pressures must follow accordingly.

Drilling into complex geologic environments often result in costly drilling problems because of the wide range of stresses and pore pressure perturbations encountered. Traditional pore pressure techniques assume the stress state is uniaxial. In these settings, changes in porosity (or some other geophysical measurement that is sensitive to changes in compaction, e.g., velocity) can be linked to changes in the vertical effective stress, because the horizontal effective stresses change as a function of the vertical. Therefore, in uniaxial settings, porosity can be correlated with the vertical effective stress. Indeed, traditional workflows to predict pore pressure establish relationships between porosity and the vertical effective stress (Bowers, 1995). However, in complex geologic settings, loading is non-uniaxial and, therefore, the horizontal stresses are independent of the vertical. As a result, all three stress components ( $\sigma_v$ ,  $\sigma_h$ , and  $\sigma_H$ ), as well as deviatoric (shear) stress, may contribute to changes in volume.

Basins where the stress state varies locally are ubiquitous around the world (salt bodies, fault zones, anticlines, synclines, continental margins, fold-and-thrust belts, etc.). An example of such a complex geologic setting where the stress state is non-uniaxial is the deepwater Gulf of Mexico Mad Dog Field. The presence of an allochthonous salt sheet in the Mad Dog Field changes the stress regime due to lateral push from the salt. (Nikolinakou et al., 2013); this creates local changes in the horizontal and, in turn, mean and shear stresses. Consequently, the stress state in Mad Dog is not uniaxial. More recent

techniques attempt to incorporate the horizontal stresses to account for non-uniaxial stress state by using the mean effective stress to calculate pore pressure (Goult, 1998; Harrold et al., 1999). Nevertheless, such attempts fail to account for the deviatoric (shear) stress component in the development of pore pressure, which can lead to either under- or over-prediction of pore pressures.

My thesis evaluates the relative contribution of both mean stress and deviatoric (shear) stress to the development of pore pressure. I focus on the traditional vertical effective stress (VES) and mean effective stress (MES) methods to predict pore pressure, and the new full stress tensor (FES) approach. My methodology and results reveal that pore pressure is driven by a combination of both mean stress and deviatoric (shear) stress.

In Chapter 2, I predict pore pressure in the deepwater Gulf of Mexico Mad Dog Field, using the VES, MES, and FES methods. I use ultra-high resolution sonic velocity data, geomechanical modeling, and the Modified Cam Clay soil model. I compare the predicted pore pressures against those that were measured while drilling. I show that the FES predicts pressures that more closely match those measured.

In Chapter 2, I also provide a solution to quantify the fraction of pore pressure induced by the mean stress and the fraction of pore pressure induced by the shear stress. This is a key contribution of my thesis. By quantifying both, we are able to determine the amount of pore pressure that will be neglected if a vertical stress-based (VES) or a mean stress-based (MES) approach is used.

In Chapter 3, I present the new University of Texas Full Application of Stress Tensor to Predict Pore Pressure (UT-FAST-P<sup>3</sup>) online software that I developed. I created the software to be a learning tool that predicts pore pressure based on the VES approach, the MES approach, and the FES approach. Specifically, I wrote the program to communicate how pore pressure and stress interact in non-uniaxial settings. My software

provides a step forward in communicating the importance of accounting for both mean stress and deviatoric (shear) stress when predicting pore pressure.

In summary, my thesis contributes to our overall understanding of the interaction of pressure and stress in the subsurface. It employs an improved pore pressure prediction technique (FES method) that is applicable in a wide range of complex geological environments where the traditional VES and MES methods underperform. Therefore, it contributes to enhancing the safety and efficiency of drilling operations.

## **Chapter 2: Influence of Mean and Deviatoric (shear) Stress on Pore Pressure Prediction at the Mad Dog Field, Gulf of Mexico**

### **ABSTRACT**

We predict pore pressure at the Mad Dog Field, GoM, using three different approaches that are based on (i) vertical effective stress (VES), (ii) mean effective stress (MES), and (iii) the full stress tensor (FES). A large salt body within the Mad Dog Field creates non-uniaxial stress conditions; the ratio of horizontal to vertical effective stress ( $K_0$ ), which is constant in uniaxial basins, changes around the salt body. This leads to either an elevation or a reduction in mean and/or deviatoric (shear) stress. In order to account for this non-uniaxial stress state, we couple velocities with geomechanical modeling to incorporate the full stress tensor in our FES workflow. This provides a significant improvement over the traditional VES and MES approaches, which can only account for mean and deviatoric (shear) stresses proportional to the vertical stress (through  $K_0$ ). Moreover, our FES workflow closely predicts the measured pressures below salt, whereas the traditional method under-predicts pressures up to 0.6 ppg. We show that accounting for the deviatoric (shear) stress drives this improvement. We also closely predict pressure in front of the salt where deviatoric (shear) is elevated and the mean total stress is reduced; in contrast, the traditional VES method under-predicts by as much as 1.4 ppg. Overall, our FES methodology and results predict pressures that more closely match the observed, and reveal that pore pressure is driven by a combination of mean stress and deviatoric (shear) stress. Furthermore, the impact of our study extends beyond salt bodies; our methodology can improve pressure prediction in geological environments where the stress state is not uniaxial, such as anticlines, synclines, continental margins or fold-and-thrust belts.

## 2.1 INTRODUCTION

Overpressure occurs when the pore pressure exceeds the hydrostatic pressure. The presence of overpressure drives fluid flow and impacts the stress state. This can lead to slope instability (Dugan and Flemings, 2002), creation of local fault networks (Cartwright, 1994), and sediments less compacted than those under hydrostatic conditions (Sangrey, 1977). In the oil and gas industry, overpressure is a key input into the exploration and production stages of operations, and special attention is required when drilling through overpressured zones (Fertl et al., 1994). Notable effects include blown reservoir seals, kicks, blowouts, loss of circulation, borehole collapse, and stuck pipe (Sweatman et al., 1999).

The porosity of overpressured rocks is often observed to be higher than the porosity of normally pressured rocks at the same depth (Gibson, 1958; Rubey and Hubbert, 1959). This is commonly interpreted to be the result of sedimentation occurring so rapidly that it exceeds the ability of the pore fluids to escape, forcing the fluids to bear a portion of the overlying load (Gordon and Flemings, 1998; Hart et al., 1995; Rubey and Hubbert, 1959; Swarbrick et al., 2001). As a result, overpressure prevents the porosity from decreasing at the rate it would during burial under normal pressure conditions (Rubey and Hubbert, 1959).

There are a variety of empirical ways to determine overpressure in the subsurface. It is empirically established that void ratio ( $e$ ; Table 2.1) is proportional to the log of vertical effective stress ( $\log(\sigma'_v)$ ) (e.g., Long et al., 2011):

$$e = e_0 - C_c \log(\sigma'_v) \quad (1)$$

where  $e_0$  and  $C_c$  are lithology-dependent constants. Void ratio is a measure of the pore volume, and is related to porosity ( $n$ ) through:

$$e = \frac{n}{1-n} \quad (2)$$

The vertical effective stress is the difference between the vertical total stress ( $\sigma_v$ ) and the pore pressure (u):

$$\sigma'_v = \sigma_v - u \quad (3)$$

By combining equations 1 and 3, pore pressure can be solved for directly:

$$u = \sigma_v - \sigma'_v = \sigma_v - 10^{\left(\frac{e_0 - e}{c_c}\right)} \quad (4)$$

In the field, void ratio (or porosity) is seldom directly measured; therefore, other methods have been developed to estimate the degree of compaction, and thus pore pressure, using velocity (Bowers, 1995; Eaton, 1975; Flemings et al., 2002; Hart et al., 1995), resistivity (Eaton, 1975), or density (Long et al., 2011).

Velocity is commonly used in conventional drilling operations. It has the advantage of being acquired either above ground (seismic) or along the trajectory of a well (sonic), and is less impacted by borehole conditions than other logs. Hart et al. (1995) used the empirical relationship from Issler (1992) to map velocity to porosity (or void ratio):

$$n = \frac{e}{1+e} = 1 - \left(\frac{\Delta t_{ma}}{\Delta t}\right)^{1/x} \quad (5)$$

where  $\Delta t_{ma}$  is the matrix travel time,  $\Delta t$  is the travel time, and x is an acoustic formation factor (all travel times measured in slowness, e.g.,  $\mu s \cdot ft^{-1}$ ), and then applied equation 4 to predict pressure. Others have directly mapped velocity to effective stress. Bowers (1995) used a power law relationship to describe a velocity – effective stress relationship and predict pressure:

$$v = v_0 + A(\sigma'_v)^B \quad (6)$$

where v is velocity,  $v_0$  is the velocity of seawater (velocity at zero effective stress), and A and B are lithology-dependent constants calibrated to existing data.

All of these approaches are grounded on the assumption that the vertical effective stress ( $\sigma'_v$ ) is the only independent stress component; therefore, volume changes are a function of the vertical effective stress. These methods work well as long as compaction is uniaxial across the field. However, in many locations around the world, local perturbations in the stress field mean that the horizontal stresses are decoupled from the vertical. For example, in salt systems, the emplacement of a salt body changes the stress state and creates nonvertical loading (Alberty and McLean, 2003; Nikolinakou et al., 2012). In these cases, void ratio changes depend on vertical stress as well as non-vertical stress components. In other words, simple vertical effective stress models fail in any geological environment where the stress state is not uniaxial (i.e., anticlines, synclines, continental margins, or fold-and-thrust belts).

To address locations where the stress state is not uniaxial, some techniques have been modified to use the mean effective stress (Alberty and McLean, 2003; Goult, 1998; Harrold et al., 1999). Using poroelasticity theory, changes in porosity can be expressed as a function of the mean effective stress, not the vertical effective stress (Goult, 1998). This theory, however, neglects to account for deviatoric (shear) induced stresses that also contribute to compaction (Nikolinakou et al., 2018).

For these reasons, there is now a focus on new methods that incorporate the full stress state (mean and shear stress) to determine pore pressure (Flemings and Saffer, 2018; Goult, 2004; Hauser et al., 2014; Heidari et al., in press; Nikolinakou et al., 2018). The full stress tensor incorporates all stress components into pressure prediction by independently taking into account the contribution of both the mean effective stress and the deviatoric (shear) stress into compaction.

In this study, we review soil compaction and stress states, the vertical effective stress (VES) and mean effective stress (MES) methods to predict pore pressure, we

present the full stress tensor (FES) method, and we apply each method in the deepwater Gulf of Mexico Mad Dog Field. We compare our prediction results against those measured while drilling from the Modular dynamic formation tester (MDT) tool. Overall, our methodology and results show that pore pressure is driven by a combination of mean stress and deviatoric (shear) stress, and highlight the importance of deviatoric (shear) stress-induced pressures. Furthermore, the impact of our study extends beyond salt bodies; the methodology used and insights gained are applicable to geological environments around the world where the stress state is non-uniaxial (fault zones, anticlines, synclines, continental margins, fold and-thrust-belts).

<b>Symbol</b>	<b>Description</b>	<b>Dimension*</b>	<b>Units</b>
TVDSS	True vertical depth from sea surface	$L^1$	ft
$Z_{wd}$	Water depth	$L^1$	ft
$Z_{bsf}$	Depth beneath seafloor	$L^1$	ft
$Z$	Depth	$L^1$	ft
$n$	Porosity	-	-
$e$	Void ratio	-	-
$v$	Velocity	$L^{-1} T^{-1}$	ft/s
$\Delta t_{ma}$	Matrix travel time	$L^{-1} T^{-1}$	$\mu\text{s}/\text{ft}$
$\Delta t$	Travel time	$L^{-1} T^{-1}$	$\mu\text{s}/\text{ft}$
MDT	Modular dynamic formation tester	$M^1 L^{-1} T^{-2}$	psi
$u_{MDT}$	MDT pore pressure measurement	$M^1 L^{-1} T^{-2}$	psi
$u_{VES}$	VES pore pressure	$M^1 L^{-1} T^{-2}$	psi
$u_{MES}$	MES pore pressure	$M^1 L^{-1} T^{-2}$	psi

Table 2.1: Nomenclature. \*M = mass, L = Length, and T = time.

$u_{FES}$	FES pore pressure	$M^1 L^{-1} T^{-2}$	psi
A	Velocity – vertical effective stress fitting parameter	$M^1 L^{-1} T^{-2}$	psi
B	Velocity – vertical effective stress fitting parameter	-	-
$A_e$	Velocity – equivalent effective stress fitting parameter	$M^1 L^{-1} T^{-2}$	psi
$B_e$	Velocity – equivalent effective stress fitting parameter	-	-
$u_h$	Hydrostatic pore pressure	$M^1 L^{-1} T^{-2}$	psi
$u_e$	Excess pore pressure	$M^1 L^{-1} T^{-2}$	psi
$\sigma_1$	Maximum principal effective stress	$M^1 L^{-1} T^{-2}$	psi
$\sigma_2$	Intermediate principal effective stress	$M^1 L^{-1} T^{-2}$	psi
$\sigma_3$	Minimum principal effective stress	$M^1 L^{-1} T^{-2}$	psi
$\sigma'_1$	Maximum principal total stress	$M^1 L^{-1} T^{-2}$	psi
$\sigma'_2$	Intermediate principal total stress	$M^1 L^{-1} T^{-2}$	psi
$\sigma'_3$	Minimum principal total stress	$M^1 L^{-1} T^{-2}$	psi
$\sigma_v$	Vertical total stress	$M^1 L^{-1} T^{-2}$	psi
$\sigma'_v$	Vertical effective stress	$M^1 L^{-1} T^{-2}$	psi
$\sigma_m$	Mean total stress	$M^1 L^{-1} T^{-2}$	psi
$\sigma_{m,K_0}$	Mean total stress under uniaxial strain	$M^1 L^{-1} T^{-2}$	psi
$\sigma_{m,K}$	Mean total stress (geomech. model)	$M^1 L^{-1} T^{-2}$	psi
$\sigma'_m$	Mean effective stress	$M^1 L^{-1} T^{-2}$	psi
$\sigma'_{m,K_0}$	Mean effective stress under uniaxial strain	$M^1 L^{-1} T^{-2}$	psi
$\sigma'_{m,K}$	Mean effective stress (geomech. model)	$M^1 L^{-1} T^{-2}$	psi
q	Deviatoric (shear) stress	$M^1 L^{-1} T^{-2}$	psi
$K_0$	Uniaxial effective stress ratio	-	-

Table 2.1: (continued)

K	Effective Stress ratio	-	-
$\Delta u_{\sigma_m}$	Increment of pore pressure due to non- $K_0$ mean total stress	$M^1 L^{-1} T^{-2}$	psi
$\Delta u_q$	Increment of pore pressure due to non- $K_0$ deviatoric (shear) stress	$M^1 L^{-1} T^{-2}$	psi
$\rho_b$	Bulk density	$M^1 L^{-3} T^0$	$g/cm^3$
$\rho_{sw}$	Seawater density	$M^1 L^{-3} T^0$	$g/cm^3$
g	Acceleration of gravity	$L T^{-2}$	$ft/s^2$
$\phi$	Friction angle	degree	$^\circ$
$\lambda$	Slope of elasto-plastic (loading) line	$M^0 L^0 T^0$	-
$\kappa$	Slope of elastic (unloading) line	$M^0 L^0 T^0$	-
$e_\lambda$	Intercept of elasto-plastic (loading) line at unit mean effective stress	$M^0 L^0 T^0$	-
$e_\kappa$	Intercept of elastic (unloading) line at unit mean effective stress	$M^0 L^0 T^0$	-
PPG	Pounds per gallon	$M^1 L^{-3}$	lbs/gal

Table 2.1: (continued)

## 2.2 SOIL COMPACTION AND STRESS STATES

Void ratio (level of compaction) is a function of the full stress state: the mean effective stress and the deviatoric (shear) stress. The mean effective stress ( $\sigma'_m$ ) is the average of the principal effective stresses:

$$\sigma'_m = \frac{\sigma'_1 + \sigma'_2 + \sigma'_3}{3} \quad (7)$$

The deviatoric (shear) stress ( $q$ ) is the difference between the principal total stresses:

$$q = \sqrt{\frac{(\sigma_1 - \sigma_2)^2 + (\sigma_1 - \sigma_3)^2 + (\sigma_3 - \sigma_2)^2}{2}} \quad (8)$$

Critical state soil models capture the interrelation between mean effective stress, deviatoric (shear) stress, and void ratio. The Modified Cam Clay (MCC) is one widely

used soil model (Wood, 1990) because of its relative simplicity and small number of input parameters (Hashash and Whittle, 1992).

The MCC model describes the, material compaction, stress states, and their interrelation in a mean effective stress vs. deviatoric (shear) stress ( $\sigma'_m:q$ ) plot (Figure 2.1A), and a void ratio vs. mean effective stress ( $e:\sigma'_m$ ) plot (Figure 2.1B). The isotropic stress state represents a loading condition where all principal stress components are equal, and consequently, the deviatoric (shear) stress is (equation 8) zero. This is represented by the horizontal axis in the  $\sigma'_m:q$  plot (Figure 2.1A) and by the dotted black line in ( $e:\sigma'_m$ ) plot (Figure 2.1B). The critical stress state (solid black paths in Figure 2.1 A, B) defines the limiting strength of a material; a material subjected to stresses at critical state will experience failure. The uniaxial stress state (red paths in Figure 2.1 A, B) represents a loading condition where deformation is vertical (no lateral strain) and the ratio of maximum to minimum principal effective stress ( $K_0$ ) is constant:

$$K_0 = \frac{\sigma'_3}{\sigma'_1} \quad (9)$$

Any other stress state (e.g., green paths in Figure 2.1 A, B) is defined by the ratio of minimum to maximum principal effective stress ( $K$ ):

$$K = \frac{\sigma'_3}{\sigma'_1} \quad (10)$$

During consolidation, the void ratio (or porosity) of a material decreases as mean effective stress increases. This deformation is primarily plastic (Craig, 2004; Wood, 1990). In  $e:\sigma'_m$  space, individual stress states (with constant stress ratio,  $K$ ) result in unique compression curves (Figure 2.1B), with the general equation for the loading (plastic) path given by:

$$e = e_\lambda - \lambda \ln(\sigma'_m) \quad (11)$$

where  $e_\lambda$  is the intercept at unit mean effective stress, and  $\lambda$  is the slope. The parameter  $e_\lambda$  depends on the stress state ( $K$ ). For a material undergoing isotropic compaction ( $K=1$ ), the equation for the loading path is given by:

$$e = e_{\lambda,iso} - \lambda \ln(\sigma'_e) \quad (12)$$

where  $e_{\lambda,iso}$  is the intercept of the isotropic loading path at unit mean effective stress, and  $\sigma'_e$  is the equivalent effective stress. The equivalent effective stress represents the mean effective stress of a material undergoing isotropic compression. Hence, the equivalent effective stress is a uniform stress state (no shear).

The general equation for the unloading (elastic) path is given by:

$$e = e_\kappa - \kappa \ln(\sigma'_m) \quad (13)$$

where  $e_\kappa$  is the intercept at unit mean effective stress, and  $\kappa$  is the slope. The loading and unloading paths are linear in  $e:\ln(\sigma'_m)$  space, and curved in  $e:\sigma'_m$  space (Figure 2.1B).

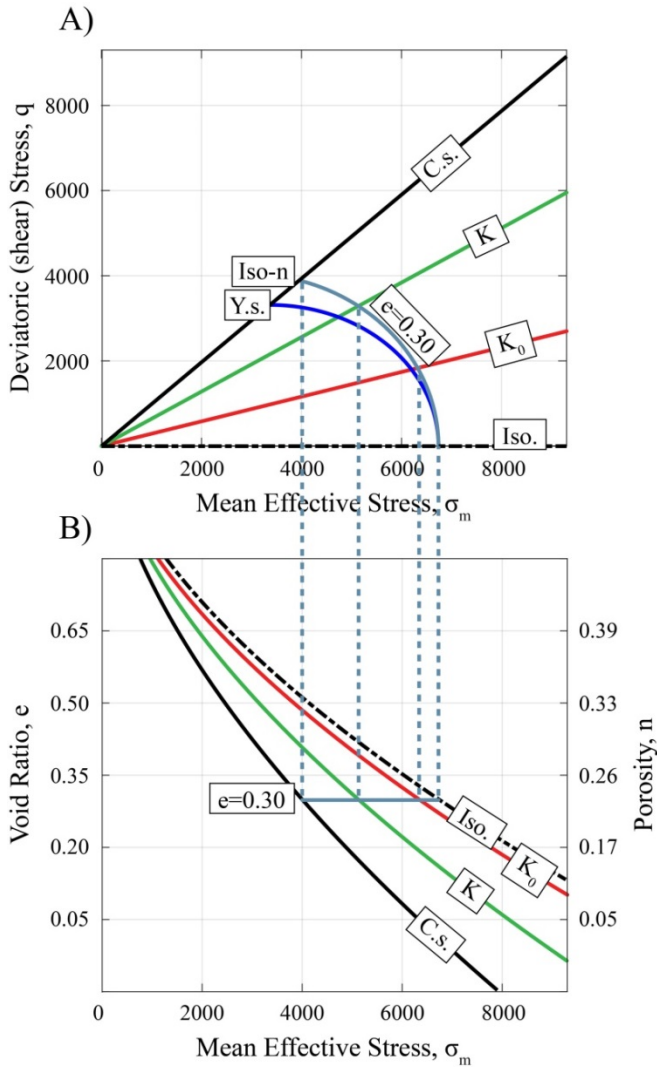


Figure 2.1: Stress paths and volumetric responses of a material compacted with various stress ratios: isotropic (Iso.;  $K=1$ ; dash-dot black path), critical state (C.s.; solid black path), uniaxial ( $K_0$ ; red path), and anything in between ( $K$ ; green paths). A) In  $\sigma'_m$ : $q$  space, iso-porosity curve (iso-n; solid turquoise) captures relationship between mean effective stress and deviatoric (shear) stress for given porosity (horizontal turquoise line in (B)). Yield surface (Y.s.; bright blue) is shown for comparison. B) In  $\sigma'_m$ : $e$  space, compression curves capture relationship between void ratio (or porosity) and mean effective stress for different stress states. Same void ratio corresponds to different mean effective stresses, depending on stress ratio ( $K$ ).

In  $\sigma'_m:q$  space, compression with a constant stress ratio (equation 10) is represented with a line, the slope of which is defined by the ratio of deviatoric (shear) stress to mean effective stress (Figure 2.1A):

$$\eta = \frac{q}{\sigma'_m} \quad (14)$$

where  $\eta=0$  for the isotropic stress state,  $\eta=M$  for the critical stress state,  $\eta=\eta_{K_0}$  for the uniaxial stress state, and  $\eta=\eta_K$  for any other stress state. According to the MCC model, the slope  $M$  is a function of the friction angle ( $\phi$ ) in triaxial compression:

$$M = \frac{6\sin\phi}{3-\sin\phi} \quad (15)$$

and the slope  $\eta_{K_0}$  is solved for numerically:

$$\frac{\eta_{K_0}(1+\nu')(1-\Lambda)}{3(1-2\nu')} + \frac{3\eta_{K_0}\Lambda}{M^2-\eta_{K_0}^2} = 1 \quad (16)$$

where  $\nu'$  is Poisson's ratio for soil in terms of effective stresses, and  $\Lambda=(\lambda-\kappa)/\lambda$ . In typical Gulf of Mexico mudrocks, plastic deformation is much larger than the elastic deformation ( $\lambda \gg \kappa$ ). Thus, the slope of the uniaxial compression line (equation 16) can be simplified to:

$$\eta_{K_0} = \frac{-3 + \sqrt{9 + 4\left(\frac{6\sin\phi}{3-\sin\phi}\right)^2}}{2} \quad (17)$$

Combining equations 9 and 14 provides the uniaxial stress ratio ( $K_0$ ) as a function of the uniaxial slope ( $\eta_{K_0}$ ):

$$K_0 = \frac{3-\eta_{K_0}}{3+2\eta_{K_0}} \quad (18)$$

Combining equations 17 and 18 allows the uniaxial stress ratio ( $K_0$ ) to be calculated as a function of the friction angle ( $\phi$ ). The slope  $\eta_K$  can be expressed as a function of the effective stress ratio ( $K$ ; equation 10):

$$\eta_K = \frac{3(1-K)}{1+2K} \quad (19)$$

The yield surface (bright blue curve in Figure 2.1A) defines the stress level at which a material yields, and marks the limit of the elastic-plastic domain:

$$\frac{\sigma'_m}{\sigma'_e} = \left( \frac{M^2}{M^2 + \eta^2} \right) \quad (20)$$

The equivalent effective stress controls the size of the yield surface and is found at the intersection of the yield surface with the isotropic axis.

The iso-porosity surface (turquoise curve in Figure 2.1A) represents all combinations of mean effective stress and deviatoric (shear) stress that have the same porosity and is described by:

$$\frac{\sigma'_m}{\sigma'_e} = \left( \frac{M^2}{M^2 + \eta^2} \right)^{\frac{\lambda - \kappa}{\lambda}} \quad (21)$$

Given the assumption that the plastic deformation is much larger than the elastic deformation ( $\lambda \gg \kappa$ ), the equation for the iso-porosity surface (equation 21) can be simplified to:

$$\frac{\sigma'_m}{\sigma'_e} = \left( \frac{M^2}{M^2 + \eta^2} \right) \quad (22)$$

Equation 22 represents an ellipse, and coincides with the MCC description for a yield surface (bright blue curve in Figure 2.1A). The elliptical iso-porosity curve reveals that, for a given void ratio (or porosity), the mean effective stress can vary by up to a magnitude of two, depending on the level of deviatoric (shear) stress.

In this study, we use the iso-porosity curves (equation 22) to provide the basic framework to present the full stress tensor (FES) method to predict pore pressure, compare with the vertical effective stress (VES) and mean effective stress (MES) methods, and quantify the relative contributions of mean effective stress and deviatoric (shear) stress to pore pressure.

### **2.3 PORE PRESSURE METHODS: VES, MES, AND FES**

We next review the vertical effective stress (VES) and mean effective stress (MES) methods to predict pore pressure, and present the full stress tensor (FES) method.

### 2.3.1 Vertical Effective Stress (VES) Method

The vertical effective stress (VES) method is based on the assumption that the stress state is uniaxial, with  $\sigma'_h = \sigma'_3$  and  $\sigma'_v = \sigma_1$ . Under this assumption, both mean effective stress and deviatoric (shear) stresses are a function of the vertical effective stress ( $\sigma'_v$ ) and the uniaxial effective stress ration, ( $K_0$ ; equation 9):

$$\sigma'_{m,K_0} = \frac{\sigma'_v(1+2K_0)}{3} \quad (23)$$

and

$$q_{K_0} = \sigma'_v(1 - K_0) \quad (24)$$

The vertical effective stress can be obtained from field measurements in uniaxial conditions. For example, at a calibration well, a relationship is established between void ratio (or e.g., porosity, density, resistivity, or velocity) and the vertical effective stress to define the compaction trend (Bowers, 1995; Eaton, 1975; Flemings et al., 2002; Hart et al., 1995; Long et al., 2011). In the routine application of the VES method, pore pressure is then calculated as the difference between the vertical total and effective stresses:

$$u = \sigma_v - \sigma'_v \quad (25)$$

where  $\sigma_v$  is the vertical total stress, which is calculated by integrating the weight of the water column with the weight of the overlying formation densities:

$$\sigma_v = \rho_{sw}gZ_{wd} + \int_{Z_{wd}}^{Z_{bsf}} \rho_b g dz \quad (26)$$

where  $\rho_{sw}$  is the density of seawater,  $g$  is the acceleration of gravity,  $Z_{wd}$  is the water depth,  $Z_{bsf}$  is the depth beneath the seafloor,  $\rho_b$  is the bulk density of the sediments, and  $z$  is the depth.

In  $\sigma'_m$ : $q$  space (Figure 2.2), uniaxial compaction has a slope  $\eta_{K_0}$  (equation 17; red line in Figure 2.2). For a given field measurement (e.g., porosity or velocity), the mean effective stress under uniaxial strain ( $\sigma'_{m,K_0}$ ) can be found from the intersection of the

uniaxial compaction line (equation 17; red line in Figure 2.2) and the iso-porosity curve (equation 22; black ellipse in Figure 2.2) corresponding to the field measurement:

$$\sigma'_{m,K_0} = \sigma'_e \left( \frac{M^2}{M^2 + \eta K_0^2} \right) \quad (27)$$

We derive the mean total stress from the vertical total stress (equation 26), the mean effective stress under uniaxial strain (equation 27), and the uniaxial effective stress ratio (equation 18):

$$\sigma_{m,K_0} = \sigma_v - \frac{2\sigma'_{m,K_0}(1-K_0)}{1+2K_0} \quad (28)$$

(see Appendix A for full derivation of  $\sigma_{m,K_0}$ )

In order to schematically compare the VES method with the MES and FES methods, pore pressure ( $u_{VES}$  in Figure 2.2) is calculated as the difference between the mean total and effective stresses:

$$u_{VES} = \sigma_{m,K_0} - \sigma'_{m,K_0} \quad (29)$$

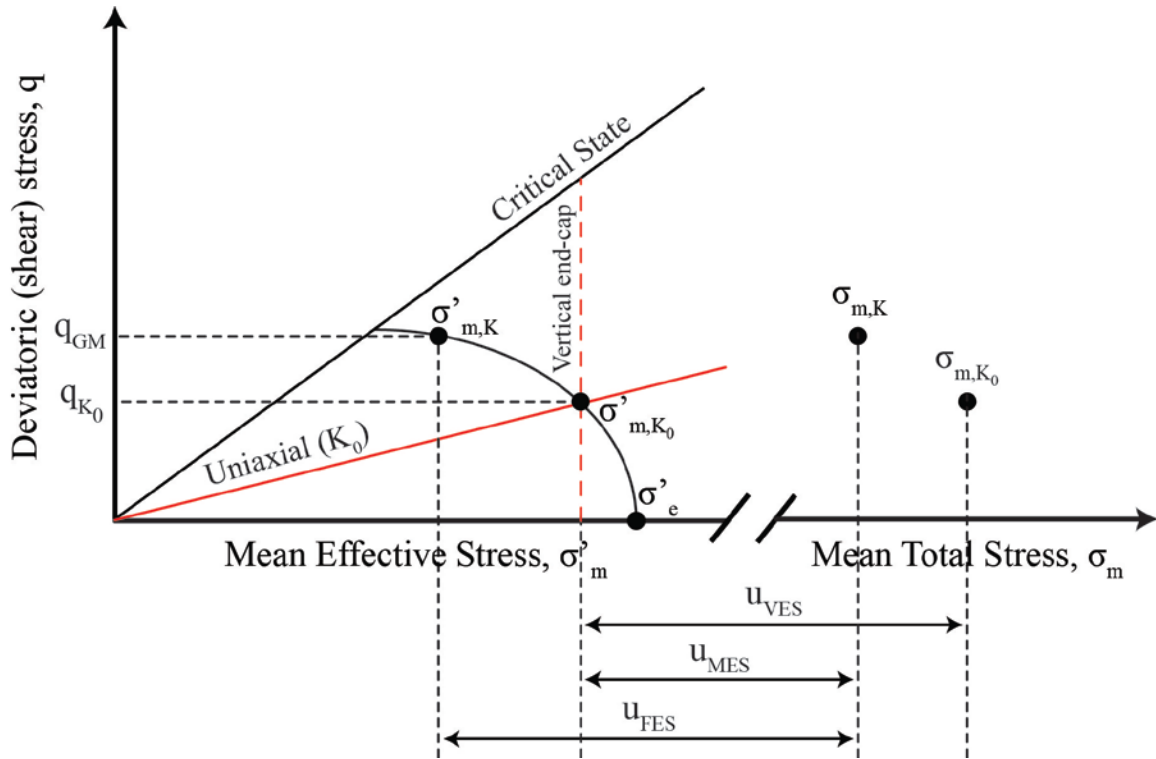


Figure 2.2: Schematic showing how pore pressure is calculated for the VES, MES, and FES methods. The VES and MES methods obtain mean effective stress from a uniaxial porosity (velocity) vs. mean effective stress relationship. Both methods assume a unique relationship between porosity and mean effective stress (vertical end-cap (dashed red line)). The FES method obtains mean effective stress from porosity and deviatoric (shear) stress acquired from a geomechanical model. The VES method derives the mean total stress from the overburden, whereas the MES and FES methods acquire the mean total stress from a geomechanical model.

### 2.3.2 Mean Effective Stress (MES) Method

In locations where the stress state varies, the horizontal stresses are decoupled from the vertical (equation 10). Although there are various forms of the MES method (Alberty and McLean, 2003; Gouly, 1998; Harrold et al., 1999), the collective assumption is that porosity and mean effective stress share a unique relationship (poroelasticity theory). This means that the iso-porosity line is vertical in  $\sigma'_m:q$  space (referred to as vertical end-cap; dashed red line in Figure 2.2). The mean total stress is

then modified to account for any non-uniaxial external loading; oftentimes a geomechanical model provides an estimate of the mean total stress.

Here we assume that the unique relationship between velocity and mean effective stress is established under uniaxial conditions. Therefore, the mean effective stress in the MES method is the same as the mean effective stress in the VES method. Like the VES method, we use equation 27 to calculate the mean effective stress for the MES method. Graphically, this is the intersection of the uniaxial compaction line (equation 17; red line in Figure 2.2) and the iso-porosity surface (equation 22; black ellipse in Figure 2.2).

The non-uniaxial external loading component is incorporated in the mean total stress. Any difference in the mean total stress from its uniaxial value (equation 28) drives the predicted pore pressure. Oftentimes, a geomechanical model provides an estimate of the mean total stress.

We calculate MES pore pressure ( $u_{MES}$ ) as the difference between the mean total stress from the geomechanical model ( $\sigma_{m,K}$ ) and the mean effective stress under uniaxial strain ( $\sigma'_{m,K_0}$ ):

$$u_{MES} = \sigma_{m,K} - \sigma'_{m,K_0} \quad (30)$$

The difference between the VES and MES mean total stress is the difference in the predicted pressure (Figure 2.2).

### 2.3.3 Full Stress Tensor (FES) Method

The full stress tensor (FES) method incorporates all stress components into pressure prediction by taking into account the non-uniaxial (K) contribution of both the mean effective stress and the deviatoric (shear) stress into compression. Hence, the fundamental difference between the FES method and the VES/MES methods is that the FES method does not assume the relationship between void ratio and mean effective

stress is unique; rather, it incorporates the dependence of this relationship on the deviatoric (shear) stress.

The FES method requires a geomechanical model to provide the total stress state: deviatoric (shear) stress and mean total stress. We couple the deviatoric (shear) stress with the iso-porosity surface (equation 22; Figure 2.2), and subtract the resulting mean effective stress ( $\sigma'_{m,K}$ ) from the mean total stress obtained from the geomechanical model to calculate pore pressure:

$$u_{FES} = \sigma_{m,K} - \sigma'_{m,K} \quad (31)$$

MES and FES share the same mean total stress ( $\sigma_{m,K}$ ), but have a different mean effective stress ( $\sigma'_{m,K_0}$  vs.  $\sigma'_{m,K}$ ). Both the total and effective stresses are different in VES.

## **2.4 APPLICATION OF VES, MES, AND FES METHODS**

### **2.4.1 Data and Methods**

We apply the VES, MES, and FES approaches to predict pore pressure around the salt body at the Mad Dog Field (Figure 2.3). We use a combination of seismic, well log, and pressure data to characterize the stresses and predict pressure. The data include Modular Dynamics Tester (MDT) pore pressure measurements, gamma ray, resistivity, sonic velocities acquired during logging-while-drilling (LWD), and mean total and deviatoric (shear) stresses acquired from a series of static 2-D plane-strain drained geomechanical models (Figure 2.3C). Discovery well 826-1 (Figure 2.3B) outboard the Mad Dog salt body is used to develop a predictive relationship. We evaluate our prediction results in wells 826-1, 825-1, 826-5, and 782-1 (Figure 2.3B).

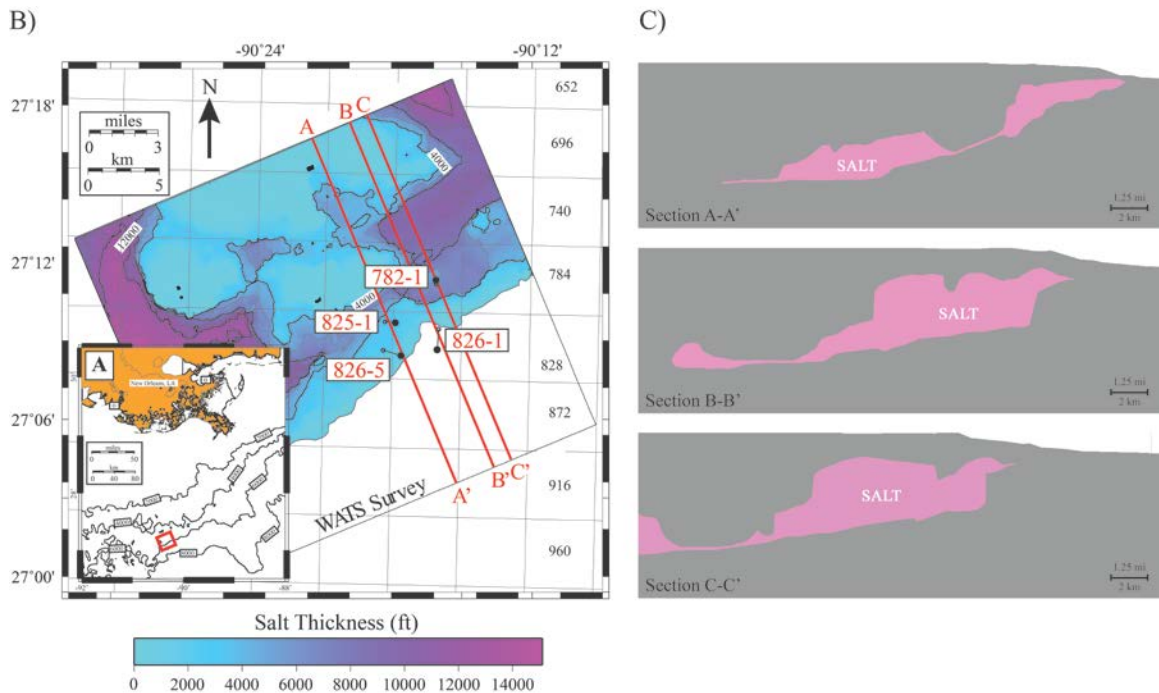


Figure 2.3: Location, salt thickness, and cross-sectional profiles of the Mad Dog Field, Gulf of Mexico. (A) The Mad Dog Field is located approximately 190 mi southwest of New Orleans and extends over the Green Canyon. (B) A large-scale 3D wide-azimuth towed-streamer (WATS) survey is used to define the seafloor bathymetry and salt body (seismic data provided by BP and Partners). Pore pressure is predicted in four wells: 825-1, 826-1, 826-5, and 782-1. The smaller red dots mark the surface well locations, and the large black dots mark the bottom hole locations. (C) Interpreted cross-sections A-A', B-B', and C-C' of the salt body (shown in red on B) are used to build the geomechanical models.

#### 2.4.2 Mad Dog Field

The Mad Dog Field was discovered by BP in 1998. The field is located approximately 190 miles southwest of New Orleans (Figure 2.3A). Water depths range from 4000 feet to 7000 feet (Merrell, 2012). The major producing reservoir at Mad Dog consists of a large north-south trending compressional anticline with early Miocene sands interpreted to be turbidite deposits (Dias et al., 2009). The main structural feature is a large allochthonous salt body, with the top of the salt approximately 3280 feet below the

seafloor. The salt is part of the Sigsbee salt canopy, which comprises the Sigsbee Escarpment.

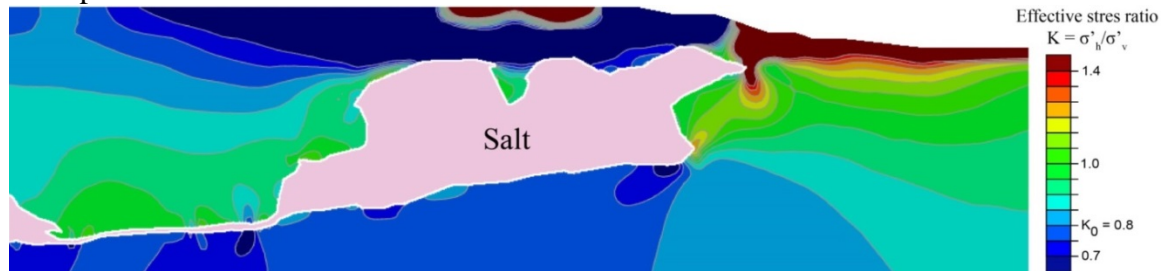


Figure 2.4: Effective stress ratio ( $K$ ) in sediments around Mad Dog salt along section B-B' (Figure 3C). The stress ratio is higher than the uniaxial value,  $K_0=0.8$ :  $K=1$  in the minibasin (isotropic stress state) and  $K>1$  in front of the salt, indicating elevated horizontal stresses (Heidari et al., in press).

### 2.4.3 Geomechanical Model

Because of loading from the Mad Dog salt body, the stress state is not uniaxial; the fraction of horizontal to vertical stress, which is constant in uniaxial basins ( $K_0$ ), changes around the salt body. This leads to either an elevation or a reduction in mean and/or deviatoric (shear) stress around the salt body.

We develop static 2D plane-strain drained geomechanical models (Heidari et al., in press). These static models use the present-day geometry of salt to provide an estimate of the total stresses (mean total stress and deviatoric (shear) stress) around the Mad Dog salt body. The geometry of the salt body is defined using seismic data provided by BP & Partners (Figure 2.3). The salt is modeled as viscoelastic and the sediments as poroelastoplastic material, using MCC (Wood, 1990). Input parameters are calibrated based on experimental work on Gulf of Mexico mudrocks (Casey et al., 2015; Casey and Germaine, 2013, 2014). A summary of the input parameters for the geomechanical models is listed in Table 2.

Symbol	Description	Sediments	Salt	Units
$\phi$	Sediment friction angle	20	-	degrees
$\lambda$	Slope of elasto-plastic (loading) line	0.03	-	-
$\kappa$	Slope of elastic (unloading) line	0.13	-	-
$\rho$	Density	143.6	137.3	lb/ft <sup>3</sup>
$\nu'$	Poisson's ratio for soil in terms of effective stresses	0.46	0.25	-
E	Young's modulus	-	4500	ksi
$\eta$	Viscosity	-	1.45 <sup>12</sup>	ksi

Table 2.2: List of input parameters for the geomechanical models.

#### 2.4.4 Assumptions

In our analyses we make the following assumptions: (1) We assume the material behavior of the mudrocks in the Mad Dog field is described by the MCC model and that the friction angle ( $\phi$ ) of the sediments is constant and equal to 20 degrees. (2) We assume elastic deformation is negligible compared to inelastic deformation ( $\kappa \ll \lambda$ ), thereby replacing equation 21 with equation 22. (3) We assume that velocity is directly related to porosity. (4) We assume plane-strain deformation. (5) We assume the sands measured for pressure at calibration well 826-1 to be in pressure equilibrium with the bounding mudrocks (Flemings et al., 2002; Merrell et al., 2014).

#### 2.4.5 Calibration

We calibrate a predictive relationship between mudrock velocity and the equivalent effective stress using the equation proposed by Heidari et al. (in press):

$$v = v_0 + A_e(\sigma'_e)^{B_e} \quad (32)$$

where  $A_e$  and  $B_e$  are lithology-dependent constants calibrated to existing data at well 826-1. This is based on the assumption that velocity is directly related to porosity (equation

5), and that porosity is a function of the equivalent effective stress (equations 2 and 12). Thus, equation 32 provides the predictive relationship to link measured mudrock velocities to the equivalent effective stress.

To constrain this predictive relationship between mudrock velocity and the equivalent effective stress (equation 32), we first identify the mudrock layers at calibration well 826-1 using a combination of gamma-ray and resistivity logs and record their sonic velocities. We pick the nearest mudrock velocities above and below each sand measured for pressure. We assume the pressure of the bounding mudrocks to be equal to the pressure in the sands. At calibration well 826-1, twenty-nine MDT pressure measurements acquired during drilling were used and tied to corresponding mudrock velocities.

For each MDT pressure measurement location, we acquire the mean total stress and the deviatoric (shear) stress from the geomechanical model. We calculate the mean effective stress ( $\sigma'_m$ ) as the difference between the mean total stress ( $\sigma_m$ ) and the MDT pressure measurement ( $u_{MDT}$ ) (Figure 2.5):

$$\sigma'_m = \sigma_m - u_{MDT} \quad (33)$$

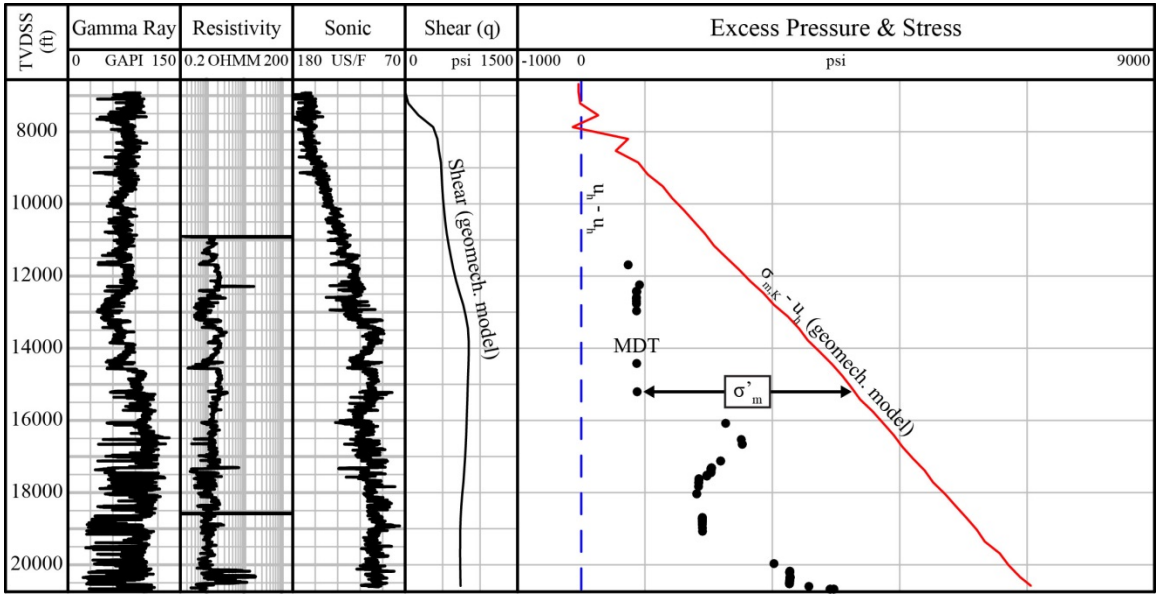


Figure 2.5: Calibration well 826-1. Gamma ray, resistivity and sonic logs acquired while drilling. Shear stress obtained from the geomechanical model. MDT measurements (black dots) and total mean stress,  $\sigma_m$  (less hydrostatic pressure) obtained from the geomechanical model (red line). The mean effective stress ( $\sigma'_m$ ) is calculated as the difference between the mean total stress and the MDT pressure measurements.

We reduce each combination of mean effective stress and deviatoric (shear) stress into an equivalent effective stress using equation 22 (Figure 2.6 A, B). This transformation removes the effect of deviatoric (shear) stress while allowing the original level of compaction to be represented by the equivalent effective stress.

Lastly, we apply equation 32 to correlate mudrock velocity to the equivalent effective stress (Figure 2.6C). We obtain an  $A_e$  value of 7.5, a  $B_e$  value of 0.78, and achieve a coefficient of determination ( $R^2$ ) of 0.78 for the line of best fit. This relationship enables iso-porosity curves to be generated from the equivalent effective stress through equation 22 at any location where a velocity measurement is available. Figure 2.6D shows the final iso-porosity curves calibrated to the Mad Dog Field.

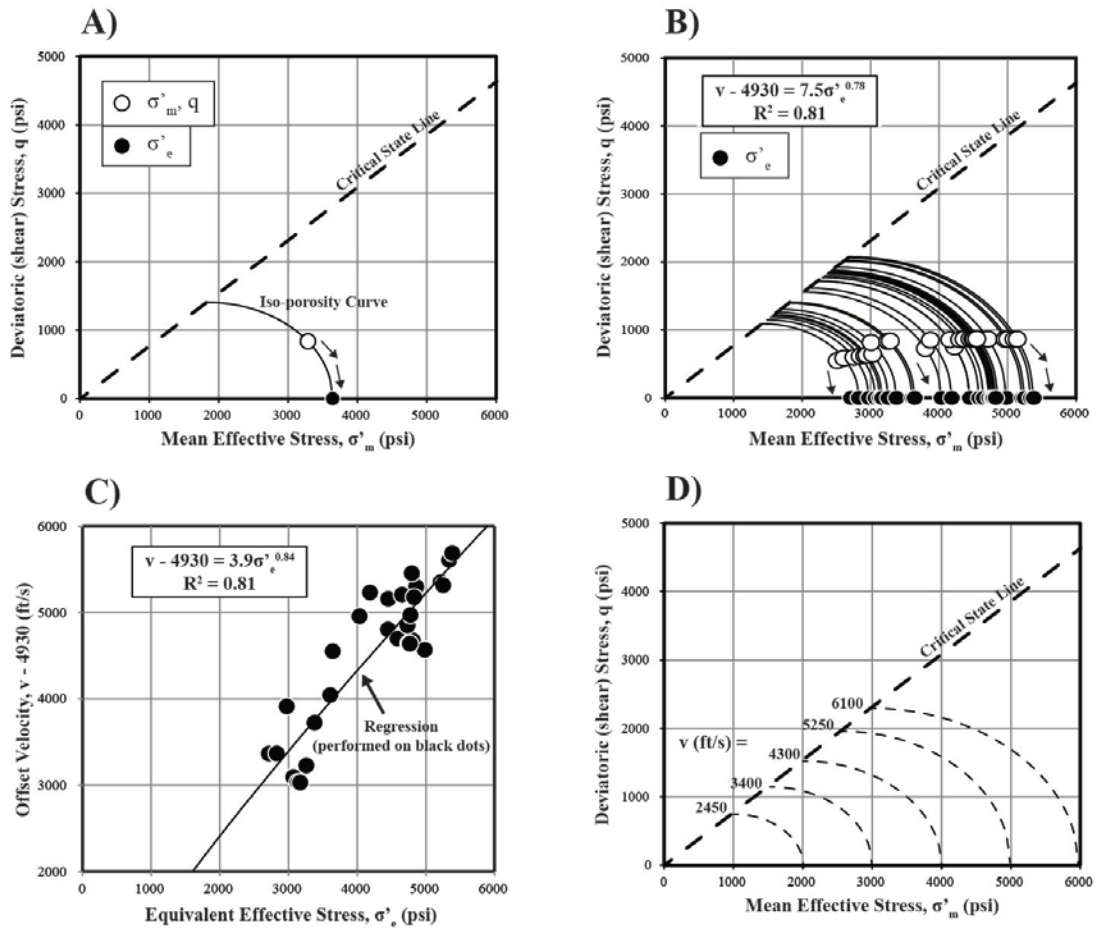


Figure 2.6: Diagram depicting relationship between velocity ( $v$ ), original stress state (open circles), and equivalent effective stress (filled circles) used to develop a predictive relationship. Pressure measurements are acquired at calibration well 826-1. A) The mean effective stress-deviatoric (shear) stress combination (or original stress state, open circle) is transformed into an equivalent effective stress (filled circle) using equation 22 (graphically, the intersection of the iso-porosity curve with x-axis, where  $q = 0$ ). B) The process described in (A) is repeated for the remainder of MDT locations where pressure measurements allowed for the calculation of mean effective stress (Figure 2.5). C) The equivalent effective stress and corresponding velocities are cross-correlated using linear regression analysis. D) Velocity values corresponding to iso-porosity curves in  $\sigma'_m$ : $q$  space; velocity values calculated from the equivalent effective stress using equation 32.

## 2.4.6 Prediction

Having established a predictive relationship for the Mad Dog Field, we next demonstrate how to predict pore pressure using the VES, MES, and FES methods. We focus on predicting pressure along wells where wireline sonic velocity data is available. We first determine the velocities of the mudrock intervals along each well that will be used to predict pressure. We manually pick the wireline sonic velocities every 30-40 ft using gamma ray and resistivity logs to locate the mudrocks. Once the velocities are picked, we apply a smoothing average of 11 samples to reduce any noise or small changes in lithology. The smoothed sonic velocities are then used to calculate the equivalent effective stress for each point (equation 32; Figure 2.7A). Based on the equivalent effective stresses, the iso-porosity surfaces are constructed (equation 22; Figure 2.7B); the iso-porosity surfaces provide the framework to predict pore pressure for the VES, MES, and FES methods.

To apply the VES workflow, we first calculate the mean effective stress under uniaxial strain from the equivalent stress, using equation 27. The slope  $\eta_{K_0}$  is found as a function of the friction angle (equation 17;  $\phi=20$  deg.). This resulting mean effective stress is illustrated in Figure 2.7C as the intersection of the iso-porosity curve with the uniaxial compression line ( $\eta_{K_0}$ ). We obtain the vertical total stress from equation 26; we assume the seawater density to be constant ( $1.023\text{g/cm}^3$ ) and acquire the sediment densities from the wireline bulk density log. We apply equation 28 to calculate the mean total stress with the  $K_0$  ratio acquired from equation 18, and use equation 29 to calculate the VES pore pressure ( $u_{\text{VES}}$ ).

To apply the MES workflow, we use the uniaxial compression line ( $\eta_{K_0}$ ; equation 17) to obtain the mean effective stress under uniaxial strain (as in the VES method, Figure 2.7C). Both the VES and MES approaches assume that the unique relationship

between mean effective stress and velocity is established under uniaxial conditions; therefore, they share the same mean effective stress. The mean total stress is acquired from the geomechanical model ( $\sigma_{m,K}$ ), and MES pore pressure ( $u_{MES}$ ) is calculated from equation 30.

To apply the FES workflow, we use the geomechanical model to estimate the deviatoric (shear) stress and the mean total stress. The mean effective stress ( $\sigma'_{m,K}$ ) is calculated through equation 22 coupled with the deviatoric (shear) stress. This is illustrated in Figure 2.7C as the intersection of the iso-porosity curve with the deviatoric (shear) stress acquired from the geomechanical model ( $q_{GM}$ ). The MES and FES methods share the same mean total stress ( $\sigma_{m,K}$ ). FES pore pressure ( $u_{FES}$ ) is calculated from equation 31.

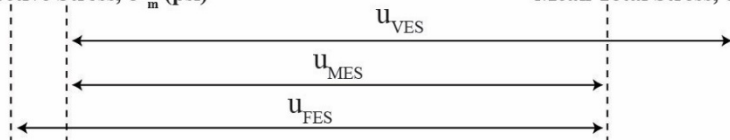
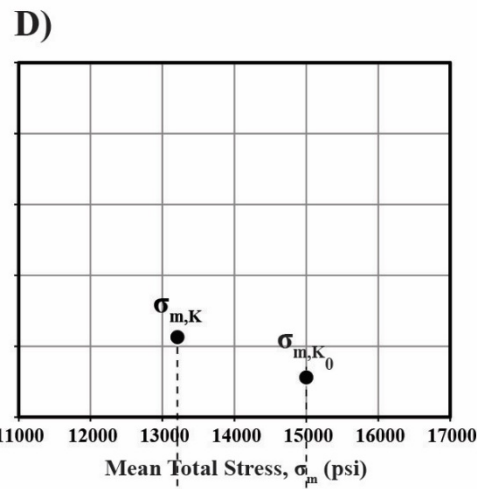
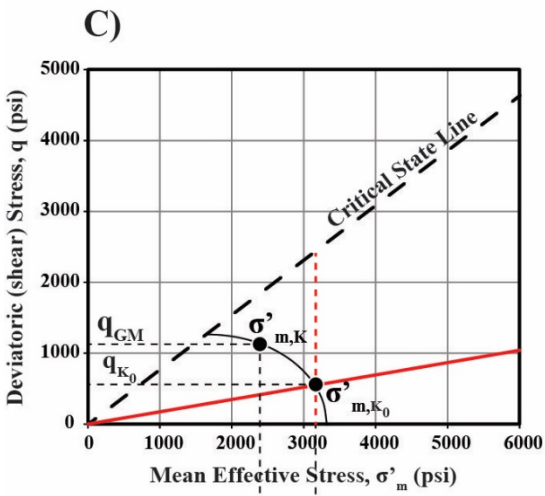
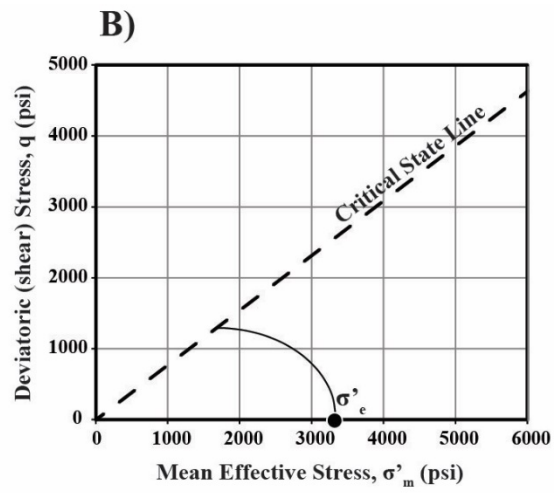
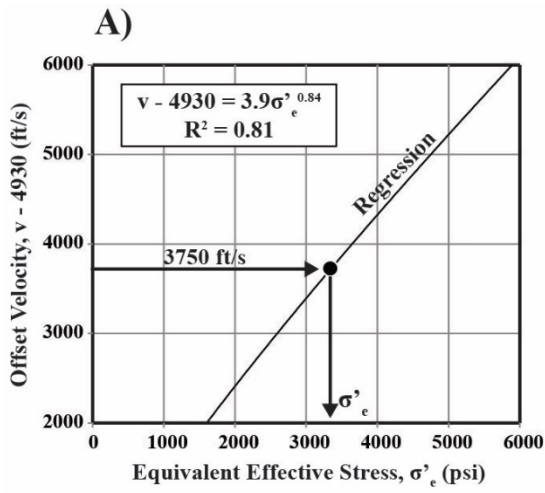


Figure 2.7: Example VES, MES, and FES pore pressures prediction from a single velocity measurement. A) The equivalent effective stress ( $\sigma'_e$ ) is determined from the measured velocity using equation 32. B) An iso-porosity curve is generated from  $\sigma'_e$  (equation 22). C) VES and MES methods: mean effective stress ( $\sigma'_{m,K_0}$ ) is obtained from intersection of iso-porosity curve and uniaxial compression line ( $\eta_{K_0}$ ; equation 17); FES method: mean effective stress ( $\sigma'_{m,K}$ ) is obtained from intersection of iso-porosity curve with deviatoric (shear) stress ( $q_{GM}$ ) obtained from geomechanical model. D) Mean total stress under uniaxial strain ( $\sigma_{m,K_0}$ ) for VES derived from vertical total stress and  $K_0$  (equation 28); Mean total stress ( $\sigma_{m,K}$ ) for MES and FES obtained from geomechanical model. Pore pressure is calculated as difference between mean total stress and mean effective stress (VES: equation 29; MES: equation 30; FES: equation 31).

## 2.5 RESULTS

We compare the predicted pore pressures from the VES, MES, and FES methods against those measured during drilling (MDT) at four wells in the Mad Dog Field. Three of the four wells we analyze penetrate the salt body. We quantify the increment of pore pressure due to non- $K_0$  mean total stress and deviatoric (shear) stress, and report the resulting pore pressures in excess pressure,  $u_e$  (pore pressure less the hydrostatic pressure).

The increment of pore pressure due to non- $K_0$  stress represents the amount of pore pressure induced by mean total stress and deviatoric (shear) stress that are different than those proportional to  $K_0$  (Figure 2.8). We calculate the increment of pore pressure due to non- $K_0$  mean total stress as the difference between the non-uniaxial mean total stress ( $\sigma_{m,K}$ ; obtained from geomechanical model) and the uniaxial mean total stress ( $\sigma_{m,K_0}$ ; equation 28):

$$\Delta u_{\sigma_m} = \sigma_{m,K} - \sigma_{m,K_0} \quad (34)$$

Similarly, we calculate the increment of pore pressure due to non- $K_0$  deviatoric (shear) stress as the difference between the uniaxial mean effective stress ( $\sigma'_{m,K_0}$ ; equation 27) and the non-uniaxial mean effective stress ( $\sigma'_{m,K}$ ; obtained from geomechanical model):

$$\Delta u_q = \sigma'_{m,K_0} - \sigma'_{m,K} \quad (35)$$

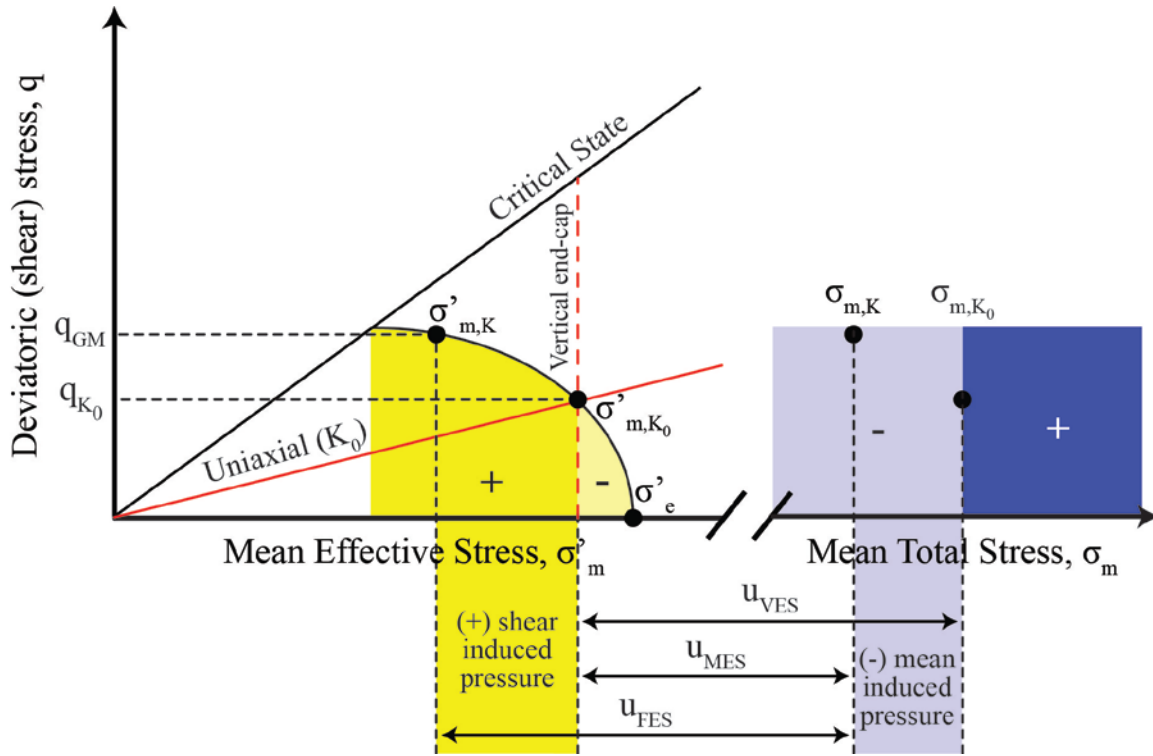


Figure 2.8: Schematic showing how to quantify the increment of pore pressure due to non- $K_0$  mean total stress and deviatoric (shear) stress. In this example, increment of pore pressure due to non- $K_0$  mean total stress is negative, and deviatoric (shear) stress is positive.

# Pressure Prediction along Calibration Well 826-1

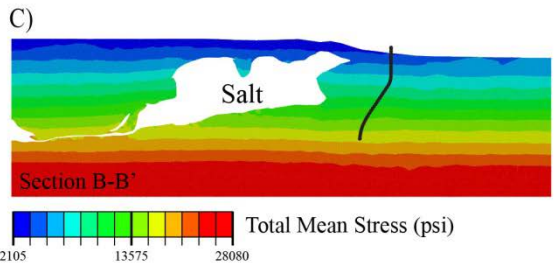
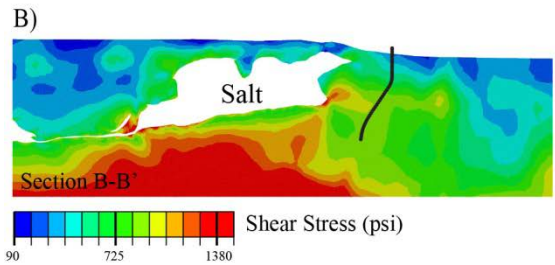
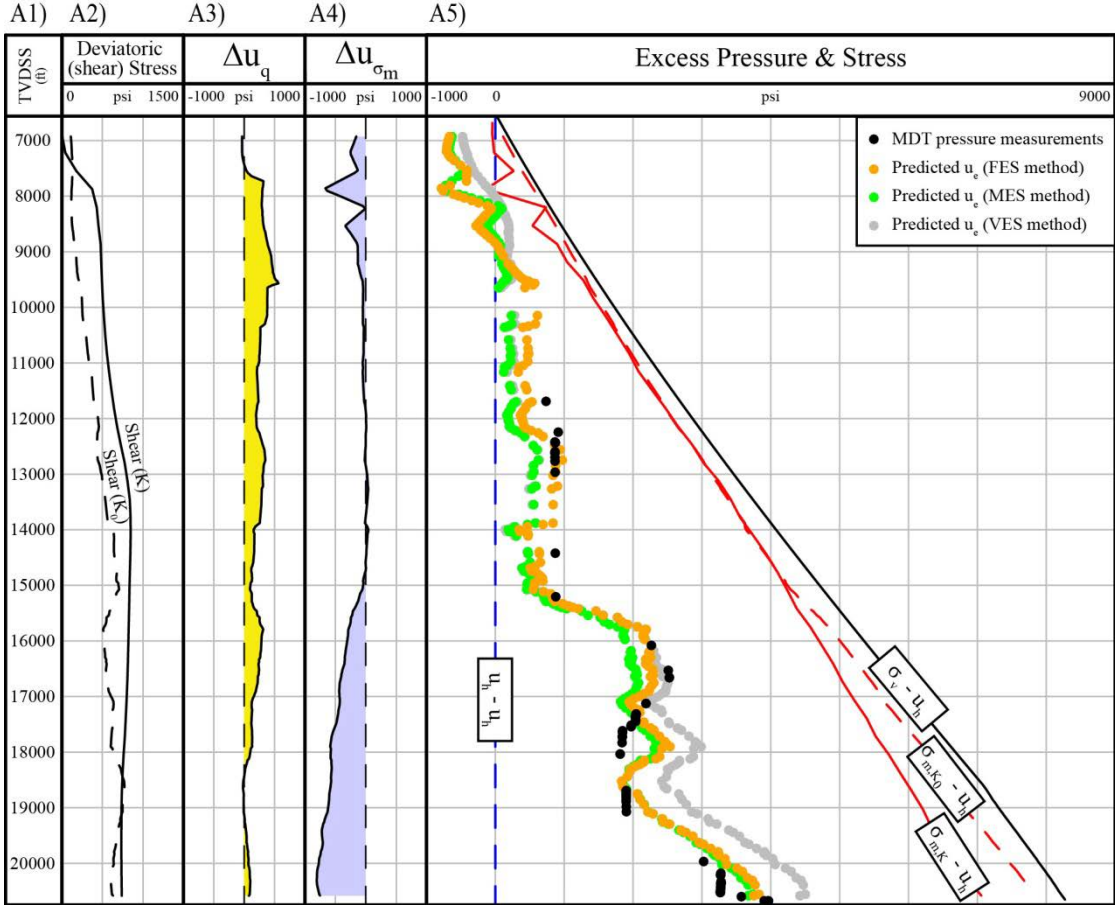


Figure 2.9: Calibration well 826-1. A1) True vertical depth subsea (TVDSS). A2) Deviatoric (shear) stress from geomechanical model (Shear (K)) and proportional to  $K_0$  (Shear ( $K_0$ )). A3) Increment of pore pressure due to geomechanical deviatoric (shear) stress greater than  $K_0$  deviatoric stress (positive  $\Delta u_q$ ; dark yellow) or lower than  $K_0$  (negative  $\Delta u_q$ ; light yellow) A4) Increment of pore pressure due to geomechanical mean total stress greater than  $K_0$  (positive  $\Delta u_{\sigma_m}$ ; dark purple) or lower than  $K_0$  (negative  $\Delta u_{\sigma_m}$ ; light purple); A5) Stress and pressure less hydrostatic value,  $u_h$ : vertical total stress ( $\sigma_v$ ; solid black line), mean total stress from geomechanical model ( $\sigma_{m,K}$ ; solid red line), mean total stress proportional to  $K_0$  ( $\sigma_{m,K_0}$ ; dashed red line), MDT pressure measurements (black dots); pore pressures predicted by the FES (orange dots), MES (green dots) and VES approach (gray dots). B) Contours of deviatoric (shear) stresses from geomechanical model along section B-B' (Figure 2.3). C) Contours of mean total stresses from geomechanical model along section B-B' (Figure 2.3).

We first explore the predicted mudrock pore pressures at calibration well 826-1 using the VES, MES, and FES approaches (Figure 2.9). Well 826-1 was drilled in front of the salt body in 6,734 ft of water. Above 9,000 ft TVDSS, all three methods predict pressure near or below the hydrostatic gradient. The negative pressures are the result of a poorly constrained velocity – effective stress relationship in the shallow depths where no MDT measurements were available for calibration purposes.

From 9,500-15,000 ft TVDSS, the VES and MES methods predict nearly equal pressures (gray vs. green dots in Figure 2.9A5). This is because the geomechanical model is indicating the mean total stress is nearly uniaxial ( $K_0$ ) (solid red line vs. dashed red line in Figure 2.9A5); thus, the increment of pore pressure due to non- $K_0$  mean total stress is negligible (Figure 2.9A4). However, the FES method is predicting higher pressures than VES and MES. This is because the geomechanical model is indicating an elevation in deviatoric (shear) stress (solid line vs. dashed line in Figure 2.9A2). Thus, the increment of pore pressure due to non- $K_0$  deviatoric (shear) stress is positive (Figure 2.9A3). This positive increment of pressure drives the FES pore pressure up relative to the VES and MES methods, which are unable to account for the increase in non- $K_0$  deviatoric (shear) stress. On average, the FES method is predicting pressures 235 psi (~0.38 ppg) higher than the MES and VES methods, and is more closely matching the measured (MDT) pressures.

Along the long the interval 15,000-18,000 ft TVDSS, the increment of pore pressure due to non- $K_0$  mean total stress is negative, which is driving the MES and FES pressures down relative to VES, and the increment of pore pressure due to non- $K_0$  deviatoric (shear) stress is positive, which is driving the FES pressure up relative to the VES and MES methods. Accordingly, the FES method predicts pressure considerably below the VES method and slightly higher than the MES method.

From 18,000 ft TVDSS to the bottom of the well, the increment of pore pressure due to non- $K_0$  mean total stress is negative, whereas the increment of pore pressure due to non- $K_0$  deviatoric (shear) stress is minor. Hence, the MES and FES methods predict similar pressures, which are significantly lower than those predicted by the VES method by an average of 650 psi (~0.65 ppg).

For the majority of the well, the FES method predicts pressures that closely match those measured by the MDT tool (black dots in Figure 2.9A5). This is because well 826-1 was used to calibrate a predictive relationship for the FES method, and extrapolated to predict pressures for the VES and MES methods.

# Pressure Prediction along Well 825-1

A1) A2) A3) A4) A5)

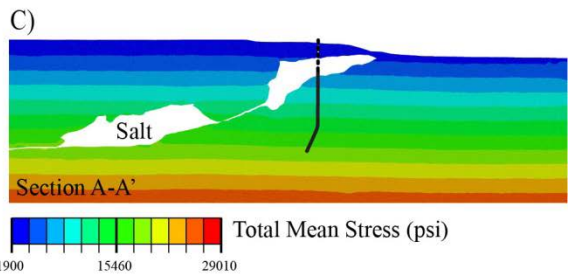
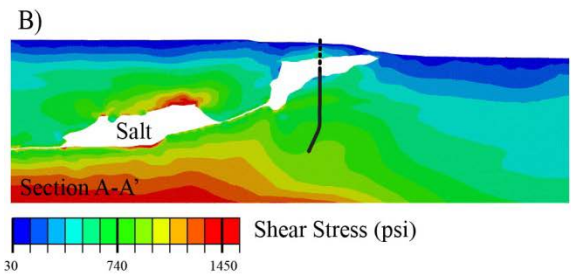
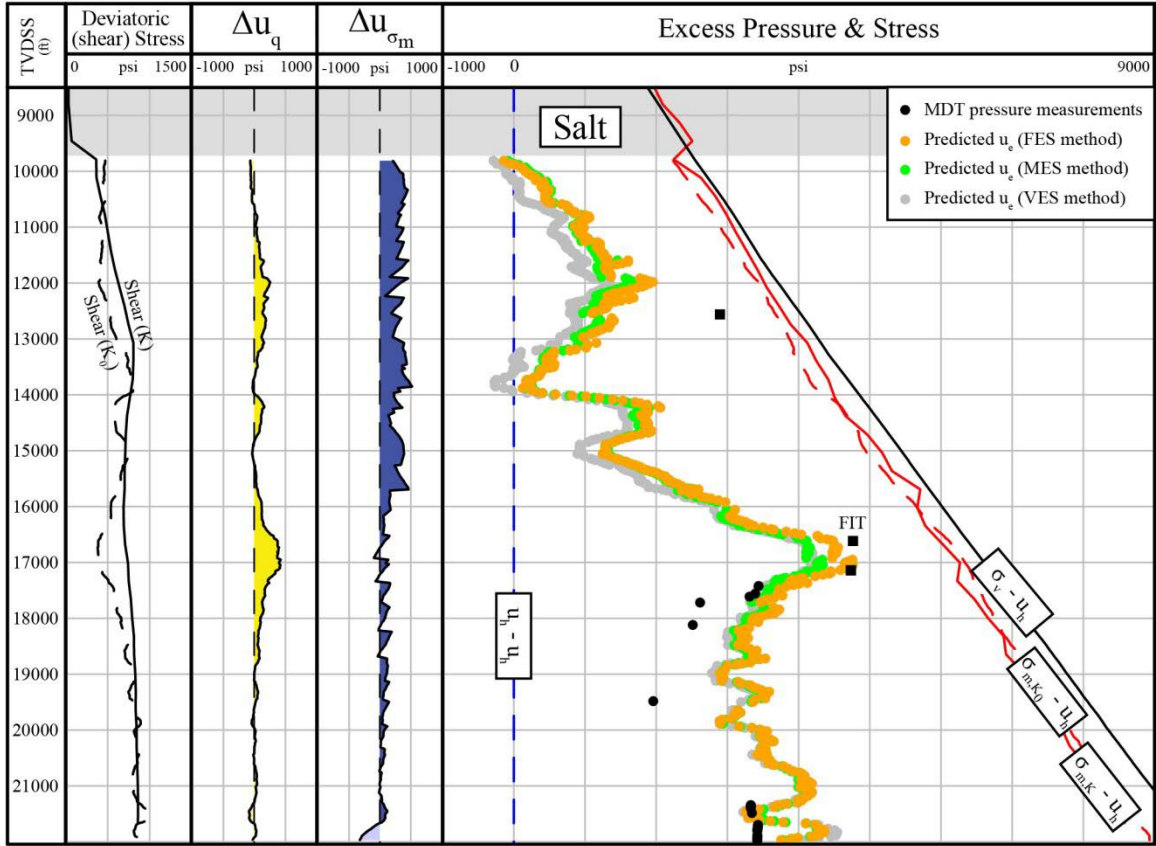


Figure 2.10: Well 825-1 results. A1) True vertical depth subsea (TVDSS). A2) Deviatoric (shear) stress from geomechanical model (Shear (K)) and proportional to  $K_0$  (Shear ( $K_0$ )). A3) Increment of pore pressure due to geomechanical deviatoric (shear) stress greater than  $K_0$  deviatoric stress (positive  $\Delta u_q$ ; dark yellow) or lower than  $K_0$  (negative  $\Delta u_q$ ; light yellow) A4) Increment of pore pressure due to geomechanical mean total stress greater than  $K_0$  (positive  $\Delta u_{\sigma_m}$ ; dark purple) or lower than  $K_0$  (negative  $\Delta u_{\sigma_m}$ ; light purple); A5) Stress and pressure less hydrostatic value,  $u_h$ : vertical total stress ( $\sigma_v$ ; solid black line), mean total stress from geomechanical model ( $\sigma_{m,K}$ ; solid red line), mean total stress proportional to  $K_0$  ( $\sigma_{m,K_0}$ ; dashed red line), MDT pressure measurements (black dots); pore pressures predicted by the FES (orange dots), MES (green dots) and VES approach (gray dots). B) Contours of deviatoric (shear) stresses from geomechanical model along section A-A' (Figure 2.3). C) Contours of mean total stresses from geomechanical model along section A-A' (Figure 2.3).

We next study well 825-1 (Figure 2.10), which was drilled in 5,014 ft of water and penetrates 2,585 ft of salt. The base of the salt is located at a depth of 9,795 ft TVDSS. There is no record of pressure measurements in the upper section below the salt.

For the majority of the well, the geomechanical model is indicating that both the mean total stress (Figure 2.10A5) and the deviatoric (shear) stress (Figure 2.10A2) are elevated relative to  $K_0$ . Thus, the increment of pore pressure due to non- $K_0$  mean total stress (Figure 2.10A4) and non- $K_0$  deviatoric (shear) stress are positive (Figure 2.10A3). As a result, the MES predicts higher pressures than the VES (green vs. gray dots in Figure 2.10A5), and the FES predicts higher pressures than both the VES and MES (orange vs. gray vs. green dots in Figure 2.10A5).

From 16,000-18,000 ft TVDSS, the increment of pore pressure due to non- $K_0$  mean total stress is minor, whereas the increment of pore pressure due to non- $K_0$  deviatoric (shear) stress is positive, reaching a maximum value of nearly 500 psi. This results in FES predicting higher pressures than both the VES and MES methods.

For the remainder of the well, the stress conditions are largely  $K_0$ . Therefore, all three methods predict similar results. However, from 17,000-19,500 ft TVDSS, all three methods predict substantially higher pressures than those measured (black dots in Figure 2.10A5).

# Pressure Prediction along Well 826-5

A1) A2) A3) A4) A5)

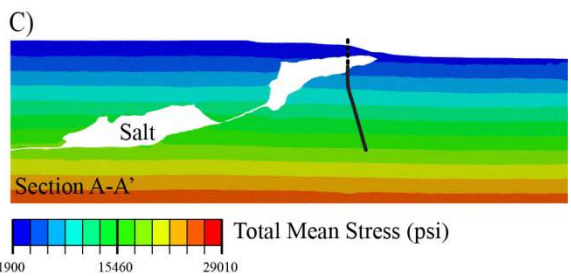
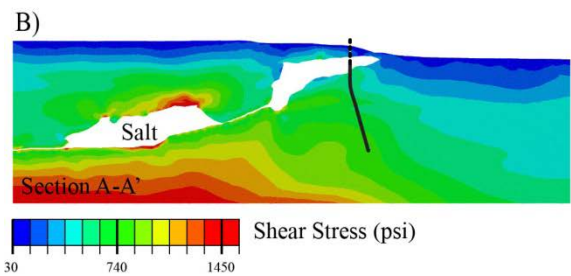
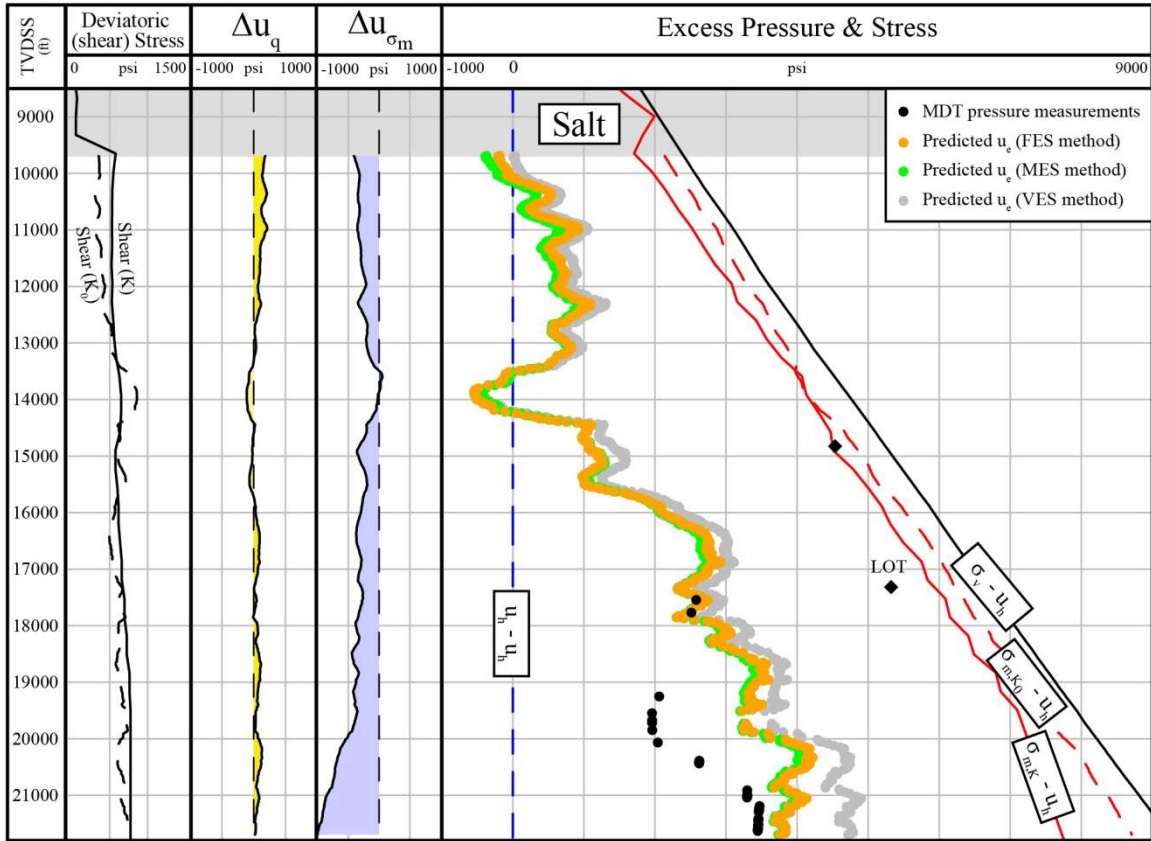


Figure 2.11: Well 826-5 results. A1) True vertical depth subsea (TVDSS). A2) Deviatoric (shear) stress from geomechanical model (Shear (K)) and proportional to  $K_0$  (Shear ( $K_0$ )). A3) Increment of pore pressure due to geomechanical deviatoric (shear) stress greater than  $K_0$  deviatoric stress (positive  $\Delta u_q$ ; dark yellow) or lower than  $K_0$  (negative  $\Delta u_q$ ; light yellow) A4) Increment of pore pressure due to geomechanical mean total stress greater than  $K_0$  (positive  $\Delta u_{\sigma_m}$ ; dark purple) or lower than  $K_0$  (negative  $\Delta u_{\sigma_m}$ ; light purple); A5) Stress and pressure less hydrostatic value,  $u_h$ : vertical total stress ( $\sigma_v$ ; solid black line), mean total stress from geomechanical model ( $\sigma_{m,K}$ ; solid red line), mean total stress proportional to  $K_0$  ( $\sigma_{m,K_0}$ ; dashed red line), MDT pressure measurements (black dots); pore pressures predicted by the FES (orange dots), MES (green dots) and VES approach (gray dots). B) Contours of deviatoric (shear) stresses from geomechanical model along section A-A' (Figure 2.3). C) Contours of mean total stresses from geomechanical model along section A-A' (Figure 2.3).

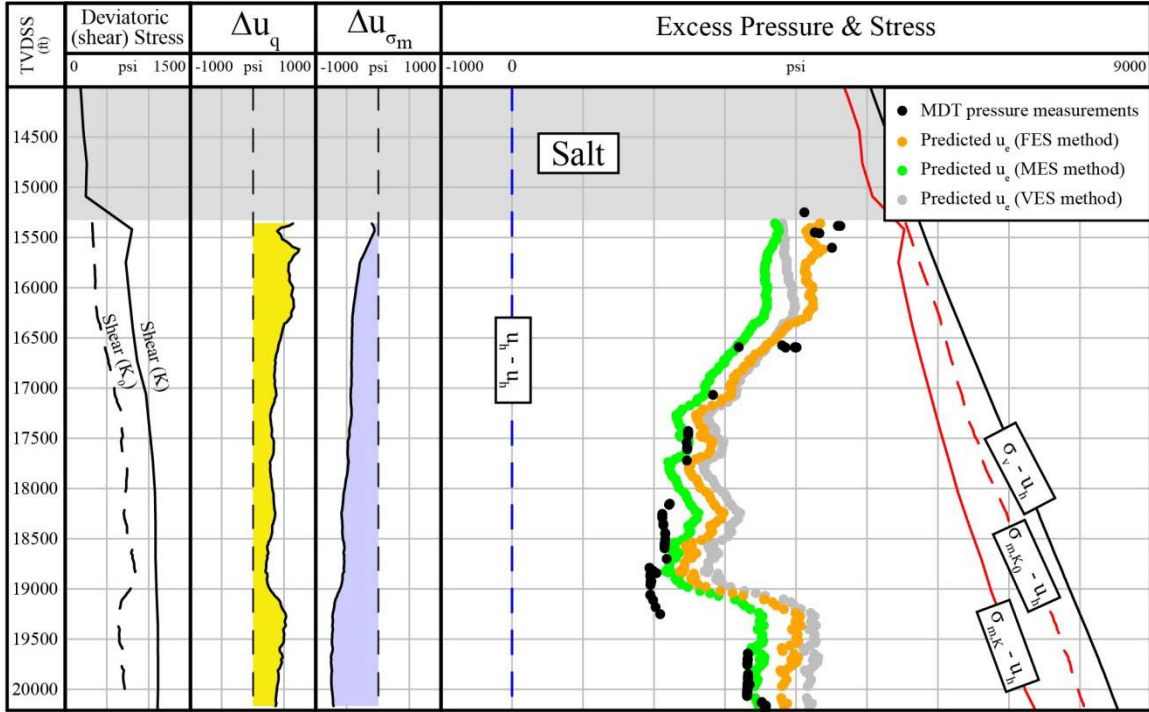
Well 826-5 (Figure 2.11) was drilled in 5,092 ft of water and penetrates 2,711 ft of salt. There are no available pressure measurements for the upper subsalt section.

For the majority of the well both the MES and FES predicted nearly equal pore pressures, which are lower than those predicted by the VES method (green vs. orange vs. gray dots in Figure 2.11A5). This is because the geomechanical model is indicating that the mean total stress is lower than uniaxial ( $K_0$ ) (solid red line vs. dashed red line in Figure 2.11A5), and the deviatoric (shear) stress is similar to uniaxial ( $K_0$ ) (solid line vs. dashed line in Figure 2.11A2). Therefore, the increment of pore pressure due to non- $K_0$  mean total stress is negative (Figure 2.11A4), and the increment of pore pressure due to non- $K_0$  deviatoric (shear) stress is minor (Figure 2.11A3).

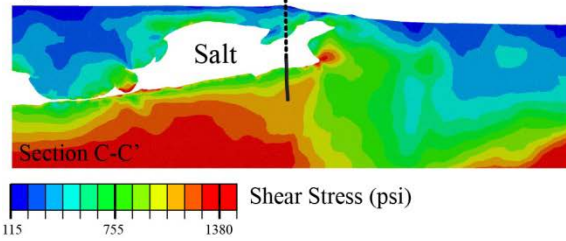
From 17,500-18,000 ft TVDSS, the MES and FES methods predict pressures that match those measured (black dots in Figure 2.11A3). However, for the remainder of the well where MDT pressure measurements are available, all three methods predict pressures significantly higher than those measured.

# Pressure Prediction along Well 782-1

A1) A2) A3) A4) A5)



B)



C)

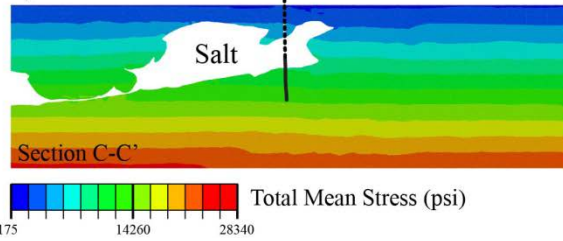


Figure 2.12: Well 782-1 results. A1) True vertical depth subsea (TVDSS). A2) Deviatoric (shear) stress from geomechanical model (Shear (K)) and proportional to  $K_0$  (Shear ( $K_0$ )). A3) Increment of pore pressure due to geomechanical deviatoric (shear) stress greater than  $K_0$  deviatoric stress (positive  $\Delta u_q$ ; dark yellow) or lower than  $K_0$  (negative  $\Delta u_q$ ; light yellow) A4) Increment of pore pressure due to geomechanical mean total stress greater than  $K_0$  (positive  $\Delta u_{\sigma_m}$ ; dark purple) or lower than  $K_0$  (negative  $\Delta u_{\sigma_m}$ ; light purple); A5) Stress and pressure less hydrostatic value,  $u_h$ : vertical total stress ( $\sigma_v$ ; solid black line), mean total stress from geomechanical model ( $\sigma_{m,K}$ ; solid red line), mean total stress proportional to  $K_0$  ( $\sigma_{m,K_0}$ ; dashed red line), MDT pressure measurements (black dots); pore pressures predicted by the FES (orange dots), MES (green dots) and VES approach (gray dots). B) Contours of deviatoric (shear) stresses from geomechanical model along section C-C' (Figure 2.3). C) Contours of mean total stresses from geomechanical model along section C-C' (Figure 2.3).

Lastly, well 782-1 (Figure 2.12) was drilled in 4,423 ft of water and penetrates a salt thickness of 5,000 ft, which is nearly double the thickness of salt any other well penetrates in this study.

For the entirety of the well below the salt, the geomechanical model is indicating that the mean total stress is markedly lower than  $K_0$  (solid red line vs. dashed red line in Figure 2.12A5), whereas the deviatoric (shear) stress is markedly higher than  $K_0$  (solid line vs. dashed line in Figure 2.12A2). Hence, the increment of pore pressure due to non- $K_0$  mean total stress is negative (Figure 2.12A4), and the increment of pore pressure due to non- $K_0$  deviatoric (shear) stress is positive (Figure 2.12A3). These induced pressures created a wide difference in predicted pressures by the VES, MES and FES methods (gray vs. green vs. orange dots in Figure 2.12A3).

Within the first 300 ft directly below the salt, the FES method predicts pressures that match those measured, whereas the VES and MES methods predict pressures that are lower (black dots in Figure 2.12A5). At ~16,600 ft TVDSS, there is one MDT measurement that matches the MES pressure; however, there are three other MDT measurements that the VES and FES methods more closely match. For the remainder of the well, both the VES and FES methods consistently predict pressures higher than those measured, whereas the lower pressures predicted by the MES method are closer to those measured.

## **2.6 DISCUSSION**

The contribution of mean and deviatoric (shear) stress is fundamentally important to the development of overpressure. At the Mad Dog Field, the stress state varies locally; therefore, the mean effective stress and deviatoric (shear) stress are not proportional to  $K_0$ . Our study provides an approach to evaluate the margin of error if the traditional VES or MES approaches are applied through the calculation of non- $K_0$  mean total stress and

deviatoric (shear) stress. The VES method assumes uniaxial stress conditions; therefore, any deviation from the  $K_0$  stress state will be reflected in the increment of pore pressure due to non- $K_0$  mean total stress and deviatoric (shear) stress. The MES method assumes a unique relationship between porosity and mean effective stress that is independent of the deviatoric (shear) stress. Nevertheless, the MES method accounts for any non- $K_0$  loading through the modification of the mean total stress using a geomechanical model; therefore, any deviation from the  $K_0$  stress state will be reflected in the increment of pore pressure due to non- $K_0$  deviatoric (shear) stress.

The non- $K_0$  contribution of mean and deviatoric (shear) stress in the development of pore pressure is best illustrated directly below the salt in well 782-1 (Figure 2.12). The available MDT pressure measurements provide a unique opportunity to compare the predicted pressures against those observed. At the base of the salt, the geomechanical model indicates that the increment of pore pressure due to non- $K_0$  mean total stress is minor (Figure 2.12A4), whereas the deviatoric (shear) stress is significant (Figure 2.12A3). As a result, both the VES and MES underpredict pressure by as much as 1,000 psi; in contrast, pore pressures predicted by the FES method closely match the observed pressures. This is important, because drilling through the base of salt is a hazardous and expensive challenge (Sweatman et al., 1999). In fact, a report in 2006 found that nearly half of the wells in the deepwater Gulf of Mexico have experienced problems exiting the base of salt (Viceer et al., 2006). By capturing the non- $K_0$  increase in deviatoric (shear) stress below salt, the FES method improves pore pressure prediction.

The importance of incorporating the effect of deviatoric (shear) stress in pore pressure prediction is illustrated along a “hypothetical” well in front of the Mad Dog salt body (Figure 2.13), where elevated horizontal stresses (Figure 2.4) result in high deviatoric (shear) stress (Figure 2.13B). Along this well, the geomechanical mean total

stress (solid red line in Figure 2.13A5) is lower than the uniaxial one (dashed red line in Figure 2.13A5); however, the geomechanical deviatoric (shear) stress is higher than  $K_0$  (Figure 2.13A3). As a result, the VES method overpredicts pressure by 1.4 ppg compared to the FES method (gray vs. orange dots in Figure 2.13A5). This presents a serious threat to drilling operators who must maintain an appropriate mud weight window to avoid dangerous blowouts or, in this case, prevent fracturing the formation and losing mud (Bruce and Bowers, 2002).

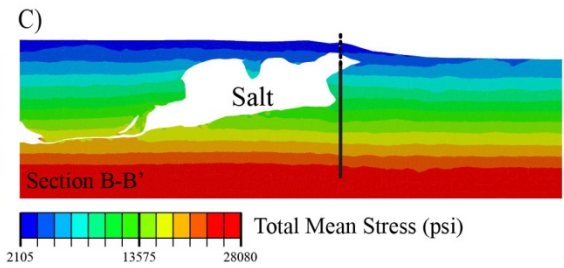
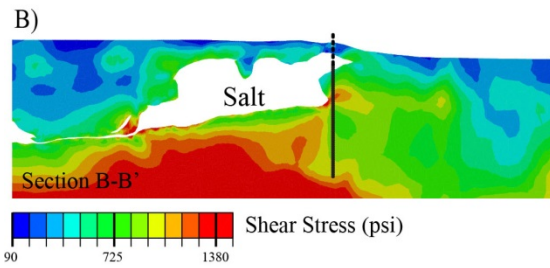
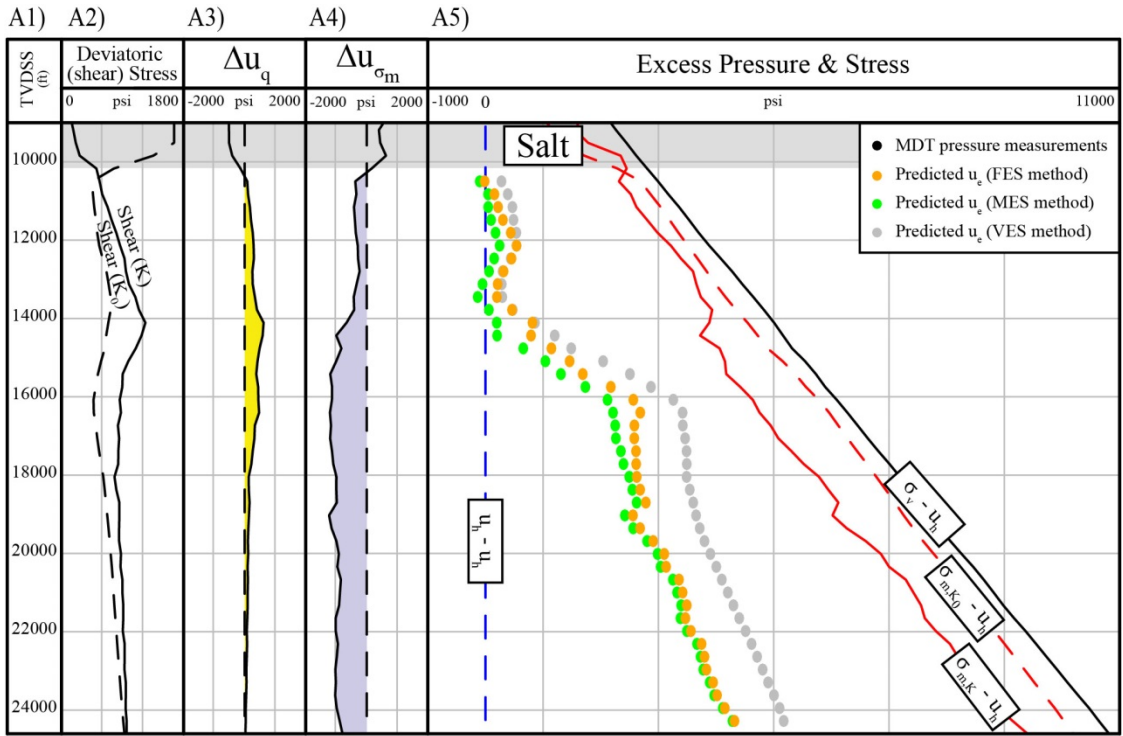


Figure 2.13: Hypothetical well in front of salt body, in area of elevated deviatoric (shear) stress (Figure 2.4). A1) True vertical depth subsea (TVDSS). A2) Deviatoric (shear) stress from geomechanical model (Shear (K)) and proportional to  $K_0$  (Shear ( $K_0$ )). A3) Increment of pore pressure due to geomechanical deviatoric (shear) stress greater than  $K_0$  deviatoric stress (positive  $\Delta u_q$ ; dark yellow) or lower than  $K_0$  (negative  $\Delta u_q$ ; light yellow) A4) Increment of pore pressure due to geomechanical mean total stress greater than  $K_0$  (positive  $\Delta u_{\sigma_m}$ ; dark purple) or lower than  $K_0$  (negative  $\Delta u_{\sigma_m}$ ; light purple); A5) Stress and pressure less hydrostatic value,  $u_h$ : vertical total stress ( $\sigma_v$ ; solid black line), mean total stress from geomechanical model ( $\sigma_{m,K}$ ; solid red line), mean total stress proportional to  $K_0$  ( $\sigma_{m,K_0}$ ; dashed red line), MDT pressure measurements (black dots); pore pressures predicted by the FES (orange dots), MES (green dots) and VES approach (gray dots). B) Contours of deviatoric (shear) stresses from geomechanical model along section B-B' (Figure 2.3). C) Contours of mean total stresses from geomechanical model along section B-B' (Figure 2.3).

Despite the fact that the FES method accounts for the independent contribution of both mean and deviatoric (shear) stress to pore pressure, there still remain intervals where the predicted pressures do not match those observed. We propose three reasons for these potential discrepancies, which we believe to be most significant: (1) calibration limitations; (2) stress dependency; and (3) centroid effects.

First, the success of the FES pressure prediction method declines in sections that are farther away from the calibration well. Changes in lithology will result in a different relationship between velocity and equivalent effective stress than the one we used (Figure 2.6C). Although we only used well 826-1 for calibration purposes, an alternative would be to incorporate the MDT pressure measurements available at every well to calibrate a more robust relationship between velocity and the equivalent effective stress.

Second, we assume the friction angle throughout our field to be constant. In their study of resedimented Gulf of Mexico mudrock, Casey et al. (2016) document that the friction angle can decrease by a factor of 4 over stresses ranging from 1-10,000 psi. This variation is significant and suggests our results may be more accurate if we were to account for a friction angle that changes with stress. A future approach would be to incorporate a friction angle dependent of the stresses into the MCC to determine its effect on pore pressure prediction.

A third reason for the discrepancy between those measured (MDT) and those predicted could be due to centroid effects. Pore pressure prediction is carried out on mudrocks because they provide consistent indicators of fluid pressures (Athy, 1930; Dutta, 2002), whereas MDT pressure measurements are carried out on sands because of their high permeability. Interpreting differences in predicted mudrock pressures and measured sand pressures is a common challenge in pressure analysis; such differences do not necessarily reflect a deficiency in the pore pressure prediction model.

The pressures within a rotated sand body will follow the hydrostatic gradient, whereas the pressures of the bounding mudrocks will approximately follow the lithostatic pressure gradient (Flemings and Lupa, 2004; Flemings et al., 2002; Stump et al., 1998). Depending on the degree of rotation, the pressures at the peak of a rotated sand body can be significantly greater than the bounding mudrock, and the pressures at the base can be significantly lower (Flemings et al., 2002).

The geologic cross section in Figure 2.14 illustrates the overall structural geometry of the Mad Dog Field. The structure is primarily horizontal far field where the calibration well 826-1 is located. Therefore, we remain confident in our assumption that the pressures measured in the permeable sands are equal to the bounding mudrocks and are appropriate for calibration purposes at this location. Directly below the salt, however, there is indication of structural disturbance. This suggest there may be rotation of the sand bodies in the wells that penetrate the salt (wells 825-1, 826-5, and 782-1), and may provide a reasonable defense for the pressures differences due to centroid effects.

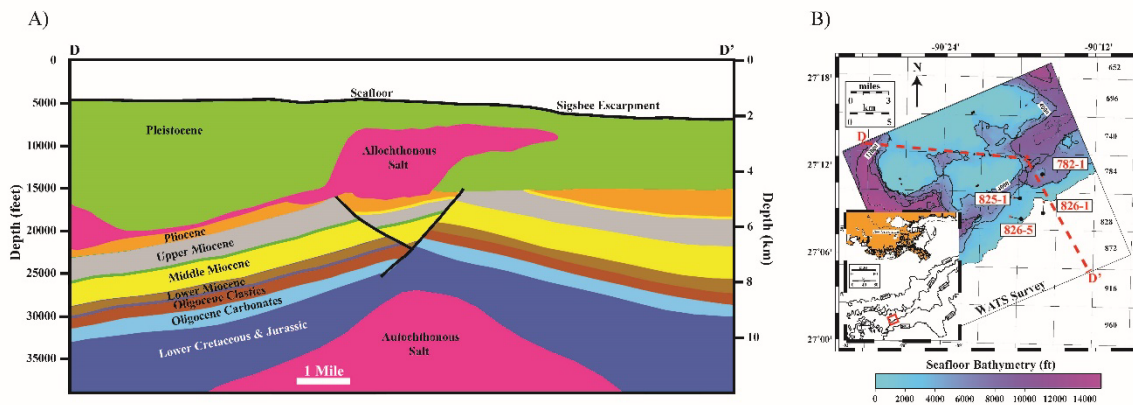


Figure 2.14: Geologic cross section of Mad Dog Field. Figure modified from Merrell et al. (2014).

## 2.7 CONCLUSIONS

We present an improved (FES) method to predict pore pressure in complex stress settings and analyze our results against the VES and MES methods at the Mad Dog Field.

We show the following:

1. Compaction and, therefore, pore pressure is driven by a combination of mean and deviatoric (shear) stresses.
2. Geomechanical modeling coupled with velocities improves prediction of pore pressures.
3. The FES method accounts for any stress state and significantly improves upon the traditional VES method, which is limited to uniaxial stress states, and the MES method, which neglects to account for local variations of deviatoric (shear) stress. A workflow that can account for any stress state is especially important directly below and to the sides of salt where the majority of drilling problems occur, because the variations in deviatoric (shear) stress and mean total stress result in a stress state considerably different than the stress conditions at far-field calibration wells.
4. At the Mad Dog wells we studied, the increment of pore pressure due to non- $K_0$  total mean stress can reach up to 1.5 ppg (Figure 2.13A4). Similarly, the increment of pore pressure due to non- $K_0$  deviatoric (shear) stress can reach up to 1 ppg (Figure 2.12A3)

## Chapter 3: UT-FAST-P<sup>3</sup> GeoFluids Software

### ABSTRACT

I have developed the University of Texas Full Application of Stress Tensor to Predict Pore Pressure (UT-FAST-P<sup>3</sup>) software as learning tool to illustrate how pore pressure and stress interact in non-uniaxial settings. I present pore pressure prediction concepts based on the vertical effective stress (VES) method, the mean effective stress (MES) method, and the full stress tensor (FES) method. I employ the Modified Cam Clay model to link volumetric deformation to mean and deviatoric (shear) stress. I designed the program to be calibrated from a (i) power-law relationship between velocity and vertical effective stress under uniaxial strain conditions and (ii) a frictional strength value; stress conditions are changed through the effective stress ratio when predicting pore pressure. I communicate the results in a velocity vs. mean effective stress plot and a mean stress vs. deviatoric (shear) stress plot. Overall, I built the program to explicitly show how various stress states can correspond to a single measured velocity, and to provide insight into the contribution of mean and deviatoric (shear) stress to compression and pore pressure development.

### 3.1 INTRODUCTION

The University of Texas Full Application of Stress Tensor to Predict Pore Pressure (UT-FAST-P<sup>3</sup>) is a MATLAB-based pore pressure prediction software. The software calculates pore pressure from velocity using the vertical effective stress (VES) approach, the mean effective stress (MES) approach, and the full stress tensor (FES) approach, and allows for a side-by-side comparison of each method. The software outputs:

- Compaction curves in velocity vs. mean effective space for difference stress states (isotropic, critical state, uniaxial ( $K_0$ ), and any stress ratio,  $K$ )

- Mean total and effective stresses
- Pore pressures
- Variation of pore pressures as a function of effective stress ratio (ranging from extensional failure to compressional failure)

The user calibrates the software with i) a power-law relationship between velocity and vertical effective stress (Bowers, 1995) under uniaxial strain conditions, and ii) a frictional strength value ( $\phi$ ). The user then enters a measured velocity and overburden value, as well as an effective stress ratio (K) at the target location to predict pore pressure. The program is designed to allow users to explore the influence of mean and deviatoric (shear) stress on predicted pore pressure for the three approaches by changing the effective stress ratio at the target location. The program illustrates how various stress states can correspond to a single measured velocity, and allows the user to examine the relative contributions of mean and deviatoric (shear) stresses to pore pressure for a range of effective stress ratios (K).

In this chapter I first present the assumptions, the material model, and the equations to predict pore pressure; I then present three simulations to demonstrate how the three methods predict different pressures based on a single velocity when stress conditions are varied; I conclude by discussing the differences between the three methods.

### **3.2 MATERIAL MODEL SET-UP AND ASSUMPTIONS**

1. I assume the vertical stress is principal, and the two horizontal stresses are equal ( $\sigma'_H = \sigma'_h$ ; triaxial conditions).
2. I assume the friction angle is constant (model input value).
3. I assume the material stress-strain behavior is described by the Modified Cam Clay (MCC) model (Wood, 1990). This is a model from the family of critical state

soil mechanics that accounts for the contribution of both mean and deviatoric (shear) stress to compression and pore pressure generation. Under triaxial conditions, the mean effective stress ( $\sigma'_m$ ) is defined as:

$$\sigma'_m = \frac{\sigma'_v + 2\sigma'_h}{3} \quad (1)$$

and the deviatoric (shear) stress (q) as:

$$q = \sigma'_v - \sigma'_h \quad (2)$$

The MCC model describes the material stress-strain behavior of each stress state in void ratio vs. mean effective stress ( $e:\sigma'_m$ ) space and mean effective stress vs. deviatoric (shear) stress ( $\sigma'_m:q$ ) space. The isotropic stress state represents a loading condition where all principal stress components are equal and, consequently, the deviatoric (shear) stress (equation 2) is zero. The critical stress state defines the limiting strength of a material; a material subjected to stresses at critical state will experience failure. The uniaxial stress state represents a loading condition where deformation is vertical (zero lateral strain) and the ratio of horizontal to vertical effective stress ( $K_0$ ) is constant:

$$K_0 = \frac{\sigma'_h}{\sigma'_v} \quad (3)$$

( $K_0$  is assumed to be less than 1). Any other stress state is defined by the ratio of horizontal to vertical effective stress (K):

$$K = \frac{\sigma'_h}{\sigma'_v} \quad (4)$$

In  $e:\sigma'_m$  space (Figure 3.B), a given stress state with constant stress ratio (K) corresponds to a unique compression curve described by:

$$e = \frac{n}{1-n} = e_\lambda - \lambda \ln(\sigma'_m) \quad (5)$$

where n is porosity, e is the void ratio,  $e_\lambda$  is the intercept at unit mean effective stress, and  $\lambda$  is the slope. The parameter  $e_\lambda$  depends on the stress state (stress

ratio,  $K$ ). The void ratio is a measurement of the pore volume, and is related to porosity. The general equation for the unloading (elastic) path is given by:

$$e = \frac{n}{1-n} = e_{\kappa} - \kappa \ln(\sigma'_m) \quad (6)$$

where  $e_{\kappa}$  is the intercept at unit mean effective stress, and  $\kappa$  is the slope. The loading and unloading paths are linear in  $e:\ln(\sigma'_m)$  space, and curved in  $e:\sigma'_m$  space (Figure 3.B).

In  $\sigma'_m:q$  space (Figure 3.A), compression with a constant stress ratio (equation 4) is represented with a line, the slope of which is defined by the ratio of deviatoric (shear) stress to mean effective stress:

$$\eta = \frac{q}{\sigma'_m} \quad (7)$$

For the isotropic stress state,  $\eta=0$ . For the critical stress state,  $\eta=M$ ; the slope  $M$  is a function of the friction angle ( $\phi$ ): above the x axis ( $K<1$ ),  $M=M_{Ext.}$ :

$$M_{Ext.} = \frac{6\sin\phi}{3-\sin\phi} \quad (8)$$

Below the x axis ( $K>1$ ),  $M=M_{Comp.}$ :

$$M_{Comp.} = -\frac{6\sin\phi}{3+\sin\phi} \quad (9)$$

For the uniaxial stress state,  $\eta=\eta_{K_0}$ ; according to the MCC model,  $\eta_{K_0}$  is expressed as:

$$\frac{\eta_{K_0}(1+v')(1-\Lambda)}{3(1-2v')} + \frac{3\eta_{K_0}\Lambda}{M_{Ext.}^2 - \eta_{K_0}^2} = 1 \quad (10)$$

where  $v'$  is Poisson's ratio for soil in terms of effective stresses, and  $\Lambda=(\lambda-\kappa)/\lambda$ .

For any other stress state,  $\eta=\eta_K$ ; the slope  $\eta_K$  is a function of the effective stress ratio ( $K$ ; equation 4):

$$\eta_K = \frac{3(1-K)}{1+2K} \quad (11)$$

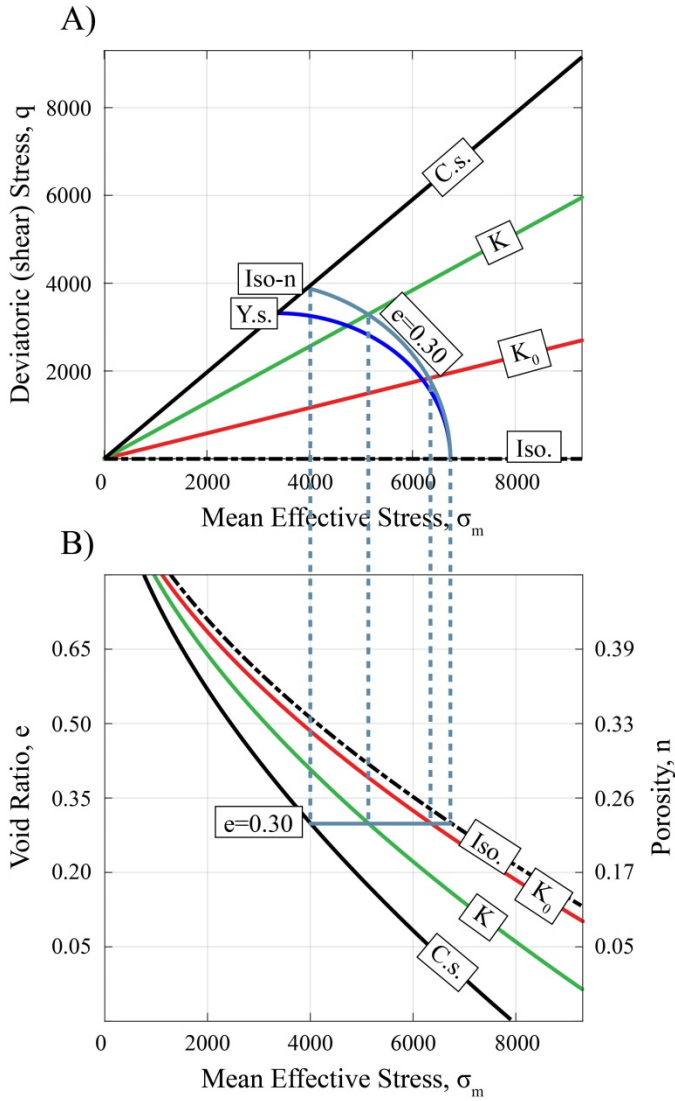


Figure 3.1: Volumetric responses of a material for various stress state: isotropic (Iso.), critical state (C.s.), uniaxial ( $K_0$ ), and arbitrary (K). A) In mean effective stress vs. deviatoric (shear) stress ( $\sigma'_m:q$ ) space, yield surface (Y.s.; dashed blue) describes elasto-plastic behavior of material. Iso-porosity surface (iso-n; solid blue) captures relationship between mean effective stress and deviatoric (shear) stress for given porosity. B) In mean effective stress vs. void ratio ( $\sigma'_m:e$ ) space, compression curves capture relationship between porosity and mean effective stress for different stress states.

In  $\sigma'_m:q$  space, the yield surface (elastoplastic behavior) is described as:

$$\frac{\sigma'_m}{\sigma'_e} = \frac{M^2}{M^2 + \eta^2} \quad (12)$$

where  $\sigma'_e$  is the equivalent effective stress (controls the size of the yield surface). The equivalent effective stress represents a uniform stress state (no shear) and is found at the intersection of the yield surface with the isotropic axis (Figure 3.A). Stress states corresponding to the same porosity form an iso-porosity surface (turquoise curve in Figure 3.A) with equation:

$$\frac{\sigma'_m}{\sigma'_e} = \left( \frac{M^2}{M^2 + \eta^2} \right)^{\frac{\lambda - \kappa}{\lambda}} \quad (13)$$

4. I assume that the elastic deformation is negligible relative to the plastic deformation (i.e.,  $\kappa \ll \lambda$ ). As a result, equation 10 simplifies to:

$$\eta_{K_0} = \frac{-3 + \sqrt{9 + 4 \left( \frac{6 \sin \phi}{3 - \sin \phi} \right)^2}}{2} \quad (14)$$

equation 3 becomes a function of the friction angle:

$$K_0 = \frac{\sigma'_h}{\sigma'_v} = \frac{3 - \eta_{K_0}}{3 + 2\eta_{K_0}} \quad (15)$$

and equation 13 simplifies to:

$$\frac{\sigma'_m}{\sigma'_e} = \frac{M^2}{M^2 + \eta^2} \quad (16)$$

The iso-porosity surface provided by equation 16 plots as an elliptical curve and coincides with the yield surface (red curve in Figure 3.A). The critical state line (M) intersects the iso-porosity curve at the crest of the ellipse (the point where the maximum value of deviatoric (shear) stress is attained).

5. I assume a power-law relationship between velocity and vertical effective stress under uniaxial strain (Bowers, 1995):

$$v = v_0 + A \sigma'_v{}^B \quad (17)$$

where  $v_0$  is the velocity of seawater, and A and B are fitting parameters ( $v_0$ , A, and B are model input parameters). Because this relationship is assumed to be

established under uniaxial strain, the vertical effective stress can be expressed as a function of the mean effective stress under uniaxial strain ( $\sigma'_{m,K_0}$ ) by combining equation 1 with equation 15:

$$\sigma'_v = \frac{3\sigma'_{m,K_0}}{(1+2K_0)} \quad (18)$$

I then relate velocity to the mean effective stress under uniaxial strain by combining equation 17 with equation 18:

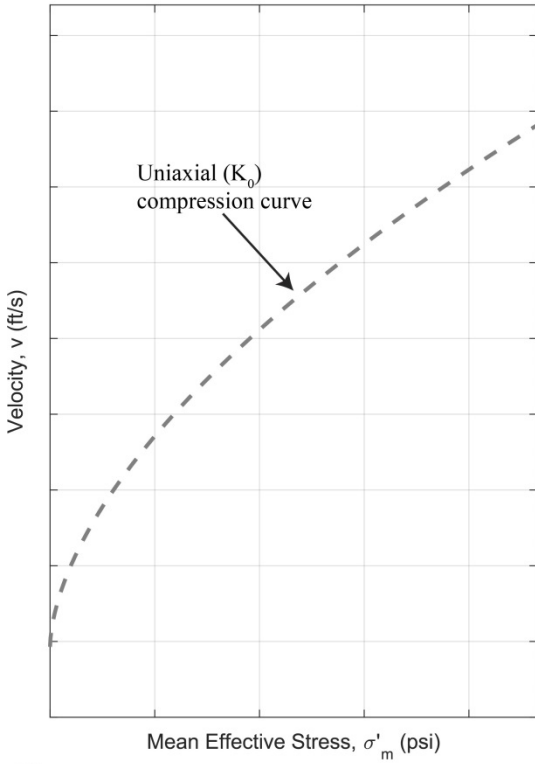
$$v = v_0 + A \left( \frac{3\sigma'_{m,K_0}}{1+2K_0} \right)^B \quad (19)$$

In velocity vs.  $\sigma'_m$  space, this is the uniaxial compression curve (Figure 3.2B).

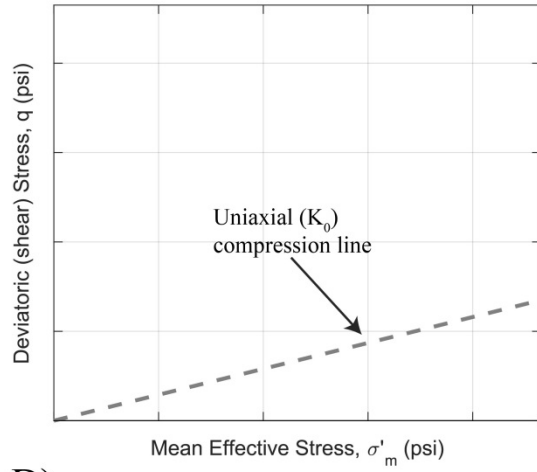
Furthermore, any point along the uniaxial compression line ( $\eta_{K_0}$ ; Figure 3.2B) in  $\sigma'_m$ : $q$  space can be linked to a velocity value through equation 19.

6. I assume a 1:1 relationship between porosity and velocity. This enables iso-porosity surfaces (equation 16) to be linked to a measured velocity value through equation 19. For any given velocity, I anchor the shape of the MCC iso-porosity surface (equation 16) to the mean effective stress along the uniaxial compression line (equation 19). This is illustrated in Figure 3.2C. This iso-porosity surface enables me to link the corresponding velocity to the mean effective stress for the isotropic stress state, critical stress state, and any stress state in between defined by  $K$  (Figure 3.2D).
7. I assume that the vertical total stress (overburden) is known (model input value)

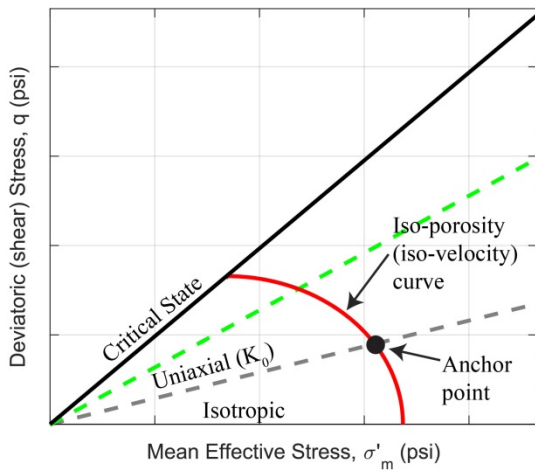
A)



B)



C)



D)

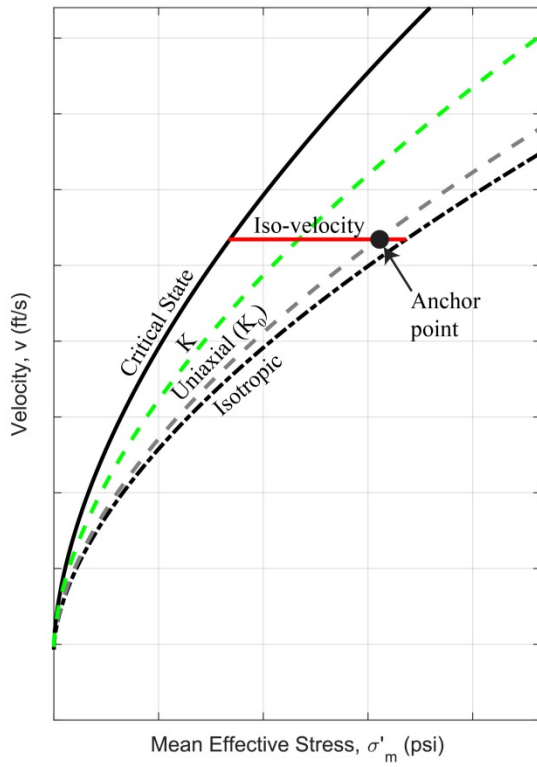


Figure 3.2: Generation of iso-porosity curve. A) The velocity – vertical effective stress relationship (equation 17) is mapped to velocity – mean effective stress assuming uniaxial strain (equation 19). B) Velocity is related to any mean effective stress along the uniaxial compression line C) Shape of iso-porosity surface (equation 13) is anchored to the mean effective stress along the uniaxial ( $K_0$ ) compression line calculated from velocity. D) The iso-porosity (iso-velocity) line is used to relate velocity to mean effective stress for the isotropic stress state, critical stress state and any stress state in between ( $K$ ).

### **3.3 DISPLAY OF RESULTS IN MEAN EFFECTIVE STRESS – DEVIATORIC (SHEAR) STRESS SPACE**

I define deformation in terms of geological conditions: an effective stress ratio ( $K$ ; equation 4) less than 1 represents extensional loading; a  $K$  ratio equal to 1 represents isotropic (uniform) loading;  $K$  greater than 1 represents compressional loading.  $K$  increases non-linearly from extensional failure to compressional failure. This is illustrated in Figure 3.3 by the colored contours and the loading cartoons. The warmer colored contours represent  $K$  ratios with higher levels of deviatoric (shear) stress; the cooler colored contours represent  $K$  ratios with lower levels of deviatoric (shear) stress. The loading cartoons represent the different stress states. From extensional failure (top) to compressional failure, the vertical stress is held constant while the horizontal stresses are increased.

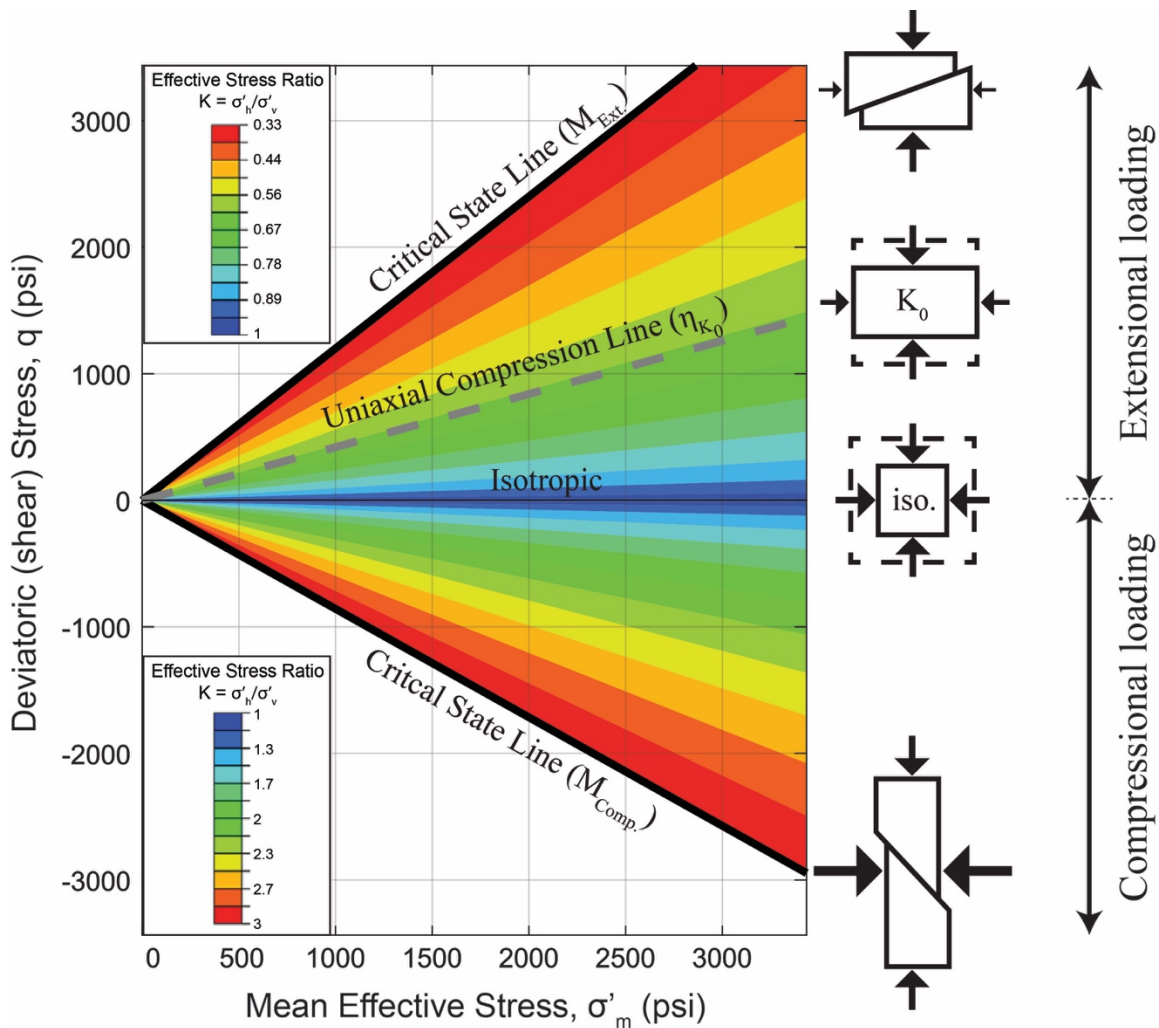


Figure 3.3: Radial compression curves corresponding to effective stress ratio ( $K$ ) varying from extensional to compressional failure. The region above the x-axis represents extensional loading in terms of geological conditions; the region below the y-axis represents compressional loading in terms of geological conditions. In this example,  $\phi=30$  deg. The slope of  $M$  in the extensional region is defined by equation 8; the slope of  $M$  in the compressional region is defined by equation 9. The loading cartoons illustrate the effective stress ratio from extensional failure (top), to uniaxial compression ( $K_0$ ), to isostatic compression (iso.), to compressional failure (bottom). For each of the stress states, the vertical stress is held constant while the horizontal stress is changed.

### 3.4 LIST OF INPUTS

The following list contains the inputs to calibrate the material model and predict pore pressure (Figure 3.4).

- Velocity model fitting parameter (A)
- Velocity model fitting parameter (B)
- Water velocity ( $v_0$ )
- Friction angle ( $\phi$ )
- Expected effective stress ratio ( $K_{exp.}$ )
- Minimum effective stress ratio ( $K_{min.}$ )
- Maximum effective stress ratio ( $K_{max.}$ )
- Velocity ( $v$ )
- Vertical total stress or overburden ( $\sigma_v$ )
- True vertical depth (TVD; for plotting purposes)

**Equation 1:  $v = v_0 + A(\sigma'_v)^B$**   
 (Velocity model under uniaxial  $K_0$  strain)  
*\*Mouse over parameter names below for description*

A

B

Water velocity,  $v_0$   ft/s

Friction angle,  $\Phi$   °

( $K_0 =$  $; \eta_{K_0} =$  $; \eta_{csl}$  $)$

Effective stress ratio, K  
 (Expected) (Min.) (Max.)

K

( $\eta_K =$  $)$

Velocity,  $v$   ft/s

Total vertical stress,  $\sigma_v$   psi

True vertical depth, TVD  ft

Figure 3.4: Default inputs for UT-FAST-P<sup>3</sup> software found on home page ([Link](#)).

### 3.5 MATERIAL MODEL CALIBRATION

Fitting parameters A and B, a water velocity ( $v_0$ ), and a friction angle ( $\phi$ ) are entered into the program (Figure 3.4) to calibrate the material model. A and B are typically determined at a calibration well through a least square fit approach of velocity versus vertical effective stress (Merrell et al., 2014).

The friction angle is used to calculate the uniaxial effective stress ratio ( $K_0$ ; equation 15). The  $K_0$  ratio is used to map the vertical effective stress to mean effective stress (equation 18); this enables the relationship between velocity and vertical effective stress (equation 17) to be mapped to velocity and mean effective stress under uniaxial strain (equation 19). In  $v:\sigma'_m$  space, this is the uniaxial compression curve (Figure 3.2A).

In  $\sigma'_m:q$  space, this allows velocity values to be linked to stress states along the uniaxial compression line ( $\eta_{K_0}$ ; Figure 3.2B).

With the material model calibrated, an iso-porosity surface can be generated from any given velocity. The velocity provides a mean effective stress along the uniaxial compression line (equation 19), and the resulting mean effective stress is then used as an anchor point to attach the shape of the iso-porosity surface (equation 16).

To predict pore pressure for the VES, MES, and FES methods, an effective stress ratio ( $K=K_{exp}$ ), velocity ( $v$ ), vertical total stress ( $\sigma_v$ ), and depth (TVD) are entered into the program (Figure 3.4).

### **3.6 PORE PRESSURE FROM VES METHOD**

The VES method (Figure 3.5) is grounded on the assumption that the stress state is uniaxial; therefore, there is a direct link between the vertical effective stress and compression because all of the stress components (mean effective stress and deviatoric (shear) stress) are proportional to the vertical effective stress.

In practice, the VES method uses only the vertical stresses to calculate pore pressure. The vertical effective stress is obtained from the velocity vs. vertical effective stress relationship (equation 17), and the pore pressure is calculated as the difference between the vertical total stress and the vertical effective stress. However, because I display the results on in  $\sigma'_m:q$  space, I map the vertical stresses to mean stresses to calculate pore pressure.

The velocity input (Figure 3.4) is used to calculate the mean effective stress under uniaxial strain (equation 19). Graphically, the mean effective stress under uniaxial strain is located along the uniaxial compression line in  $\sigma'_m:q$  space ( $\eta_{K_0}$ ; equation 14; Figure 3.5B).

The vertical total stress (model input) is coupled with the uniaxial effective stress ratio (equation 15) and the mean effective stress under uniaxial strain (equation 18) to calculate the mean total stress under uniaxial strain ( $\sigma_{m,K_0}$ ):

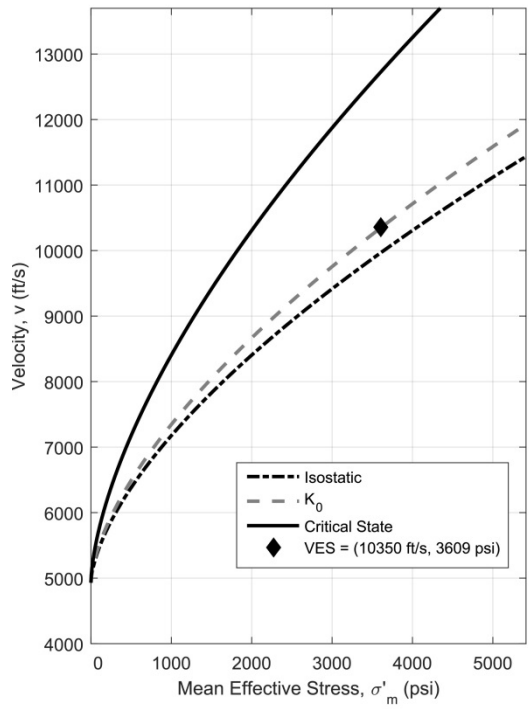
$$\sigma_{m,K_0} = \sigma_v - \frac{2\sigma'_{m,K_0}(1-K_0)}{1+2K_0} \quad (20)$$

The VES pore pressure ( $u_{VES}$ ) is calculated as the difference between the mean total stress under uniaxial strain ( $\sigma_{m,K_0}$ ) and the mean effective stress under uniaxial strain ( $\sigma'_{m,K_0}$ ):

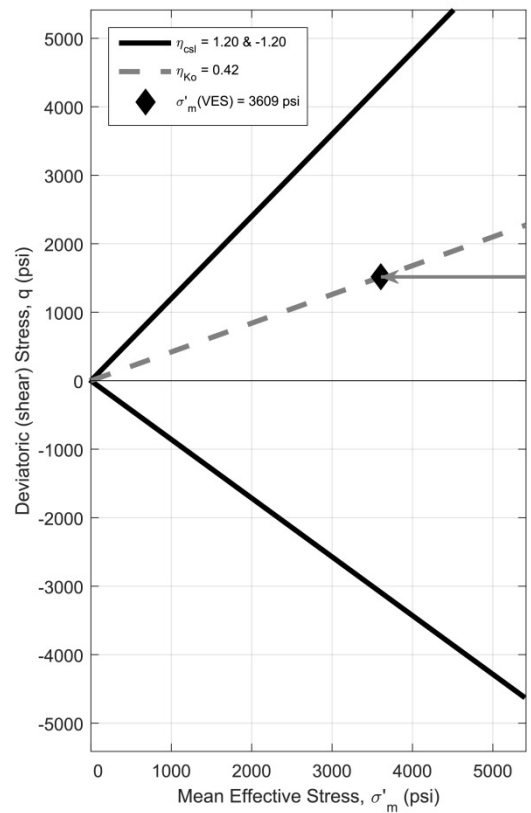
$$u_{VES} = \sigma_{m,K_0} - \sigma'_{m,K_0} \quad (21)$$

A key assumption of the VES method is that deformation is uniaxial (only in the vertical direction). Because the uniaxial effective stress ratio ( $K_0$ ) is used to calculate the mean effective stress directly from velocity (equation 19), the compaction trend is defined by a 1:1 relationship between velocity and mean effective stress, and is independent of the deviatoric (shear) stress.

A)



B)



C)

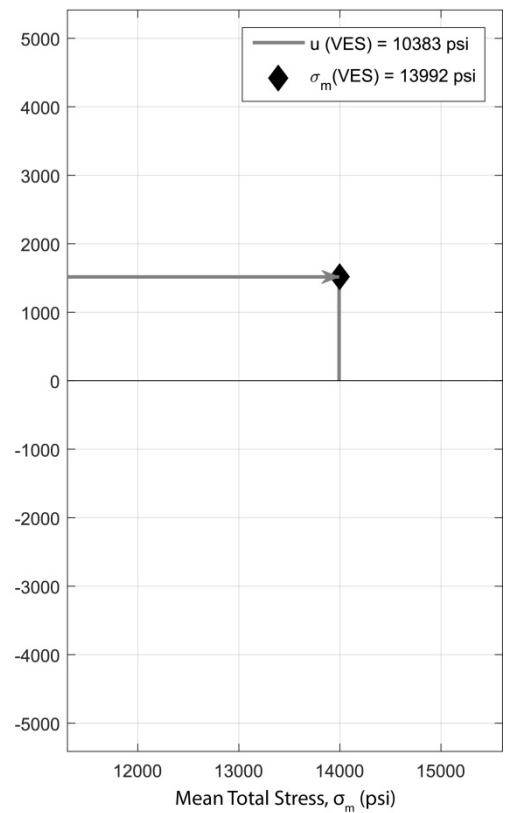


Figure 3.5: Pore pressure and stress prediction based on VES method (diamond). Results shown use default input parameters (Figure 3.4). A) Compression curves for isotropic stress state (black dash-dot curve), uniaxial stress state (gray dashed curve), and critical state state (black dashed curve). B) Compression lines for the isotropic stress state (x-axis), uniaxial stress state (dashed gray line), and critical stress state (black line); pore pressure is the difference between mean total and effective stress ( $u_{VES}$ ; gray arrow). C) Mean total stress.

### 3.7 PORE PRESSURE FROM MES METHOD

The Mean Effective Stress (MES) method (Figure 3.6) predicts pore pressure based on the poroelasticity theory. According to the poroelasticity theory, changes in porosity depend on the mean effective stress (Gouly, 1998; Harrold et al., 1999). Therefore, the MES method assumes the compaction trend is defined by a unique 1:1 relationship between velocity (assuming porosity maps 1:1 with velocity) and mean effective stress (equation 19). This relationship is usually calibrated assuming uniaxial conditions. This unique relationship means that an iso-porosity line is vertical in the mean effective stress vs. deviatoric (shear) stress space (often referred to as vertical end-cap; dashed red line in Figure 3.6B). Therefore, the VES and MES methods share the same mean effective stress, which is obtained from velocity ( $\sigma'_{m,K_0}$ ; equation 19; Figure 3.6B).

The MES method, however, allows the user to apply a correction to account for a stress state that may be different than the one used to calibrate the  $K_0$  velocity model. This is achieved through the user-defined effective stress ratio ( $K$ ; Figure 3.4). The mean total stress is calculated for the MES method ( $\sigma_{m,MES}$ ) as:

$$\sigma_{m,MES} = \sigma_v + \frac{2\sigma'_v(-1+K-2K_0+2K_0K)}{3(1+2K)} \quad (22)$$

(see Appendix B for full derivation of  $\sigma_{m,MES}$ )

The MES pore pressure ( $u_{MES}$ ) is taken as the difference between the mean total stress that has been modified by  $K$  ( $\sigma_{m,MES}$ ) and the mean effective stress under uniaxial strain ( $\sigma'_{m,K_0}$ ):

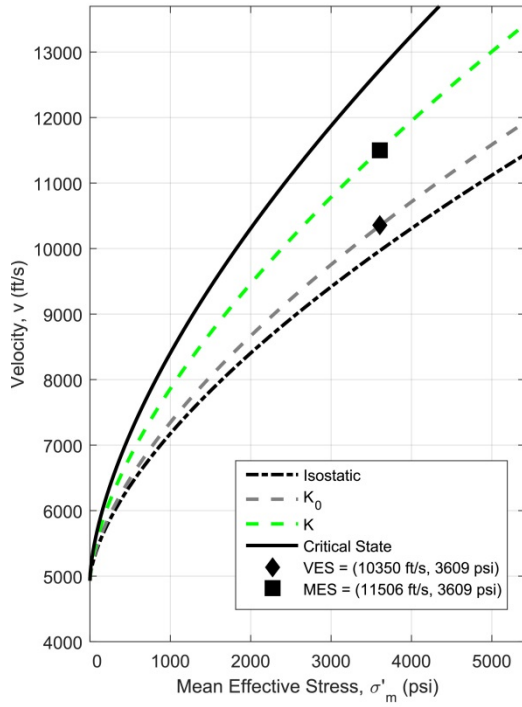
$$u_{MES} = \sigma_{m,MES} - \sigma'_{m,K_0} \quad (23)$$

The fundamental difference between the VES and MES methods is the modification of the mean total stress as a function of  $K$ . Any change in  $K$  ( $K \neq K_0$ ) will provide the MES method with a different mean total stress, and therefore a different pore pressure than the VES method. The relationship between  $K$  and the mean total stress is

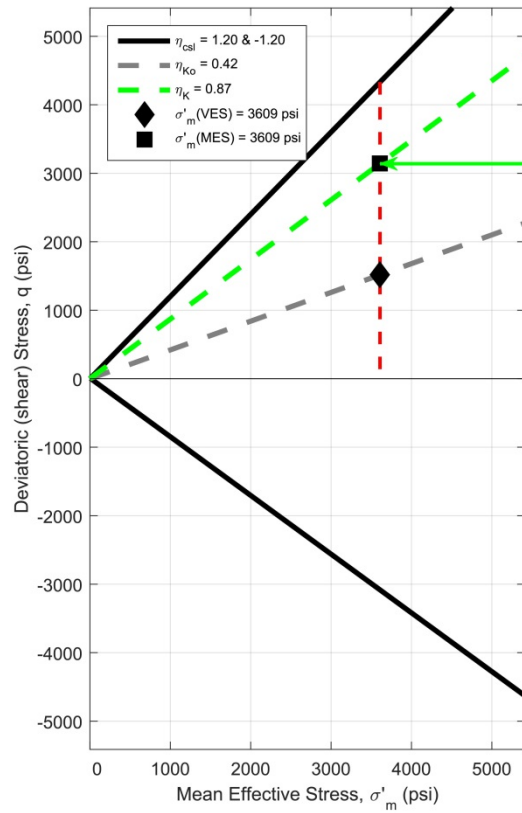
illustrated in Figure 3.7. For a given velocity and vertical total stress, an increase in  $K$  will result in an increase in the mean total stress relative to  $K_0$  conditions. This is due to an increase in the horizontal stresses. Similarly, the relationship between  $K$  and the predicted pore pressure is illustrated in (Figure 3.8). For a given velocity and vertical total stress, an increase in  $K$  will result in a monotonic increase in the predicted pore pressure relative to  $K_0$  conditions.

Many of the basins located in the Gulf of Mexico are characterized by compressional loading where the effective stress ratio is higher than uniaxial ( $K > K_0$ ). By failing to account for the horizontal stresses, pore pressures predicted by the VES method will underpredict in such locations. Other basins around the world are characterized by extensional loading where the effective stress ratio is lower than uniaxial ( $K < K_0$ ). In these areas the VES method will overpredict.

A)



B)



C)

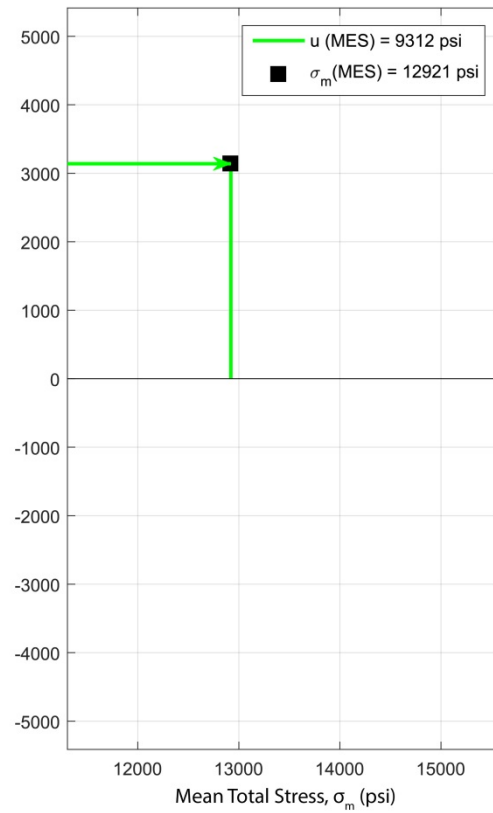


Figure 3.6: Pore pressure and stress prediction based on MES method (square). Results shown use default input parameters (Figure 3.4). A) Compression curves for isotropic stress state (black dash-dot curve), uniaxial stress state (gray dashed curve), user-defined stress state (green dashed curve), and critical stress state (black dashed curve). B) Compression lines for the isotropic stress state (x-axis), uniaxial stress state (dashed gray line), user-defined stress state (green dashed line), and critical stress state (black line). MES method assumes a 1:1 relationship between velocity and mean effective stress that is independent of deviatoric (shear) stress; therefore, the isoporosity line is vertical in  $\sigma'_m:q$  space (red dashed line). Pore pressure is the difference between mean total and effective stress ( $u_{MES}$ ; green arrow). C) Mean total stress.

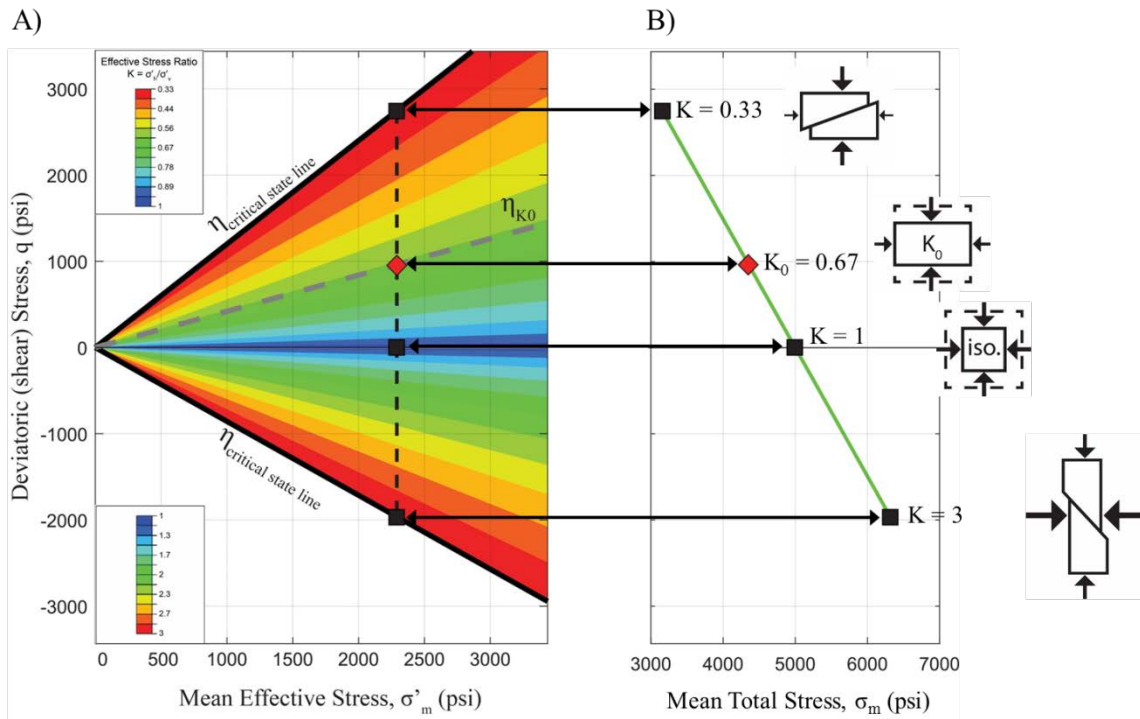


Figure 3.7: A) Radial compression curves corresponding to effective stress ratio ( $K$ ) varying from extensional to compressional failure. MES method assumes a 1:1 relationship between velocity and mean effective stress that is independent of deviatoric (shear) stress; therefore, the iso-porosity line is vertical in  $\sigma'_m$ : $q$  space (black dashed line). B) Change in mean total stress (green line) and therefore pore pressure (black arrows between A and B figures) as a function of  $K$  (from extensional failure to compressional failure).

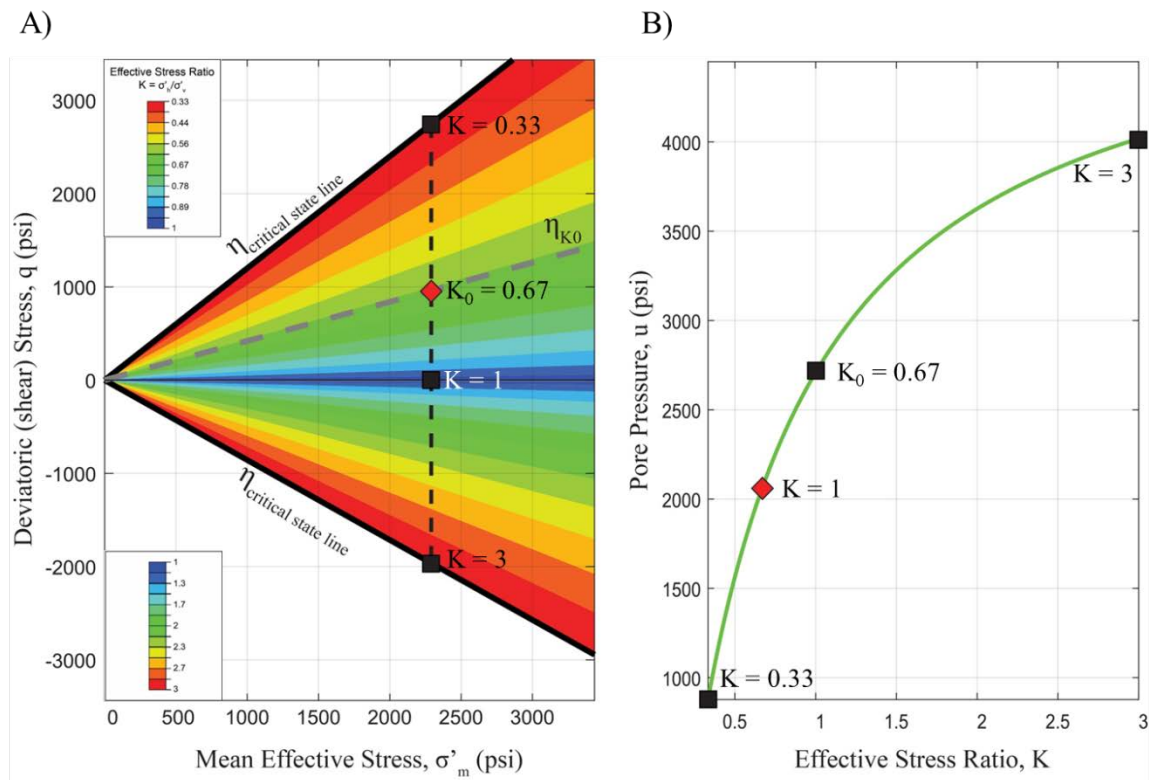


Figure 3.8: A) Radial compression curves corresponding to effective stress ratio ( $K$ ) varying from extensional to compressional failure. MES method assumes a 1:1 relationship between velocity and mean effective stress that is independent of deviatoric (shear) stress; therefore, the iso-porosity line is vertical in  $\sigma'_m$ : $q$  space (black dashed line). B) Change in pore pressure predicted by the MES method (green curve) as a function of stress ratio  $K$  (from extensional to compressional failure).

### 3.8 PORE PRESSURE FROM FES METHOD

The Full Stress Tensor (FES) method (Figure 3.9) incorporates all stress components into pressure prediction by taking into account the non-uniaxial ( $K$ ) contribution of both the mean effective stress and the deviatoric (shear) stress into compression. The relationship between porosity and mean effective stress is non-unique because it depends on the deviatoric (shear) stress. This is illustrated in Figure 3.2: For a given velocity, as the stress state is changed from  $K_0$  (dashed gray line in Figure 3.2C) to

K (dashed green line in Figure 3.2C), the increase in deviatoric (shear) stress reduces the mean effective stress (Figure 3.2C). This is because both mean effective stress and deviatoric (shear) stress contribute to compaction. Therefore, higher deviatoric (shear) stress means that less mean effective stress is needed to compact to the observed porosity. The relationship between mean effective stress and deviatoric (shear) stress for a given velocity (porosity) is defined by the shape of the iso-porosity surface, according to the MCC model.

Graphically, the mean effective stress for the FES method is found by the intersection of the iso-porosity curve (red curve in Figure 3.9B) with the slope of the defined stress state (dashed green line in Figure 3.9B). Mathematically, this is found by first using the velocity (model input) to solve for the mean effective stress along the uniaxial compression line ( $\sigma'_{m,K_0}$ ; equation 19). The mean effective stress is then used to anchor the iso-porosity surface (equation 16) at this location along the uniaxial compression line (where  $\sigma'_m = \sigma'_{m,K_0}$ ;  $M = M_{Ext.}$ ;  $\eta = \eta_{K_0}$ ) and then solve for the equivalent effective stress:

$$\sigma'_e = \sigma'_{m,K_0} \left( \frac{M_{Ext.}^2 + \eta_{K_0}^2}{M_{Ext.}^2} \right) \quad (24)$$

Finally, the equation for the equivalent effective stress (equation 24) is combined with the equation for the iso-porosity surface (equation 16) to solve for the mean effective stress for the FES method ( $\sigma'_{m,FES}$ ) as a function of the vertical effective stress (obtained from velocity (model input; equation 17)) and the user-defined stress ratio ( $\eta_K$ , where  $\eta_K$  is a function of K (model input; equation 11)):

$$\sigma'_{m,FES} = \sigma'_v \left( \frac{1+2K_0}{3} \right) \left( \frac{M_{Ext.}^2 + \eta_{K_0}^2}{M_{Ext.}^2} \right) \left( \frac{M^2}{M^2 + \eta_K^2} \right) \quad (25)$$

The mean total stress for the FES method ( $\sigma_{m,FES}$ ) is calculated as:

$$\sigma_{m,FES} = \sigma_v + \frac{2\sigma'_v M^2 (M_{Ext.}^2 + \eta_{K_0}^2) (1+2K_0) (K-1)}{3M_{Ext.}^2 (1+2K) (M^2 + \eta_K^2)} \quad (26)$$

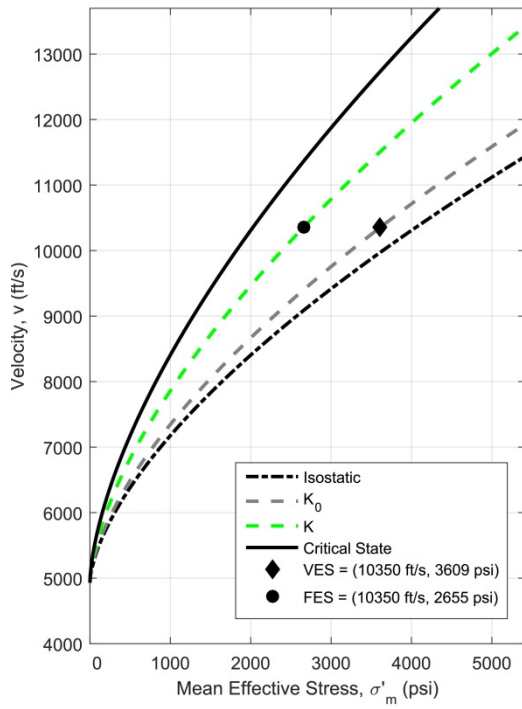
(see Appendix C for full derivation of  $\sigma_{m,FES}$ ).

The FES pore pressure is calculated as the difference between the mean total stress ( $\sigma_{m,FES}$ ) and the mean effective stress ( $\sigma'_{m,FES}$ ):

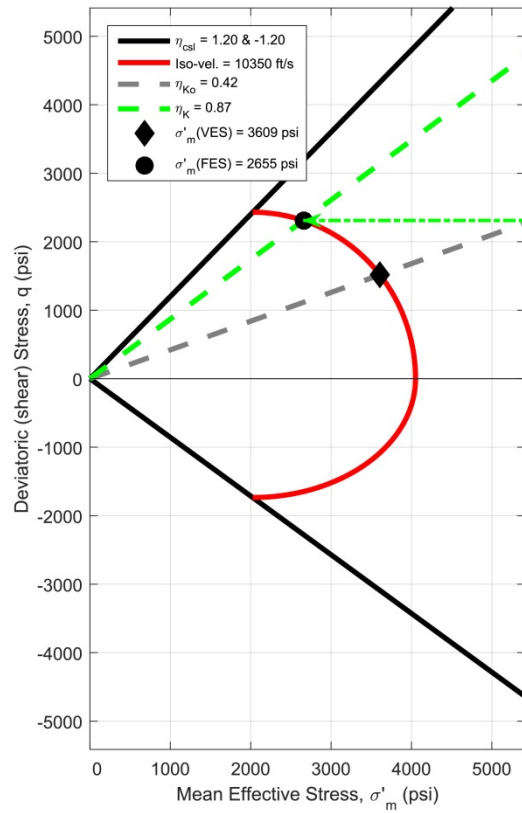
$$u_{FES} = \sigma_{m,FES} - \sigma'_{m,FES} \quad (27)$$

The fundamental difference between the FES method and the VES and MES methods is that it does not assume a unique relationship between porosity and mean effective stress; rather, it assumes a relationship between porosity, mean effective stress, and deviatoric (shear) stress. Any change in  $K$  ( $K \neq K_0$ ) will provide the FES method with a different mean total stress and a different mean effective stress (Figure 3.10), and therefore a different pore pressure (Figure 3.11) than the VES and MES methods. The FES method will always predict a pore pressure greater than or equal to the VES method.

A)



B)



C)

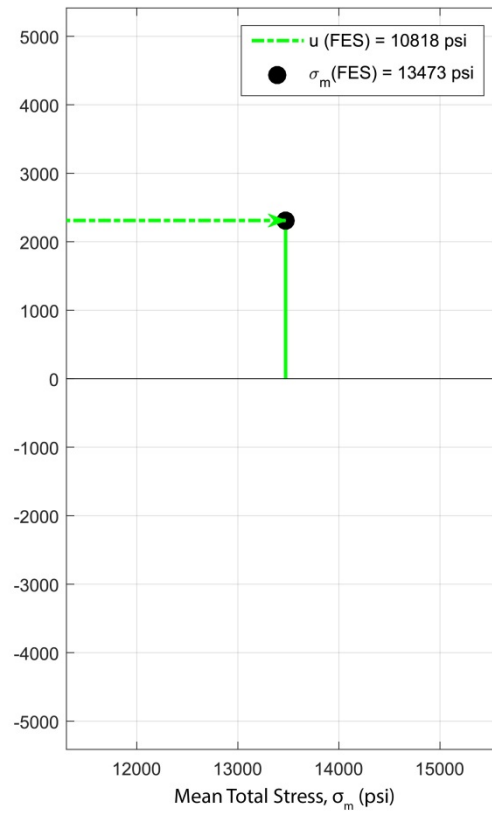


Figure 3.9: Pore pressure and stress prediction based on FES method (circle). Results shown use default input parameters (Figure 3.4). A) Compression curves for isotropic stress (black dash-dot curve), uniaxial stress (gray dashed curve), user-defined stress state (green dashed curve), and critical state (black dashed curve). B) Compression lines for the isotropic stress state (x-axis), uniaxial stress state (dashed gray line), user-defined stress state (green dashed line), and critical stress state (black line). For a given velocity, changes in mean effective stress and deviatoric (shear) stress follow curved iso-porosity path. Pore pressure is the difference between mean total and effective stress ( $u_{FES}$ ; dash-dot green arrow). C) Mean total stress.

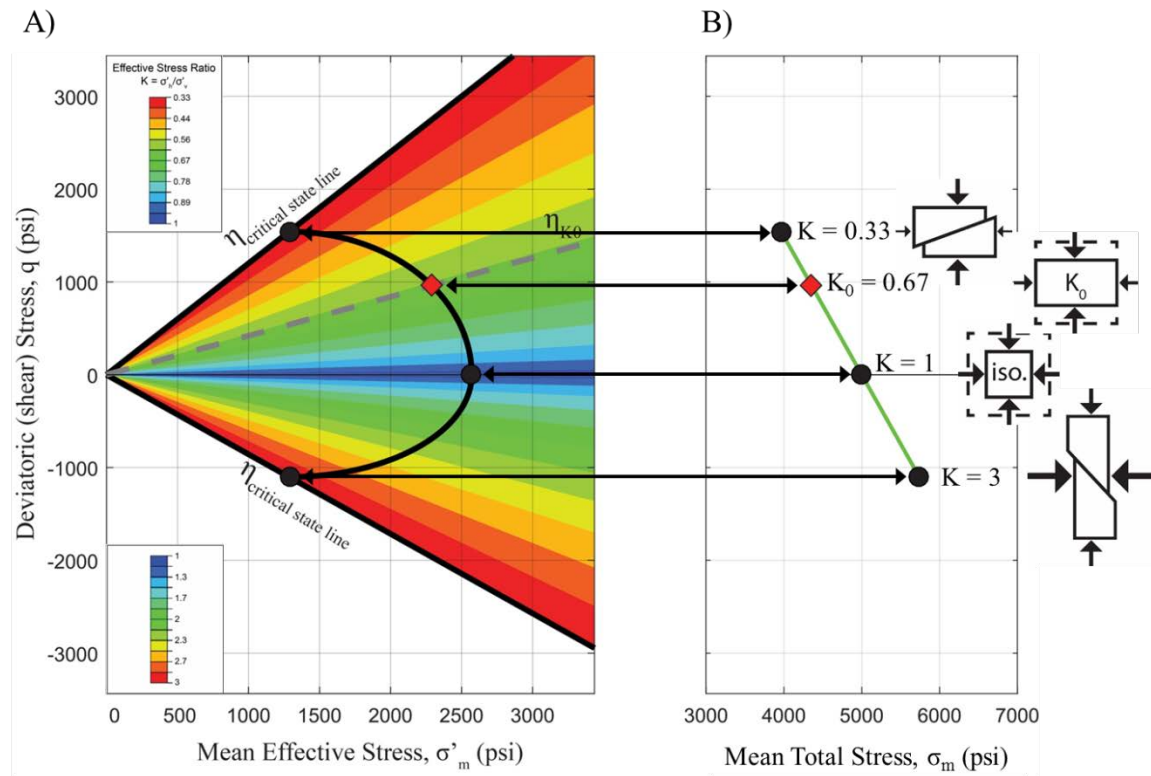


Figure 3.10: A) Radial compression curves corresponding to effective stress ratio ( $K$ ) varying from extensional to compressional failure. For a given velocity, changes in mean effective stress and deviatoric (shear) stress follow curved iso-porosity path. B) Change in mean total stress (green line) and therefore pore pressure (black arrows between A and B figures) as a function of  $K$  (from extensional failure to compressional failure).

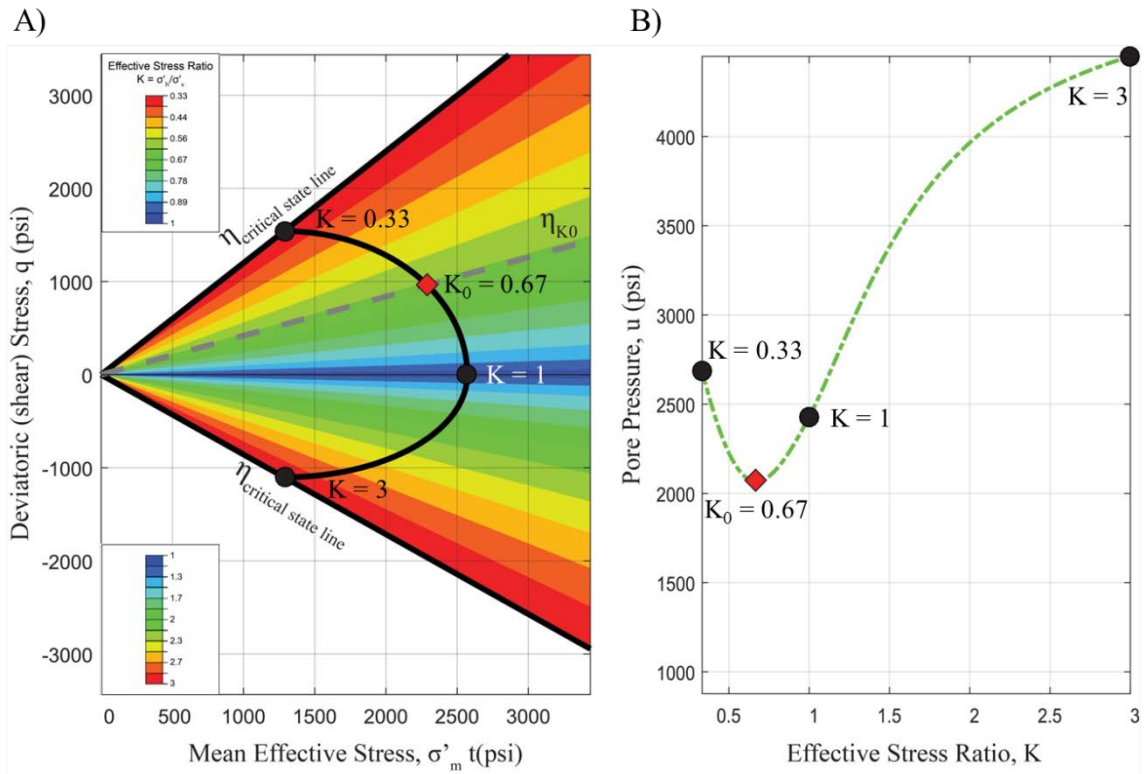


Figure 3.11: A) Radial compression curves corresponding to effective stress ratio ( $K$ ) varying from extensional to compressional failure. For a given velocity, changes in mean effective stress and deviatoric (shear) stress follow curved iso-porosity path. B) Change in pore pressure predicted by the FES method (green dash-dot curve) as a function of stress ratio  $K$  (from extensional to compressional failure).

### 3.9 SIMULATIONS

I next present three different simulations to examine how pore pressure and stress interact in different stress settings: (1) uniaxial compression, (2) isotropic compression (shear lower than uniaxial), and (3) shear higher than uniaxial. In each of the simulations presented below, the material model is calibrated using the following parameters:

- $A = 28.3$
- $B = 0.59$
- Friction angle ( $\phi$ ) = 30 deg.

- Velocity ( $v$ ) = 10,350 ft/s
- Vertical total stress ( $\sigma_v$ ) = 15,010
- True vertical depth (TVD) = 10,000 ft

### 3.9.1 Simulation 1: Uniaxial Compression

In the first simulation, stresses are assumed to be uniaxial ( $K=K_0$ ). As previously established, according to the MCC model the uniaxial effective stress ratio ( $K_0$ ) is a function of the friction angle (equation 15). For a friction angle of 30 deg.,  $K_0 = 0.67$ . Therefore, the expected effective stress ratio ( $K_{\text{expected}}$ ) is set to 0.67 and the program is run. In addition, the minimum and maximum K ratios are included to incorporate a degree of uncertainty in the expected K value. In this example,  $K_{\text{min}}$  is set to 0.3 and  $K_{\text{max}}$  is set to 1 (Figure 3.12).

**Equation 1:  $v = v_0 + A(\sigma'_v)^B$**   
 (Velocity model under uniaxial  $K_0$  strain)  
*\*Mouse over parameter names below for description*

A

B

Friction angle,  $\Phi$   °

( $K_0 =$  $; \eta_{K_0} =$  $; \eta_{csl}$  $)$

Effective stress ratio, K  
 (Expected) (Min.) (Max.)

K

( $\eta_K =$  $)$

Velocity,  $v$   ft/s

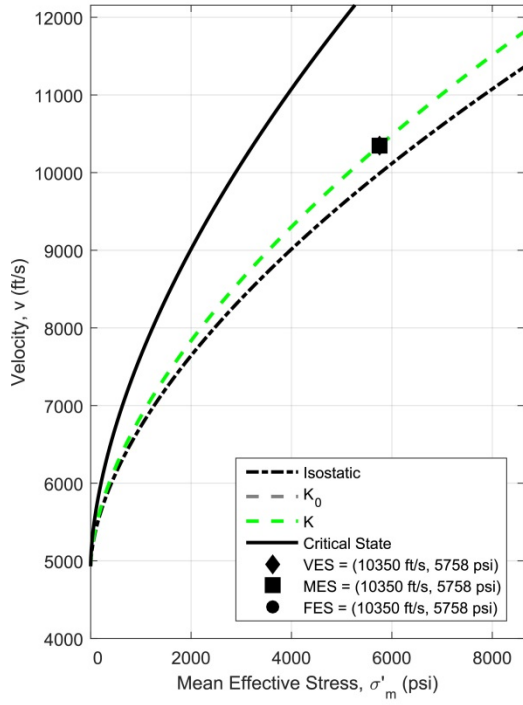
Total vertical stress,  $\sigma_v$   psi

True vertical depth, TVD  ft

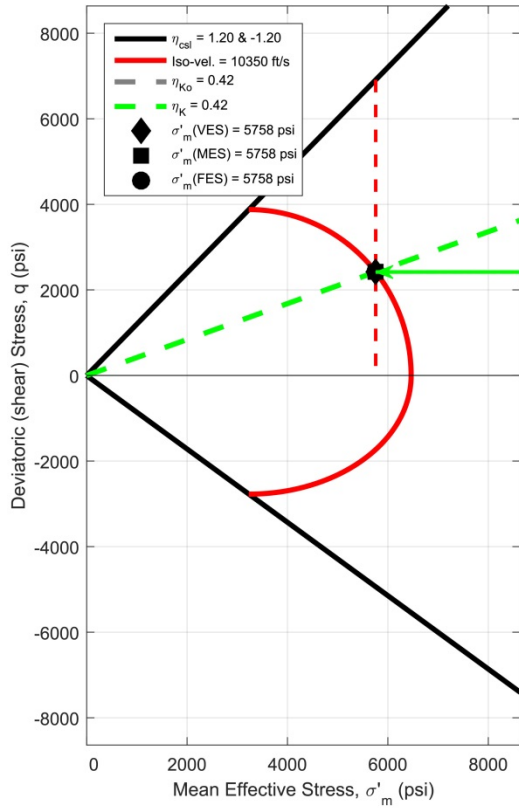
Figure 3.12: Input table for uniaxial compaction ( $K=K_0$ ).

Because we assume uniaxial conditions, the VES, MES, and FES will predict the same pore pressure. The physical meaning of  $K=K_0$  is that the compression paths (Figure 3.13 A, B) and the mean total stress (Figure 3.13C) are the same in all three methods; hence, the VES, MES, and FES share the same mean effective stress, and the same mean total stress. Therefore all three methods predict the same pore pressure (Figure 3.14).

A)



B)



C)

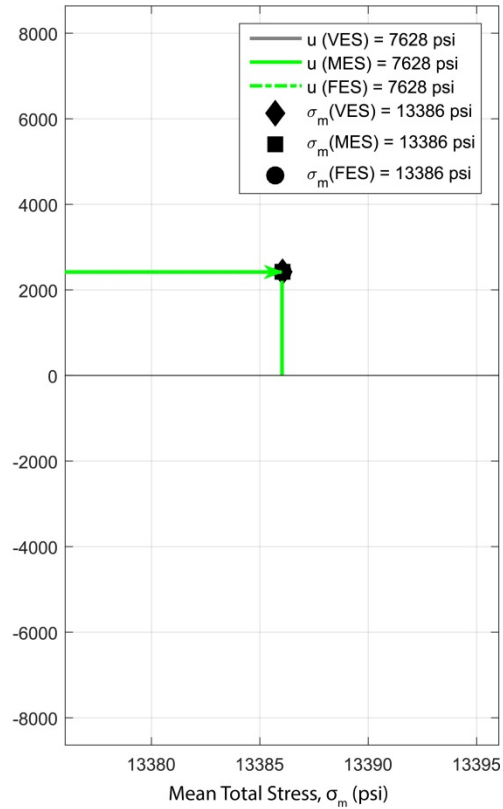


Figure 3.13: Pore pressure and stress prediction based on VES (diamond), MES (square), and FES (circle) methods. A) Compression curves for isotropic stress state (black dash-dot curve), uniaxial stress state (gray dashed curve), user-defined stress state (dashed green curve) and critical stress state (black dashed curve). B) Compression lines for the isotropic stress state (x-axis), uniaxial stress state (dashed gray line), user-defined stress state (green dashed line), and critical stress state (black line). C) Mean total stress. B, C)  $u_{VES}$  pore pressure (gray arrows);  $u_{MES}$  pore pressure (green arrows);  $u_{FES}$  pore pressure (green dash-dot arrows).

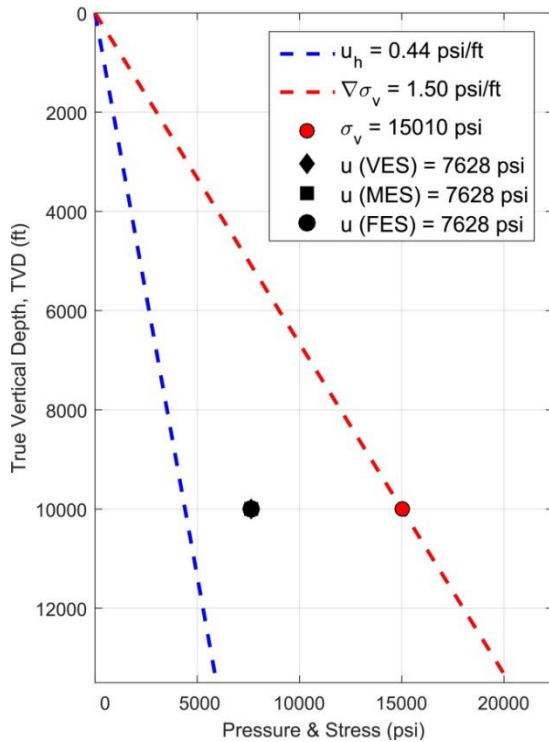


Figure 3.14: Predicted pore pressures in pressure & stress – depth plot.  $u_{VES}$  pore pressure (diamond);  $u_{MES}$  pore pressure (square);  $u_{FES}$  pore pressure (circle); hydrostatic gradient (blue dashed line); lithostatic gradient (red dashed line). The lithostatic gradient is derived from vertical total stress and user-defined input depth.

### 3.9.2 Simulation 2: Isotropic Compaction (shear lower than uniaxial)

In the second simulation, the stress state is isotropic. For an isotropic stress state, the vertical and horizontal stresses are equal and, consequently, the shear stress is zero. To simulate this, the expected effective stress ratio is set to 1 ( $K_{exp.}=1$ ), with  $K_{min.}=0.67$  and  $K_{max.}=1.1$  (Figure 3.15).

**Equation 1:  $v = v_0 + A(\sigma'_v)^B$**   
 (Velocity model under uniaxial  $K_0$  strain)  
*\*Mouse over parameter names below for description*

A	28.3		
B	0.59		
Friction angle, $\Phi$	30 °		
( $K_0 = $ <input style="border: 1px solid black; width: 40px; text-align: center;" type="text" value="0.67"/> ; $\eta_{K_0} = $ <input style="border: 1px solid black; width: 40px; text-align: center;" type="text" value="0.42"/> ; $\eta_{csl} $ <input style="border: 1px solid black; width: 40px; text-align: center;" type="text" value="1.20"/> )			
Effective stress ratio, K			
(Expected)	(Min.)	(Max.)	
K	1	0.67	1.1
( $\eta_K = $ <input style="border: 1px solid black; width: 40px; text-align: center;" type="text" value="0.00"/> )			
Velocity, v	10350	ft/s	
Total vertical stress, $\sigma_v$	15010	psi	
True vertical depth, TVD	10000	ft	
<input type="button" value="Calculate"/>			

Figure 3.15: Input table for isotropic compaction (K=1).

VES vs. MES: The MES approach calculates a higher pore pressure than the VES approach (gray arrows (VES) vs. green arrows (MES) in Figure 3.17 B, C). Both the VES and MES approaches assume a unique relationship between velocity and mean effective stress; therefore, they share the same mean effective stress (square (MES) and diamond (VES) in Figure 3.17 B). Thus, the difference in pressure is driven by the difference in mean total stress; the VES method calculates the mean total stress from equation 20 (diamond in Figure 3.16C); the MES method calculates the mean total stress from equation 22 (square in Figure 3.16C). As K is increased from  $K_0$  to isotropic, the mean total stress also increases (Figure 3.7). The MES method accounts for this increase in the mean total stress; therefore, the MES method has a higher mean total stress (Figure 3.17C), and thus a higher pore pressure.

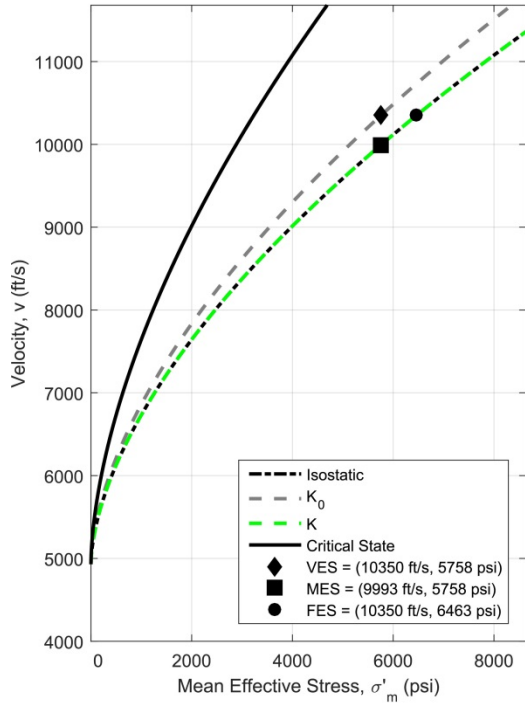
VES vs. FES: The FES approach calculates a higher pore pressure than the VES approach (gray arrows (VES) vs. dash-dot green arrows (FES) in Figure 3.17 B, C). Because  $K > K_0$ , the FES approach has a different mean effective stress and a different mean total stress than the VES method (diamond (VES) vs. circle (FES) in Figure 3.16 B, C). According to the FES method, as  $K$  is increased from  $K_0$  to isotropic, both the mean effective stress and the mean total stress increase (Figure 3.10). Only the FES method is able to account for both of these changes. Here, the FES approach predicts a higher pore pressure than the VES approach, because the increase in mean total stress is more pronounced than the increase in mean effective stress.

MES vs. FES: The FES approach calculates a lower pore pressure than the MES approach (green arrows (FES) vs. dash-dot green arrows (FES) in Figure 3.17 B, C). At isotropic conditions, the MES and FES share the same mean total stress (square (MES) and circle (FES) in Figure 3.16 B, C); therefore, the difference in pore pressure is the result of a difference in mean effective stress. Because the MES method shares a 1:1 relationship between velocity and mean effective stress, it cannot account for the reduction in decrease in deviatoric (shear) stress as the effective stress ratio is increased from  $K_0$  to  $K=1$  (Figure 3.10). Therefore, the FES approach predicts a lower pore pressure.

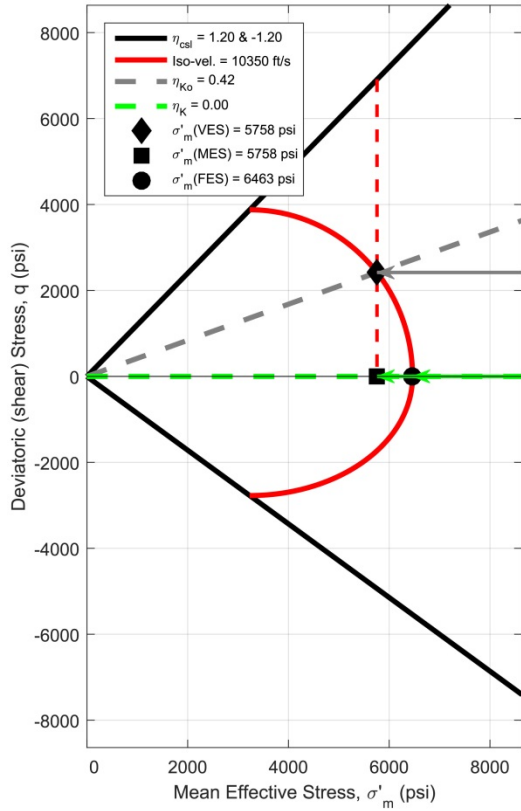
In Figure 3.17A, the predicted pore pressures for VES, MES, and FES are bounded by the lithostatic and hydrostatic gradients. If the expected effective stress ratio ( $K_{exp.}$ ) was varied from extensional to compressional failure, the VES pressure would remain constant, while the MES pressure would increase monotonically; the FES pressure would decrease to the VES value as  $K$  varies from extensional failure to  $K_0$ , and then would increase for  $K > K_0$ . This is shown in Figure 3.17B.

The margin of error set by the minimum and maximum expected effective stress ratios ( $K_{\min.}$  &  $K_{\max.}$ ) for the three methods is displayed in a pressure and stress vs. depth plot (Figure 3.18A), and a pressure vs. method plot (Figure 3.18B). At  $K_{\min.}$ , all three methods predict the same pore pressure, because  $K_{\min.}=K_0$ . At  $K_{\max.}$ , the FES method predicts the highest pore pressure.

A)



B)



C)

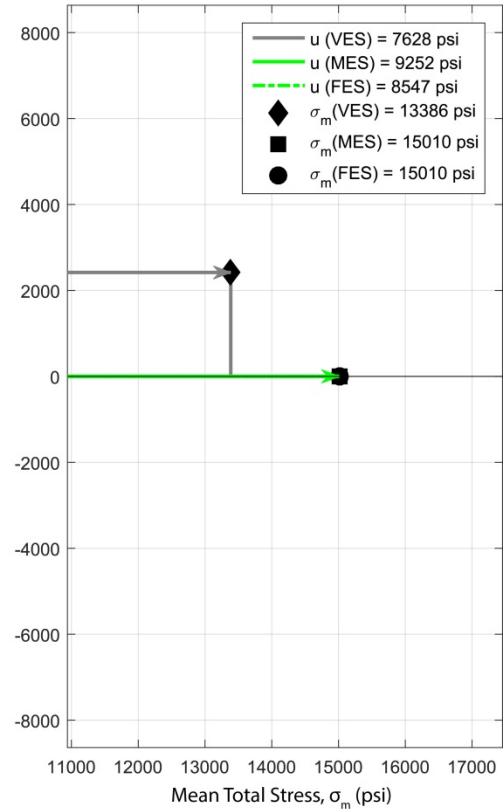


Figure 3.16: Pore pressure and stress prediction based on VES (diamond), MES (square), and FES (circle) methods. A) Compression curves for isotropic stress state (black dash-dot curve), uniaxial stress state (gray dashed curve), user-defined stress state (dashed green curve) and critical stress state (black dashed curve). B) Compression lines for the isotropic stress state (x-axis), uniaxial stress state (dashed gray line), user-defined stress state (green dashed line), and critical stress state (black line). C) Mean total stress. B, C)  $u_{VES}$  pore pressure (gray arrows);  $u_{MES}$  pore pressure (green arrows);  $u_{FES}$  pore pressure (green dash-dot arrows).

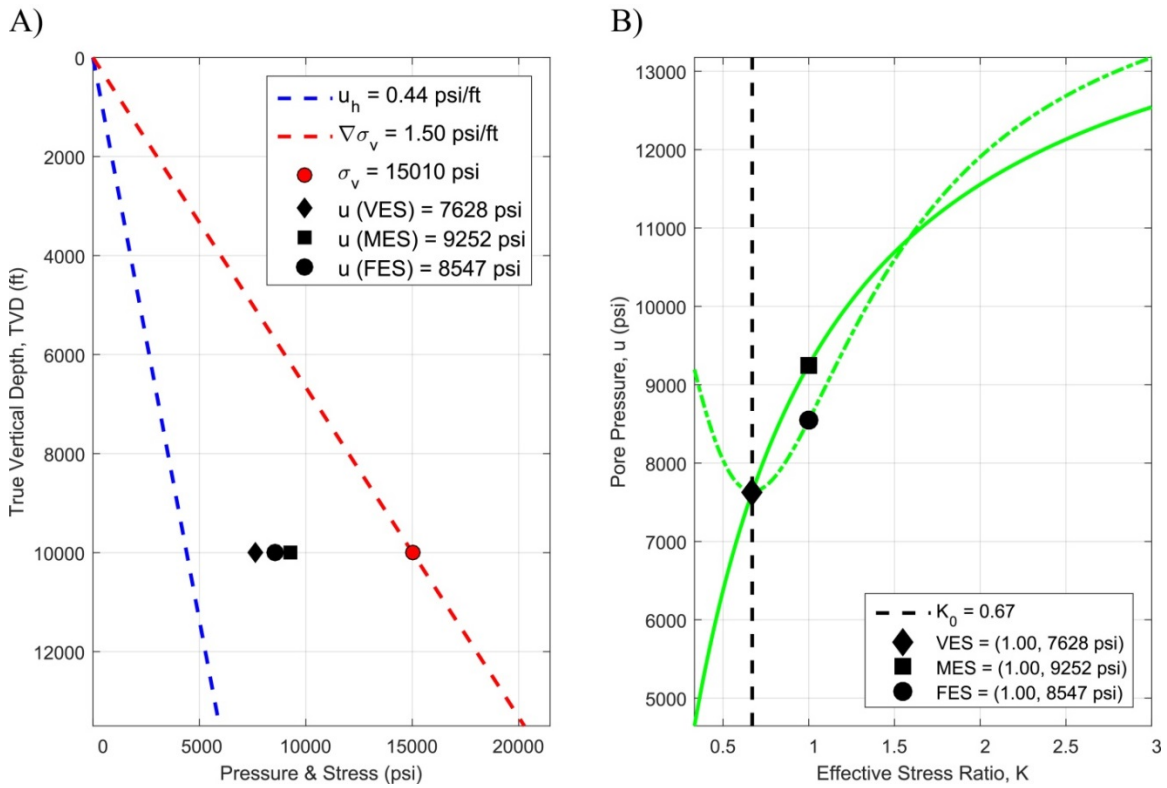


Figure 3.17: Predicted pore pressures:  $u_{ES}$  (diamond);  $u_{MES}$  (square);  $u_{FES}$  (circle) A) Predicted pore pressures in pressure & stress – depth plot: hydrostatic gradient (blue dashed line); lithostatic gradient (red dashed line). The lithostatic gradient is derived from vertical total stress and user-defined depth. B) Change in pore pressure predicted by MES (green solid curve) and FES (green dash-dot curve) as a function of stress ratio  $K$  (from extensional to compressional failure).

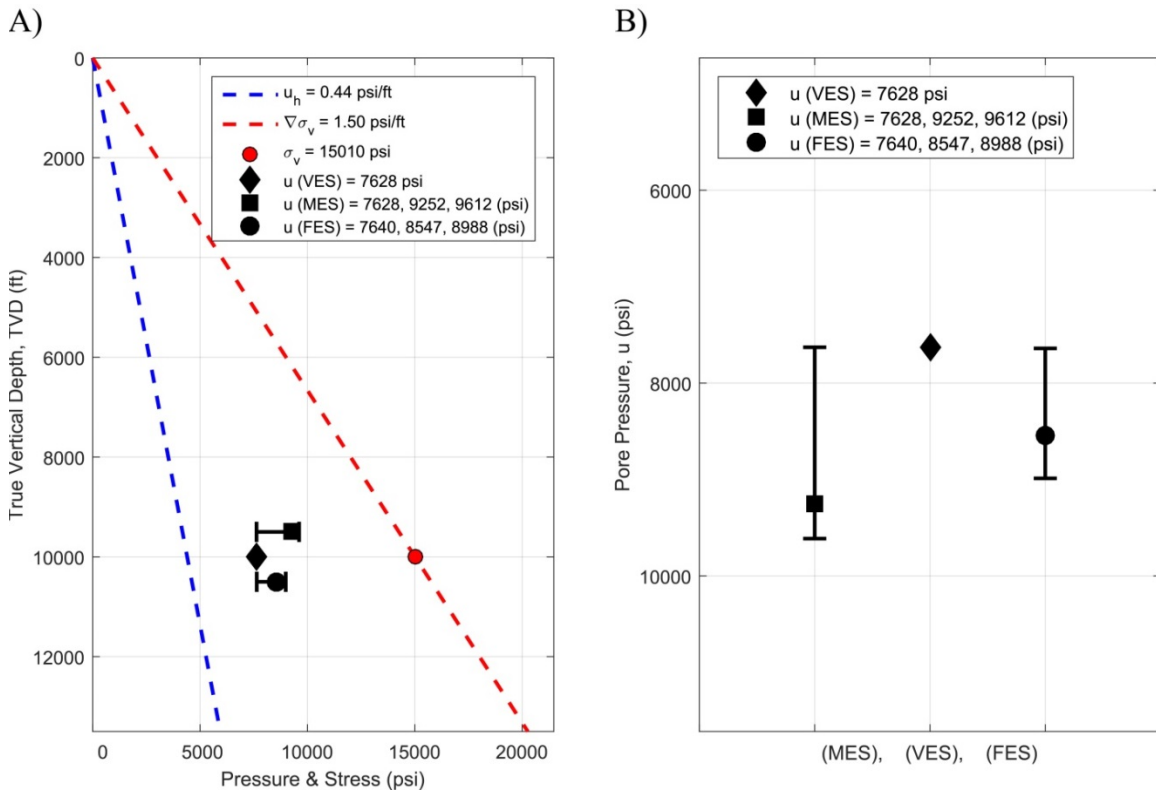


Figure 3.18: Predicted pore pressure error range:  $u_{VES}$  (diamond);  $u_{MES}$  (square);  $u_{FES}$  (circle); capped lines represent predicted pore pressure based on minimum and maximum  $K$  values ( $K_{min.}$  &  $K_{max.}$ ). A) Pressure & stress – depth plot. Depth is the same but shown graphically as different to improve clarity. B) Error range for VES, MES, and FES methods.

### 3.9.3 Simulation 3: Shear Higher than Uniaxial

In the final simulation, the deviatoric (shear) stress is higher than  $K_0$ . This is achieved by setting  $K_{exp.} < K_0$ . For this simulation,  $K_{exp.}$  is set to 0.4,  $K_{min.}$  is set to 0.3, and  $K_{max.}$  is set to 0.67 (Figure 3.19).

**Equation 1:  $v = v_0 + A(\sigma'_v)^B$**   
 (Velocity model under uniaxial  $K_0$  strain)  
 \*Mouse over parameter names below for description

A	<input type="text" value="28.3"/>	
B	<input type="text" value="0.59"/>	
Friction angle, $\Phi$	<input type="text" value="30"/> °	
( $K_0 = $ <input type="text" value="0.67"/> $ ; \eta_{K_0} = $ <input type="text" value="0.42"/> $ ; \eta_{csl} $ <input type="text" value="1.20"/> $ )$		
Effective stress ratio, K		
(Expected) (Min.) (Max.)		
K	<input type="text" value="0.4"/>	<input type="text" value="0.3"/> <input type="text" value="0.67"/>
( $\eta_K = $ <input type="text" value="1.00"/> $ )$		
Velocity, v	<input type="text" value="10350"/>	ft/s
Total vertical stress, $\sigma_v$	<input type="text" value="15010"/>	psi
True vertical depth, TVD	<input type="text" value="10000"/>	ft
<input type="button" value="Calculate"/>		

Figure 3.19: Input table for shear higher than uniaxial ( $K < K_0$ ).

VES vs. MES: The MES approach calculates a lower pore pressure than the VES approach (gray arrows (VES) vs. green arrows (MES) in Figure 3.20 B, C). Given they share the same mean effective stress (Figure 3.20A), the difference in pressure is driven by the difference in mean total stress. According to the MES method, a decrease in K with respect to  $K_0$  results in a decrease in the mean total stress (Figure 3.7). Because only the MES method accounts for the decrease in mean total stress (square in Figure 3.20C), the MES predicts a lower pore pressure than VES (green arrows (MES) vs. gray arrows (VES) in Figure 3.20 B, C).

VES vs. FES: The FES approach calculates a higher pore pressure than the VES approach (gray arrows (VES) vs. dash-dot green arrows (FES) in Figure 3.20 B, C). Because  $K < K_0$ , the FES approach has a different mean effective stress (circle in Figure 3.20C) and a different mean total stress (circle in Figure 3.20C) than the VES method

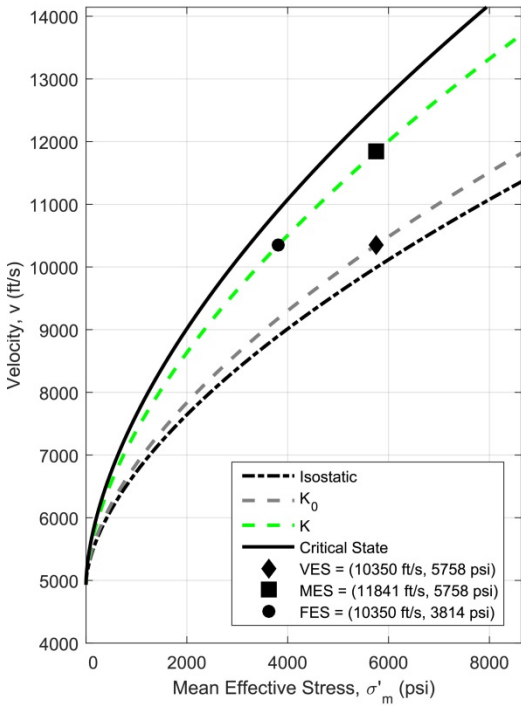
(diamond in Figure 3.20 B, C). According to the FES method, a decrease in  $K$  with respect to  $K_0$  results in a change in both the mean effective stress and the mean total stress (Figure 3.10). Only the FES method is able to account for both of these changes. Here, the FES predicts a higher pore pressure than the VES approach, because the decrease in mean effective stress is more pronounced than the decrease in mean total stress.

MES vs. FES: The FES approach calculates a higher pore pressure than the MES approach (green arrows (MES) vs. dash-dot green arrows (FES) in Figure 3.20 B, C). Because  $K < K_0$ , the FES method has a different mean effective stress (circle in Figure 3.20B) and a different mean total stress (circle in Figure 3.20C) than MES (square in Figure 3.20 B, C). A decrease in  $K$  with respect to  $K_0$  results in a decrease in both the mean effective stress and the mean total stress. Only the FES method is able to account for both of these changes. Because of the large decrease in mean effective stress, the FES predicts a higher pore pressure than the MES approach.

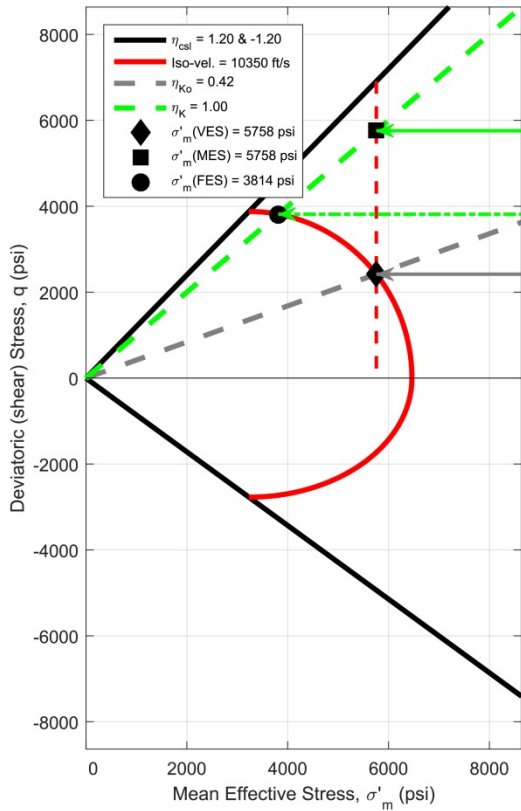
In Figure 3.21A, the predicted pore pressures for VES, MES, and FES are bounded by the lithostatic and hydrostatic gradients. If the expected effective stress ratio ( $K_{exp.}$ ) was varied from extensional to compressional failure, the VES pressure would remain constant, while the MES pressure would increase monotonically; the FES pressure would decrease to the VES value as  $K$  varies from extensional failure to  $K_0$ , and then would increase for  $K > K_0$ . This is shown in Figure 3.21B.

The margin of error set by the minimum and maximum expected effective stress ratios ( $K_{min.}$  &  $K_{max.}$ ) for the three methods is displayed in a pressure and stress vs. depth plot (Figure 3.18A), and a pressure vs. method plot (Figure 3.18B). At  $K_{min.}$ , the FES method predicts the highest pore pressure. At  $K_{max.}$ , all three methods predict the same pore pressure, because  $K_{max.} = K_0$ .

A)



B)



C)

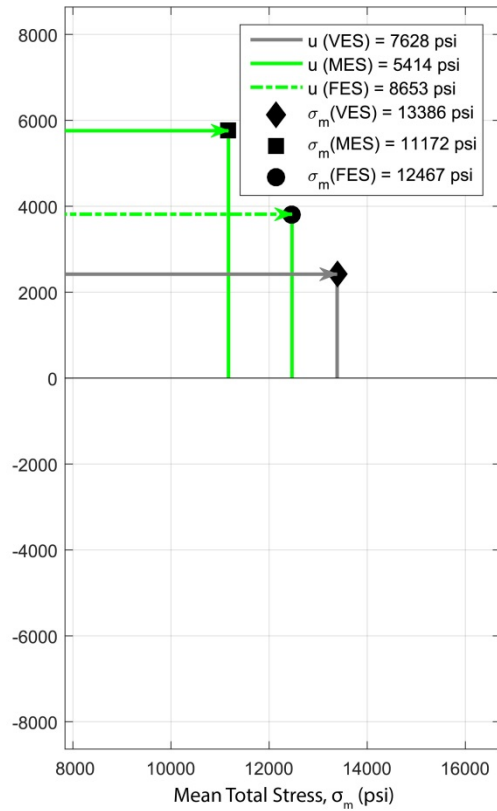


Figure 3.20: Pore pressure and stress prediction based on VES (diamond), MES (square), and FES (circle) methods. A) Compression curves for isotropic stress state (black dash-dot curve), uniaxial stress state (gray dashed curve), user-defined stress state (dashed green curve) and critical stress state (black dashed curve). B) Compression lines for the isotropic stress state (x-axis), uniaxial stress state (dashed gray line), user-defined stress state (green dashed line), and critical stress state (black line). C) Mean total stress. B, C)  $u_{VES}$  pore pressure (gray arrows);  $u_{MES}$  pore pressure (green arrows);  $u_{FES}$  pore pressure (green dash-dot arrows).

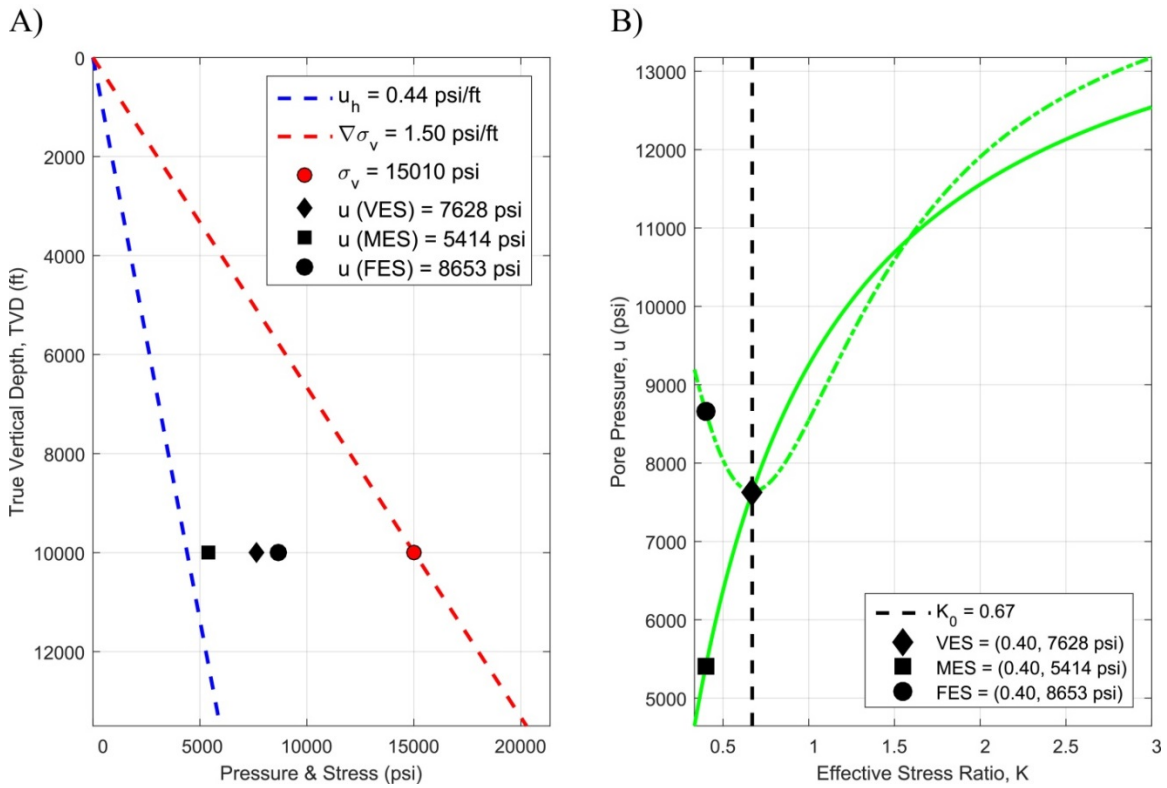


Figure 3.21: Predicted pore pressures:  $u_{ES}$  (diamond);  $u_{MES}$  (square);  $u_{FES}$  (circle) A) Predicted pore pressures in pressure & stress – depth plot: hydrostatic gradient (blue dashed line); lithostatic gradient (red dashed line). The lithostatic gradient is derived from vertical total stress and user-defined depth. B) Change in pore pressure predicted by MES (green solid curve) and FES (green dash-dot curve) as a function of stress ratio  $K$  (from extensional to compressional failure).

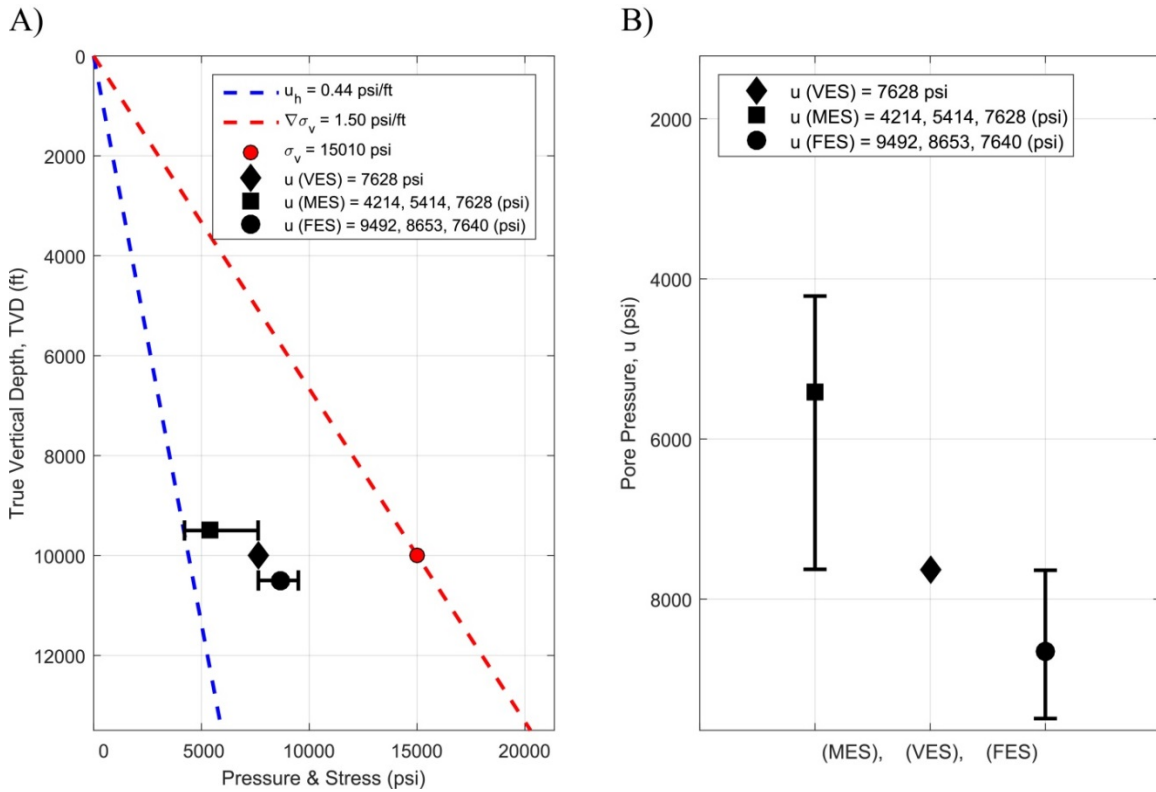


Figure 3.22: Predicted pore pressure error range:  $u_{VES}$  (diamond);  $u_{MES}$  (square);  $u_{FES}$  (circle); capped lines represent predicted pore pressure based on minimum and maximum  $K$  values ( $K_{min.}$  &  $K_{max.}$ ). A) Pressure & stress – depth plot. Depth is the same but shown graphically as different to improve clarity. B) Error range for VES, MES, and FES methods.

### 3.10 CONCLUSIONS AND DISCUSSION

I have developed UT-FAST-P<sup>3</sup> to allow users to evaluate how pore pressure and stress interact in non-uniaxial settings. This is achieved by calibrating the software with a uniaxial velocity model, where the horizontal stresses are a function of the vertical, and changing the stress conditions ( $K$ ) at the target location to calculate pore pressure.

The software illustrates that both mean and deviatoric (shear) stress contribute to the development of pore pressure. Often times in industry, either only the vertical stresses (i.e., VES approach) or the mean stresses (i.e., MES approach) are used to predict pore

pressure. In reality, both the mean and shear stresses contribute to the development of pore pressure, and must be independently accounted for if the stress conditions locally vary away from the calibration well. A traditional vertical stress-based approach is only able to account for the mean and shear stress proportional to the vertical stresses through  $K_0$ . As a consequence, a vertical stress-based method is physically limited to geological environments where the stress state is uniaxial; rarely are basins truly uniaxial. Many of the most prolific hydrocarbon reserves are located in geological environments where the stress state is not uniaxial (salt canopies, fault zones, anticlines, synclines, continental margins, etc.).

A mean stress-based approach allows for a correction to be applied if stress conditions vary away from the calibration well; this is carried out by obtaining a better estimate the mean total stress; oftentimes the mean total stress is acquired from a geomechanical model. However, because a mean stress-based approach assumes a 1:1 relationship between velocity and mean effective stress, this technique fails to account for the contribution of non- $K_0$  deviatoric (shear) stress to compression and pressure development. By examining the software, it becomes obvious that, from a single velocity, the mean effective stress can vary up to a magnitude of two, depending on the level of deviatoric (shear) stress (through  $K$ ). Therefore, by failing to account for local non- $K_0$  variations in deviatoric (shear) stress, the mean effective stress (and hence the predicted pore pressure) can be grossly miscalculated.

The FES method is formulated to account for non- $K_0$  stress states. In this software, I used iso-porosity curves based on the MCC model (Wood, 1990). The FES method is not restricted to a single compression curve; rather, the FES method interrelates velocity with both mean and deviatoric (shear) stress. The mean effective stress is calculated as a function of the deviatoric (shear) stress through the iso-porosity

surface. As a result, both the mean effective stress and mean total stress are modified to account for non- $K_0$  stress conditions.

In summary, the UT-FAST-P3 software is a learning tool to illustrate how pore pressure and stress interact in non- $K_0$  settings. It allows users to examine the relative contributions of non- $K_0$  mean and deviatoric (shear) stress to pore pressure development, and provides a way to analyze the margin of error resulting from their omission.

## Appendix A: Derivation of Mean Total Stress for VES Method

This appendix summarizes the steps I use to derive the mean total stress for the VES method in Chapter 2 (equation 28) and Chapter 3 (equation 20). I derive the mean total stress for the VES method in terms of the vertical total stress (Chapter 2, equation 26; Chapter 3, model input), the uniaxial effective stress ratio (Chapter 2, equation 17; Chapter 3, equation 14), and the mean effective stress under uniaxial strain (Chapter 2, equation 27; Chapter 3, equation 14).

With the mean total stress for the VES method ( $\sigma_{m,K_0}$ ) equal to:

$$\sigma_{m,K_0} = \sigma'_{m,K_0} + u_{VES} \quad (\text{A.1})$$

I first solve for  $\sigma'_{m,K_0}$  in terms of the known inputs. I write  $\sigma'_{m,K_0}$  in terms of the vertical effective stress using Chapter 2, equation 23, and Chapter 2, equation 18:

$$\sigma'_{m,K_0} = \frac{\sigma'_v(1+2K_0)}{3} \quad (\text{A.2})$$

I next solve for  $u_{VES}$  in terms of the known inputs. With  $u_{VES}$  written as a function of the vertical stresses:

$$u_{VES} = \sigma_v - \sigma'_v \quad (\text{A.3})$$

I start by expressing  $\sigma'_v$  in terms of  $\sigma'_{m,K_0}$  using Chapter 2, equation 23, and Chapter 2, equation 18:

$$\sigma'_v = \frac{3\sigma'_{m,K_0}}{(1+2K_0)} \quad (\text{A.4})$$

Equation A.4 allows for equation A.3 to be written in terms of the known inputs:

$$u_{VES} = \sigma_v - \frac{3\sigma'_{m,K_0}}{(1+2K_0)} \quad (\text{A.5})$$

Finally, the equation for  $\sigma_{m,K_0}$  (equation A.1) can be written in terms of the known inputs by combining equation A.2 with equation A.5:

$$\sigma_{m,K_0} = \frac{\sigma'_v(1+2K_0)}{3} + \sigma_v - \frac{3\sigma'_{m,K_0}}{(1+2K_0)} \quad (\text{A.6})$$

By reducing equation A.6, I arrive at the final equation for  $\sigma_{m,K_0}$  used in Chapter 2 (equation 28) and Chapter 3 (equation 20):

$$\sigma_{m,K_0} = \sigma_v - \frac{2\sigma'_{m,K_0}(1-K_0)}{1+2K_0} \quad (\dots)$$

## Appendix B: Derivation of Mean Total Stress for MES Method

This appendix summarizes the steps I use to derive the mean total stress for the MES method in Chapter 3 (equation 22). I derive the mean total stress for the MES method in terms of the known inputs:  $\sigma'_v$  (function of velocity; Chapter 3, equation 17),  $K_0$  (function of friction angle; Chapter 3, equation 15), and  $K$  (model input).

With the mean total stress for the MES method ( $\sigma_{m,MES}$ ) equal to:

$$\sigma_{m,MES} = \sigma'_{m,MES} + u_{MES} \quad (B.1)$$

I first solve for  $\sigma'_{m,MES}$  in terms of the known inputs. Given the VES and MES methods share the same mean effective stress ( $\sigma'_{m,MES} = \sigma'_{m,K_0}$ ), I write  $\sigma'_{m,MES}$  in terms of the vertical effective stress using Chapter 3, equation 18:

$$\sigma'_{m,MES} = \frac{\sigma'_v(1+2K_0)}{3} \quad (B.2)$$

I next solve for  $u_{MES}$  in terms of the known inputs. With  $u_{MES}$  written as a function of the vertical stresses:

$$u_{MES} = \sigma_v - \sigma'_{v,MES} \quad (B.3)$$

I start by expressing  $\sigma'_{m,MES}$  in terms  $\sigma'_{v,MES}$ :

$$\sigma'_{m,MES} = \frac{\sigma'_{v,MES}(1+2K)}{3} \quad (B.4)$$

I combine equation B.2 with equation B.3:

$$\frac{\sigma'_v(1+2K_0)}{3} = \frac{\sigma'_{v,MES}(1+2K)}{3} \quad (B.5)$$

I rearrange equation B.5 to be in terms of  $\sigma'_{v,MES}$ :

$$\sigma'_{v,MES} = \frac{\sigma'_v(1+2K_0)}{1+2K} \quad (B.6)$$

Equation B.6 allows for equation B.3 to be written in terms of the known inputs:

$$u_{MES} = \sigma_v - \frac{\sigma'_v(1+2K_0)}{1+2K} \quad (B.7)$$

Finally, the equation for  $\sigma_{m,MES}$  (equation B.1) can be written in terms of the known inputs by combining equation B.2 with equation B.7:

$$\sigma_{m,MES} = \frac{\sigma'_v(1+2K_0)}{3} + \sigma_v - \frac{\sigma'_v(1+2K_0)}{1+2K} \quad (\text{B.8})$$

By reducing equation B.8, I arrive at the final equation for  $\sigma_{m,MES}$  used in Chapter 3 (equation 22):

$$\sigma_{m,MES} = \sigma_v + \frac{2\sigma'_v(-1+K-2K_0+2K_0K)}{3(1+2K)} \quad (\dots)$$

## Appendix C: Derivation of Mean Total Stress for FES Method

This appendix summarizes the steps I use to derive the mean total stress for the FES method in Chapter 3 (equation 26). I derive the mean total stress for the FES method in terms of the known inputs:  $\sigma'_v$  (function of velocity; Chapter 3, equation 17),  $K_0$  (function of friction angle; Chapter 3, equation 15),  $K$  (model input),  $\eta_{K_0}$  (function of friction angle; Chapter 3, equation 14),  $\eta_K$  (function of  $K$ ; Chapter 3, equation 11),  $M$  (function of friction angle; if  $K \leq 1$ , Chapter 3, equation 8; if  $K > 1$ , Chapter 3, equation 9), and  $M_{Ext.}$  (function of friction angle; Chapter 3, equation 8).

With the mean total stress for the FES method ( $\sigma_{m,FES}$ ) equal to:

$$\sigma_{m,FES} = \sigma'_{m,FES} + u_{FES} \quad (C.1)$$

I first write  $\sigma'_{m,FES}$  (Chapter 3, equation 25) in terms of the known inputs:

$$\sigma'_{m,FES} = \sigma'_v \left( \frac{1+2K_0}{3} \right) \left( \frac{M_{Ext.}^2 + \eta_{K_0}^2}{M_{Ext.}^2} \right) \left( \frac{M^2}{M^2 + \eta_K^2} \right) \quad (C.2)$$

I next solve for  $u_{FES}$  (Chapter 3, equation 27) in terms of the known inputs. With  $u_{FES}$  written as a function of the vertical stresses:

$$u_{FES} = \sigma_v - \sigma'_{v,FES} \quad (C.3)$$

I start by expressing  $\sigma'_{v,FES}$  in terms of  $\sigma'_{m,FES}$ :

$$\sigma'_{v,FES} = \frac{3\sigma'_{m,FES}}{1+2K} \quad (C.4)$$

I then combine equation C.2 with equation C.4:

$$\sigma'_{v,FES} = \frac{3}{1+2K} * \sigma'_v \left( \frac{1+2K_0}{3} \right) \left( \frac{M_{Ext.}^2 + \eta_{K_0}^2}{M_{Ext.}^2} \right) \left( \frac{M^2}{M^2 + \eta_K^2} \right) \quad (C.5)$$

Next, I combine equation C.3 with equation C.5:

$$u_{FES} = \sigma_v - \frac{3}{1+2K} * \sigma'_v \left( \frac{1+2K_0}{3} \right) \left( \frac{M_{Ext.}^2 + \eta_{K_0}^2}{M_{Ext.}^2} \right) \left( \frac{M^2}{M^2 + \eta_K^2} \right) \quad (C.6)$$

Finally, the equation for  $\sigma_{m,FES}$  (equation C.1) can be written in terms of the known inputs by combining equation C.2 with equation C.6:

$$\sigma'_v \left( \frac{1+2K_0}{3} \right) \left( \frac{M_{Ext.}^2 + \eta K_0^2}{M_{Ext.}^2} \right) \left( \frac{M^2}{M^2 + \eta K^2} \right) + \sigma_v - \frac{3}{1+2K} * \sigma'_v \left( \frac{1+2K_0}{3} \right) \left( \frac{M_{Ext.}^2 + \eta K_0^2}{M_{Ext.}^2} \right) \left( \frac{M^2}{M^2 + \eta K^2} \right) \quad (C.7)$$

By reducing equation C.7, I arrive at the final derivation for the mean total stress for the FES method used in Chapter 3 (equation 26):

$$\sigma_{m,FES} = \sigma_v + \frac{2\sigma'_v M^2 (M_{Ext.}^2 + \eta K_0^2) (1+2K_0) (K-1)}{3M_{Ext.}^2 (1+2K) (M^2 + \eta K^2)} \quad (26)$$

## Bibliography

- Alberty, M. W., and McLean, M. R., Emerging trends in pressure prediction, *in* Proceedings Offshore Technology Conference2003, Offshore Technology Conference.
- Athy, L. F., 1930, Density, porosity, and compaction of sedimentary rocks: AAPG Bulletin, v. 14, no. 1, p. 1-24.
- Bowers, G. L., 1995, Pore pressure estimation from velocity data: Accounting for overpressure mechanisms besides undercompaction: SPE Drilling & Completion, v. 10, no. 02, p. 89-95.
- Bruce, B., and Bowers, G., 2002, Pore pressure terminology: The Leading Edge, v. 21, no. 2, p. 170-173.
- Cartwright, J. A., 1994, Episodic basin-wide fluid expulsion from geopressed shale sequences in the North Sea basin: Geology, v. 22, no. 5, p. 447-450.
- Casey, B., Germaine, J., Flemings, P., and Fahy, B., 2015, Estimating horizontal stresses for mudrocks under one-dimensional compression: Marine and Petroleum Geology, v. 65, p. 178-186.
- Casey, B., and Germaine, J. T., 2013, Stress dependence of shear strength in fine-grained soils and correlations with liquid limit: Journal of Geotechnical and Geoenvironmental Engineering, v. 139, no. 10, p. 1709-1717.
- , 2014, An evaluation of three triaxial systems with results from 0.1 to 100 MPa: ASTM International.
- Casey, B., Germaine, J. T., Flemings, P. B., and Fahy, B. P., 2016, In situ stress state and strength in mudrocks: Journal of Geophysical Research: Solid Earth, v. 121, no. 8, p. 5611-5623.
- Craig, R. F., 2004, Craig's soil mechanics, CRC Press.
- Dias, T. A., Tett, D. L., and Croasdaile, M. T., Evidence for a hydrodynamic aquifer in the lower Miocene sands of the Mad Dog field, Gulf of Mexico, *in* Proceedings Adapted from extended abstract from AAPG Convention, Denver, Colorado2009, Citeseer.
- Dugan, B., and Flemings, P., 2002, Fluid flow and stability of the US continental slope offshore New Jersey from the Pleistocene to the present: Geofluids, v. 2, no. 2, p. 137-146.
- Dutta, N., 2002, Geopressure prediction using seismic data: Current status and the road ahead: Geophysics, v. 67, no. 6, p. 2012-2041.
- Eaton, B. A., The equation for geopressure prediction from well logs, *in* Proceedings Fall meeting of the Society of Petroleum Engineers of AIME1975, Society of Petroleum Engineers.
- Fertl, W. H., Chapman, R. E., and Hotz, R. F., 1994, Studies in abnormal pressures, Elsevier.
- Flemings, P., and Lupa, J., 2004, Pressure prediction in the Bullwinkle Basin through petrophysics and flow modeling (Green Canyon 65, Gulf of Mexico): Marine and Petroleum Geology, v. 21, no. 10, p. 1311-1322.

- Flemings, P. B., and Saffer, D. M., 2018, Pressure and Stress Prediction in the Nankai Accretionary Prism: A Critical State Soil Mechanics Porosity-based approach: *Journal of Geophysical Research: Solid Earth*.
- Flemings, P. B., Stump, B. B., Finkbeiner, T., and Zoback, M., 2002, Flow focusing in overpressured sandstones: Theory, observations, and applications: *American Journal of Science*, v. 302, no. 10, p. 827-855.
- Gibson, R. E., 1958, The progress of consolidation in a clay layer increasing in thickness with time: *Geotechnique*, v. 8, no. 4, p. 171-182.
- Gordon, D. S., and Flemings, P. B., 1998, Generation of overpressure and compaction-driven fluid flow in a Plio-Pleistocene growth-faulted basin, Eugene Island 330, offshore Louisiana: *Basin Research*, v. 10, no. 2, p. 177-196.
- Gouly, N., 1998, Relationships between porosity and effective stress in shales: *First Break*, v. 16, no. 12, p. 413-149.
- , 2004, Mechanical compaction behaviour of natural clays and implications for pore pressure estimation: *Petroleum Geoscience*, v. 10, no. 1, p. 73-79.
- Harrold, T. W., Swarbrick, R. E., and Gouly, N. R., 1999, Pore pressure estimation from mudrock porosities in Tertiary basins, southeast Asia: *AAPG bulletin*, v. 83, no. 7, p. 1057-1067.
- Hart, B., Flemings, P., and Deshpande, A., 1995, Porosity and pressure: Role of compaction disequilibrium in the development of geopressures in a Gulf Coast Pleistocene basin: *Geology*, v. 23, no. 1, p. 45-48.
- Hashash, Y., and Whittle, A., 1992, Integration of the modified Cam-clay model in non-linear finite element analysis: *Computers and geotechnics*, v. 14, no. 2, p. 59-83.
- Hauser, M. R., Couzens-Schultz, B. A., and Chan, A. W., 2014, Estimating the influence of stress state on compaction behavior: *Geophysics*.
- Heidari, M., Nikolinakou, M., and Flemings, P., in press, Coupling geomechanical modeling with seismic pressure prediction: *Geophysics*.
- Issler, D., 1992, A new approach to shale compaction and stratigraphic restoration, Beaufort-Mackenzie Basin and Mackenzie Corridor, Northern Canada (1): *AAPG bulletin*, v. 76, no. 8, p. 1170-1189.
- Long, H., Flemings, P., Germaine, J., and Saffer, D., 2011, Consolidation and overpressure near the seafloor in the Ursa Basin, Deepwater Gulf of Mexico: *Earth and Planetary Science Letters*, v. 305, no. 1, p. 11-20.
- Merrell, M. P., 2012, Pressure and Stress at Mad Dog Field, Gulf of Mexico.
- Merrell, M. P., Flemings, P. B., and Bowers, G. L., 2014, Subsalt pressure prediction in the Miocene Mad Dog field, Gulf of Mexico: *AAPG bulletin*, v. 98, no. 2, p. 315-340.
- Nikolinakou, M., Merrell, M., Luo, G., Flemings, P., and Hudec, M., Geomechanical modeling of the Mad Dog salt, Gulf of Mexico, *in Proceedings 47th US Rock Mechanics/Geomechanics Symposium 2013*, American Rock Mechanics Association.

- Nikolinakou, M. A., Heidari, M., Flemings, P. B., and Hudec, M. R., 2018, Geomechanical modeling of pore pressure in evolving salt systems: *Marine and Petroleum Geology*.
- Nikolinakou, M. A., Luo, G., Hudec, M. R., and Flemings, P. B., 2012, Geomechanical modeling of stresses adjacent to salt bodies: Part 2—Poroelastoplasticity and coupled overpressures: *AAPG bulletin*, v. 96, no. 1, p. 65-85.
- Rubey, W. W., and Hubbert, M. K., 1959, Overthrust belt in geosynclinal area of western Wyoming in light of fluid pressure hypothesis: *Geol. Soc: America Bull*, v. 70, no. 2, p. 167-205.
- Sangrey, D. A., 1977, Marine geotechnology—state of the art: *Marine Georesources & Geotechnology*, v. 2, no. 1-4, p. 45-80.
- Stump, B. B., Flemings, P. B., Finkbeiner, T., and Zoback, M. D., Pressure differences between overpressured sands and bounding shales of the Eugene Island 330 field (offshore Louisiana, USA) with implications for fluid flow induced by sediment loading, *in Proceedings Overpressures in petroleum exploration: workshop proceedings: Elf Exploration Production Memoir 1998, Volume 22*, p. 83-92.
- Swarbrick, R. E., Osborne, M. J., and Yardley, G. S., 2001, *AAPG Memoir 76, Chapter 1: Comparison of Overpressure Magnitude Resulting from the Main Generating Mechanisms*.
- Sweatman, R., Faul, R., and Ballew, C., New solutions for subsalt-well lost circulation and optimized primary cementing, *in Proceedings SPE annual technical conference 1999*, p. 157-167.
- Viceer, S., Albertin, M., Vinson, G., Hornby, B., Ebrom, D., Heppard, P., Jay, C., and Blangy, J.-P., Improving drilling efficiency using a look-ahead vsp to predict pressure, exiting salt: five Gulf of Mexico examples, *in Proceedings Offshore Technology Conference 2006, Offshore Technology Conference*.
- Wood, D. M., 1990, *Soil behaviour and critical state soil mechanics*, Cambridge university press.